ENHANCING THE TRANSIENT STABILITY OF POWER SYSTEMS USING A THYRISTOR CONTROLLED SERIES CAPACITOR

by

Rudy Pillay Carpanen

B.Eng(Hons)

Submitted in the fulfillment of the academic requirements for the degree of Master of Science in Engineering, in the School of Electrical, Electronic and Computer Engineering, University of KwaZulu – Natal, Durban, South Africa.

March 2005

I hereby declare that all the material incorporated into this thesis is my own original and unaided work except where a specific reference is made by name or in the form of a numbered reference. The work contained herein has not been submitted for a degree at any other university.

Signed: 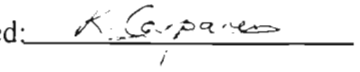

R Pillay Carpanen

This thesis is dedicated to my parents

ABSTRACT

The continuously growing demand for electric power requires transmitting larger amounts of power over long distances. An economically attractive solution to increase the power transfer through a long interconnection (up to a limit) without building new parallel circuits is to install series capacitor compensation on the transmission line. Large disturbances which constantly occur in power systems may disrupt the synchronous operation of the generators and lead to out-of-step conditions. Coordinated insertion and removal of the compensating capacitors in series with a transmission line is an approach that has been known for many years to be capable of enhancing the transient stability of power systems as well as providing additional damping to the power system oscillations. The relatively recent emergence of the thyristor controlled series capacitor (TCSC) has now made this method of transient stability enhancement practically feasible.

This thesis compares a range of different strategies that have been proposed in the literature for control of series compensating reactance to enhance transient stability. Initially a simple swing-equation model of a single-generator power system, including an idealised controllable series compensator (CSC) is used to study the fundamental characteristics of the variable impedance control and its impact on transient stability. Subsequently, a detailed model of a small study system is developed, including a detailed representation of a TCSC, for more in-depth analysis.

This detailed study system model is then used to compare three different transient stability control schemes for the TCSC, namely: generator speed-deviation based bang-bang control, discrete control based on an energy-function method, and nonlinear adaptive control. Time-domain results are presented to demonstrate the impact of the TCSC on first swing stability of the SMIB system with the above control schemes for various fault scenarios. The performance of each control scheme is also compared by evaluating the extent to which it extends the transient stability margin of the study system.

For each of the three different TCSC control approaches considered, the results show that variable impedance control of the TCSC provides further improvement in the transient stability limits of the study system over and above the improvement that is obtained by having a fixed-impedance TCSC in the system. In the case of the bang-bang and discrete control approaches, it is shown that a combination of a large steady-state value of the TCSC compensation, together with a relative small range of variable TCSC reactance under transient conditions, offers the best improvement in the transient stability limits for the studied system.

The results also show that there is little difference in the extent to which the energy-function method of TCSC control improves the transient stability limits over the improvement obtained using speed-deviation bang-bang control of the TCSC for the study system considered.

ACKNOWLEDGEMENTS

The work presented in this thesis was carried out under the supervision of Dr. Bruce S. Rigby of the School of Electrical, Electronic and Computer Engineering, University of KwaZulu – Natal, Durban. I wish to thank Dr. Rigby for his support, guidance throughout the course of this thesis, and for his commendable efforts during the correction of this thesis. I would also wish to thank Dr. Rigby for arranging much needed financial support.

In addition, I would like to thank:

Professor Edward Boje for his assistance and suggestions during several discussions on the control aspects of this work;

my family for their support, patience and their best wishes;

my friends for their support and encouragement;

the University of KwaZulu – Natal and THRIP for providing financial support;

the staff and postgraduate students of the School of Electrical, Electronic and Computer Engineering, unfortunately too many to mention by name, who have together contributed towards a friendly and simulating work environment over the years.

TABLE OF CONTENTS

CHAPTER THREE MATHEMATICAL MODELLING FOR TRANSIENT STABILITY STUDIES

CHAPTER FOUR BANG – BANG CONTROL OF THE TCSC FOR POWER SYSTEM STABILITY ENHANCEMENT

CHAPTER FIVE DISCRETE CONTROL OF THE TCSC BASED ON ENERGY FUNCTIONS FOR POWER SYSTEM STABILITY ENHANCEMENT

APPENDICES

LIST OF FIGURES AND TABLES

FIGURES

TABLES

LIST OF SYMBOLS

The commonly used symbols and notations adopted in this thesis are listed below. Other symbols used the text are explained where there first occur.

Acronyms

AVR	Automatic Voltage Regulator
CCT	Critical Clearing Time
CSC	Controllable Series Compensator
FACTS	Flexible AC Transmission Systems
IPFC	Interline Power Flow Controller
MOV	Metal Oxide Varistor
PLL	Phase Locked Loop
PSCAD	Power System Computer Aided Design
TCR	Thyristor Controlled Reactor
TCSC	Thyristor Controlled Series Capacitor
TSSC	Thyristor Switched Series Capacitor
TCSR	Thyristor Controlled Series Reactor
TSSR	Thyristor Switched Series Reactor
SMIB	Single Machine Infinite Bus
SSSC	Static Synchronous Series Compensator

Synchronous generator symbols

R_a	armature winding resistance
X_l	leakage reactance
X_d	direct axis stator self-inductive reactance
X_q	quadrature axis stator self-inductive reactance

R_f	field resistance
X_f	field leakage reactance
R_d	direct axis damper resistance
X_{kd}	direct axis damper leakage reactance
X_{mfd}	direct axis unsaturated magnetising reactance
X_{mq}	quadrature axis magnetising reactance
R_{kq}	quadrature axis damper winding resistance
X_{kq}	quadrature axis damper winding leakage reactance
H	inertia constant
D	parameter representing mechanical damping
P_m	mechanical power input to the generator
P_e	generator electrical power output
V_T	initial generator terminal voltage
ω_0	generator synchronous speed
δ	rotor angle
$\Delta\omega$	rotor speed deviation

Automatic Voltage Regulator

K_A	regulator gain
T_C	1st lead time constant
T_B	1st lag time constant
T_{C1}	2nd lead time constant
T_{B1}	2nd lag time constant

System symbols

C	capacitance
L	inductance
R	resistance
V_s	sending bus voltage
V_b	infinite bus voltage
ϕ	voltage angle difference between sending and receiving buses
R_L	transmission line resistance
X_L	transmission line reactance
X_T	transformer reactance
X_{TCSC}	overall TCSC reactance
X_{TCR}	reactance of TCR
X_C	capacitive reactance of the TCSC capacitors
X_{ORDER}	reactance order of the TCSC
X_{ORDER0}	initial steady state of the reactance order
$X_{orderMAX}$	maximum reactance order
$X_{orderMIN}$	minimum reactance order
α	firing angle of the TCSC thyristors
α_{res}	resonant point of firing angle

General

$\dot{x}$	signifies the derivative of x
pu	per-uint
$[Y]$	signifies a matrix of Y
Δ	small change operator

CHAPTER ONE

INTRODUCTION

1.1 General

Power utilities are increasingly called upon to operate transmission lines at high power transfer levels due to the steadily growing demand for electric power. As the power transfer levels increase, the margins of the stability of the power system decrease. Traditional solutions to upgrade the transmission system infrastructure have been primarily in the form of new transmission lines, substations, and associated equipment. However, as experiences have proven over the past decade or more, the process to permit, site, and construct new transmission lines has become extremely difficult, expensive, time-consuming, and controversial [1]. Moreover, because of natural conditions and environmental protections it is difficult to construct more lines or substations at present [2]. This situation, in turn, has led to a review of the traditional power generation and transmission system theory and practice in order to address the issue of how to operate the existing power system much closer to its stability limits without compromising the security of the system itself. Historically, safe and stable operation of an electric power system has been achieved by operating the system far away from its theoretical stability limits, in part because of a limited capability to control the transmission system itself under dynamic conditions. However, it has been recognised that improved dynamic control of ac power systems would allow better utilisation of these systems [3]. These circumstances, and significant developments in the area of power electronics have led to the emergence of the Flexible AC Transmission systems or FACTS concept: FACTS aims to bring the factors which influence the transfer of power in a transmission system under rapid control by means of modern, power-electronic-based compensating devices in order to allow the system safely to be pushed closer to its limits.

Kimbark [4] in fact first recognised that dynamic switching of series compensating reactance in a transmission line could improve stability. However, at that time such switching could only be carried out using mechanical circuit breakers which are not

practical for repeated fast dynamic control applications. Fig. 1.1 is an illustration of a few cycles of voltage at power system frequency [1]. This figure shows that the speed of mechanical switches (primarily circuit breakers) for conventional transmission line switching can be as fast as a couple of cycles of 50 Hz. This speed of switching in and of itself may be fast enough to solve many power system constraints. Although there is a vast improvement in switching time from mechanical to power-electronic based solutions (Fig1.1 illustrates that the speed of the power electronic electronics switches is a fraction of a cycle), the main benefit that FACTS controller solutions provide is the "cycling/repeatability" and "smooth control" that accompanies the power electronic based switching. In other words, solutions based on mechanical switches (which tend to wear out very quickly and cannot therefore be operated too often) usually have a "one and done" or "on or off" impact on power system stability. By contrast, solutions based on power electronics can provide either a smooth and continuous, or a rapidly repeatable option for power system control.

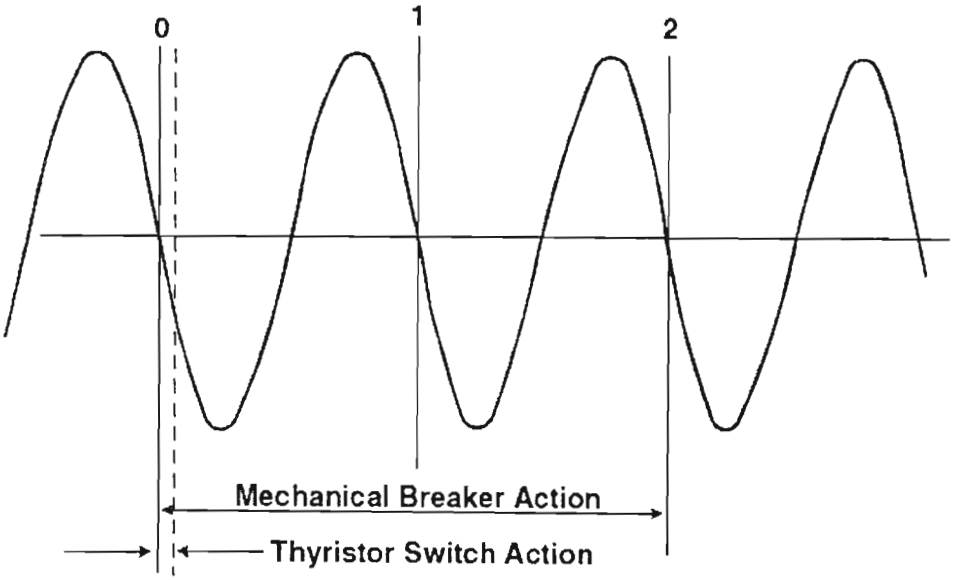

Fig. 1.1: Illustration of the speed of power system control

The high-speed response of FACTS devices provides fast and efficient control of the power transmitted through transmission lines, and dynamic control applications using these devices have now become practically feasible. As a consequence, a number of FACTS technologies have emerged with which to improve power system stability, thus allowing the system to be operated closer to its stability limits.

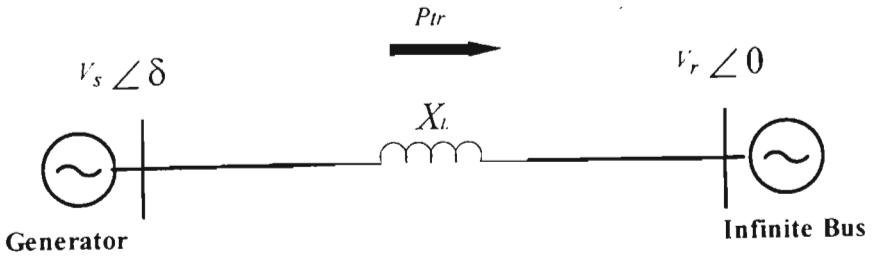

Fig. 1.2: Simplified two-area power system illustrating the factors which influence power flow

Fig. 1.2 shows a simplified diagram of a two-area power system connected by a transmission corridor. The active power P_{tr} transferred by the transmission system is given by

$$P_{tr} = \frac{|V_s||V_r|}{X_L} \sin\delta = P_{tr\max} \sin\delta \tag{1.1}$$

where,

δ = transmission angle;

$|V_s|$ = transmission system voltage at the sending bus;

$|V_r|$ = transmission system voltage at the receiving bus.

The maximum power transfer $P_{tr\max}$ in equation (1.1) is the steady-state power transfer limit of the system. However, the transient stability characteristics of the synchronous generators in the system mean that the transmission line must in practice be operated at a power level much lower than this steady state limit in order to allow sufficient margin for the generators to remain in synchronism following disturbances. One application of FACTS devices is to enhance the control of the electromechanical power oscillations between the generators and the transmission system so as to reduce the need for such large stability margins inherent in conventional power systems. This control can be used to enhance both transient and small-signal stability as required.

From equation (1.1), it is apparent that three possible levers exist for control of power flow: voltage magnitude ($|V_s|, |V_r|$), voltage phase (δ), and transmission line reactance (X_L). Various traditional approaches to control each of these levers using mechanical controllers can now be implemented with modern power-electronic-based FACTS controllers which can be divided into four categories: series controllers, shunt controllers, combined series-series controllers and combined series-shunt controllers [5]. When transmission systems are heavily stressed, the angle between sending and receiving ends is high and variation in series impedance has a large leverage on the instantaneous power transfer. The leverage with series compensation is generally much higher than can be achieved with a controlled shunt reactive system of comparable rating [6]. This thesis is concerned with one particular lever, namely compensation of the series reactance of the transmission line for line reactance control. In addition the thesis focuses primarily on one application of this lever to system stability: that is using controllable series compensation to enhance the *transient* stability of a power system.

Traditionally, fixed capacitor banks have been used in series with transmission lines to reduce their net inductive reactance and thereby to increase their maximum power transfer capability: with a capacitive compensating reactance X_{CSC} introduced in series with the transmission line in Fig. 1.2, the maximum power transfer capability at steady state is increased to $P_{tr\max} = |V_s||V_r|/(X_L - X_{CSC})$. In turn, an improvement in the transient stability margin is also achieved because of this increased power transfer capability at steady-state for a given voltage phase angle and not because of any dynamic control. Modern FACTS series compensators now allow such series compensating reactance to be controlled dynamically resulting in even further potential improvement in transient stability margins. There are several FACTS series compensators namely: Static Synchronous Series Compensator (SSSC), Interline Power Flow Controller (IPFC), Thyristor Controlled Series Capacitor (TCSC), Thyristor Switched Series Capacitor (TSSC), Thyristor Controlled Series Reactor (TCSR) and Thyristor Switched Series Reactor (TSSR) [5]. Any of these FACTS series compensators can now, in principle, be used to provide a dynamically varying series compensation for the purpose of enhancing system stability in general.

However, this thesis is particularly concerned with the use of the variable impedance capability of the TCSC for enhancing the transient stability of a power system.

1.2 Thesis Background and Objectives

Power system stability can be classified into large-signal (or transient) stability and small-signal stability phenomena. Power system operation can often be limited by small-signal stability concerns, in particular by a lack of damping in the system oscillations. However, the issue of transient stability is of interest in the operation of all power systems.

Transient stability is the ability of the power system to maintain synchronism when subjected to a severe transient disturbance such as a short-circuit or line tripping. The resulting system response involves large excursions of the generator rotor angles and is influenced by the nonlinear power-angle relationship of each generator. Stability depends on both the initial operating state of the system and the severity of the disturbance. Often, the system is altered so that the post-disturbance steady state operation differs from that prior to the disturbance. Disturbances of widely varying degrees of severity and probability of occurrence can occur on the system. The system is, however, designed and operated so as to be stable for a selected set of contingencies. The contingencies are short-circuits of different types: phase-to-ground, phase-to-phase-to-ground, or three-phase. They are usually assumed to occur on transmission lines, but occasionally bus or transformer faults are also considered. The fault is assumed to be cleared by the opening of appropriate breakers to isolate the faulted element. In some cases, high-speed reclosure of the circuit breakers may be assumed [7].

The aim of thesis is to investigate the use a particular type of FACTS series compensator, that is the TCSC, to enhance the transient stability of power systems. The thesis evaluates a range of proposed approaches for carrying out control of a TCSC for transient stability enhancement and assesses these control approaches by comparing their impact on the transient stability limits of the power system.

1.3 Thesis Layout

This thesis consists of six further chapters and appendices. In order to present the analyses of this thesis, the development of the various system models, the results and main finding of the thesis, the material has been arranged as follows.

Before an investigation of this kind could be carried out it was necessary to review the technical literature on the subject of controllable series compensation as applied to improving the transient stability of power systems. Chapter Two, in particular, provides the background theory to enhancing transient stability using controllable series compensators. This chapter also provides a literature review of the control strategies proposed for varying the reactance of a series compensator for transient stability enhancement and identifies the particular approaches to be considered for further study in the thesis.

Chapter Three presents two mathematical models used for the simulation studies and analysis in the thesis: a simple swing-equation model and a detailed nonlinear model of a single-machine infinite bus power system. The simple swing-equation model employs an idealised representation of the controllable series capacitor whereas the detailed nonlinear simulation model represents the TCSC's power electronics and internal control in some detail. The theory and operation of the TCSC is also briefly presented and the effect of short-circuit faults on the TCSC's internal controls is examined.

Chapter Four presents the results of two case studies on the single-machine infinite bus power system described in Chapter Three. Firstly, an external transient stability control loop is implemented around the TCSC to vary its compensating reactance in bang-bang mode so as to improve the transient stability of the power system following a large disturbance; the generator speed deviation is used as the input signal to the transient stability controller. Secondly, the effect of deactivating the transient stability control loop, or alternatively transferring the control of the TCSC to a damping control loop after a limited number of switchings is also considered. The effects of the size of the TCSC's controllable reactance range, as well as the severity of the fault on the transient stability margin of the power system are investigated.

Chapter Five considers an energy-function control approach to vary the TCSC's compensating reactance for transient stability enhancement, with a locally-measured input signal synthesised for use as the controller input. The performance of this energy-function controller is then compared with that of the bang-bang control approach considered in Chapter Four, again by evaluating the extent to which each method improves the transient stability limit of the power system.

Chapter Six considers a nonlinear adaptive control scheme to vary the TCSC's compensating reactance for transient stability enhancement, again using locally measured signals synthesised for use as the controller input. The performance of the non-linear adaptive control scheme is then compared with the two previous control schemes considered in Chapter Four and Chapter Five.

Finally, Chapter Seven summarises the main results from the studies carried out in the thesis and suggests further research that could be undertaken in the future.

1.4 Main Achievements and Findings of the Thesis

The previous section has outlined the contents and arrangement of the thesis. This section now summarises the main findings of the thesis and the achievements made. This thesis has:

(i) derived and programmed a MATLAB [8] time-domain simulation model of a single-machine infinite bus (SMIB) power system containing a controllable series compensator. In addition, a detailed model of a SMIB system which is more suitable for transient stability studies (including a detailed representation of the TCSC itself) has been developed in the power system simulation package PSCAD [9];

(ii) presented a detailed study of the bang-bang control approach based on generator speed deviation, for varying a TCSC's compensating reactance to enhance the transient stability of a SMIB power system. In addition, the thesis has shown the effect of size of the compensating reactance and the severity of fault on the transient stability of the system. The thesis has also demonstrated

how bang-bang control can be successfully switched to linear damping control or simply de-activated once the system has survived a transient event;

(iii) compared the performance of bang-bang control of the TCSC with two other control approaches proposed in the literature.

(iv) showed that, at least for the study system considered here, the energy function and nonlinear adaptive control schemes do not result in a significant improvement in the transient stability limit over the simple bang-bang control approach.

1.5 Research Publications

Some of the findings of this thesis have been presented at national and international conferences [10], [11] and [12].

CHAPTER TWO

REVIEW OF THE STRATEGIES FOR TRANSIENT STABILITY CONTROL

2.1 Introduction

The previous chapter has described the problems facing power utilities today and explained that Flexible AC Transmission Systems (FACTS) aim to alleviate these problems by allowing power systems to be operated closer to their stability limits without risking the security of the system. The discussions of that chapter showed that when transmission systems are heavily stressed, the angle between the sending and receiving ends is high and variation in the series compensation has a large leverage on the instantaneous power transfer. Hence FACTS series devices can therefore be used to dynamically control the power flow in a manner that tends to keep the amplitude of the generator rotor swings as low as possible following a large disturbance on the system.

This chapter initially describes how fixed series capacitive compensation can be used to extend the transient stability limit of a SMIB power system using an example of a simplified two-area power system subjected to a large disturbance; from this simple case study the fundamental operating principle of enhancing the transient stability using dynamically variable series capacitive compensation is established.

Finally, this chapter reviews various control approaches proposed in the literature for transient stability control of power systems via controllable series compensation. Approaches suited for remote positioning of the variable series compensator and the appropriate types of input signals to the controller are discussed.

2.2 Historical Perspective

In 1966, E. W. Kimbark [4] proposed the use of a switched series capacitor to change the power flow in a transmission line following a disturbance. Kimbark used the equal area criterion to predict that the transient stability of an electrical power system can be

improved by bypassing and inserting a series capacitor. The advantage of switched versus fixed series compensation is that it increases both the steady-state and the transient stability limits, and it is more economical than fixed compensation [4]. It must be noted that the analyses in [4] referred to one switching in of a series capacitor after a fault. In 1969, O. J. Smith [13] proposed that the oscillatory transients in power systems can be removed by inserting and removing a series capacitor in a transmission line. While reference [4] proposed a single switching in of a series capacitor, Smith appears to be the first to propose a coordinated insertion and removal during the transient power swings. Reference [13] states that even a small amount of switched series compensating reactance can provide a dramatic increase in the power system stability. In a subsequent paper by Smith and Webster [14], the ideas in [13] were practically implemented in a laboratory and it was shown that a generator which would have otherwise have pole-slipped following a particular system fault was successfully stabilised using coordinated switching of the series capacitance.

At the time the ideas in [4], [13], [14], and [15] were proposed, dynamically variable series compensation could only be achieved using capacitor banks switched in and out with mechanical circuit breakers; however such devices were in practice too slow and unreliable for high-speed use demanded by a dynamical control application and as a result these ideas remained on hold for nearly two decades. Recently however, progress in the field of power electronics has led to the development of high-power electronic switches with which to implement dynamically variable compensating reactances for the specific purpose of improving the transient stability of power systems. However, the following section first explains conceptually how a variable series capacitive compensating reactance is able to enhance the transient stability of power systems following large-signal disturbances.

2.3 Theory of Transient Stability Control via Variable Impedance Control

Following a large disturbance, for example a 3-phase short-circuit on the transmission line of the two area power system in Fig. 1.2, the dynamics of the system can be described using the mechanical input torque to the system and the electrical output torque of the system. Figure 2.1 shows a simplified two-area power system with the transmission line compensated with a controllable series compensator (CSC). If the

torques caused by friction, windage and core loss in a machine are ignored, any difference between the mechanical (shaft) torque and electromagnectic torque developed must cause acceleration or deceleration of the generator. If T_m represents mechanical input torque from the turbines, and T_e is the electromagnetic torque, the net torque causing acceleration or deceleration is $T_a = T_m - T_e$. A similar equation holds for accelerating or decelerating power $P_a = P_m - P_e$, where P_m is the mechanical power input to the system, and P_e is the electrical power developed for a generator. If resistance is neglected, then the electrical power developed is the same as the power transferred by the line to the receiving end (that is, $P_e = P_{tr}$).

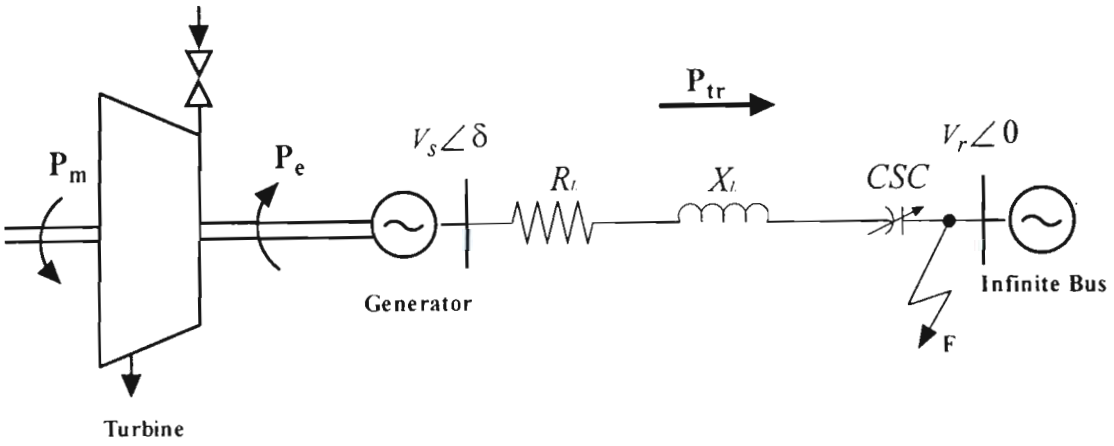

Fig. 2.1: A simplified two-area power system with a dynamically variable series compensating reactance.

Under steady-state operating conditions, the mechanical power input is equal to the electrical power developed, the accelerating power P_a is zero, the generator speed remains constant at synchronous speed and the generator rotor angle δ remains constant. However, following a disturbance, any imbalance between the mechanical input power and the electrical output power results in non-zero accelerating power which accelerates the shaft of the generator, changing its rotor angle according the swing equation [7]:

$$\frac{2H}{\omega_0}\frac{d^2\delta}{dt^2} = P_m - P_e \qquad (2.1)$$

where,

$$P_e = \frac{|V_s||V_r|}{X_L - X_{CSC}} \sin\delta \tag{2.2}$$

and: P_e = electrical power output;

P_m = mechanical power input to the system;

P_a = accelerating power;

H = inertia constant of the machine;

ω_0 = synchronous speed;

δ = generator rotor angle (with respect to a frame rotating at ω_0);

t = time.

The time derivative of the rotor angle is generator speed deviation $\Delta\omega$:

$$\frac{d\delta}{dt} = \omega - \omega_0 = \Delta\omega \tag{2.3}$$

At steady-state when the machine runs at constant speed, $\frac{d\delta}{dt}$ is zero since the generator electrical speed is equal to the synchronous speed and $\frac{d^2\delta}{dt^2}$ is likewise zero. The mechanical power input to the system is assumed to be constant throughout this analysis. If the system experiences a three-phase short circuit fault at the receiving end (as illustrated at point F in Fig. 2.1), the power P_{tr} transmitted to the receiving end in Fig. 2.1 becomes zero since V_r in equation (2.2) becomes zero. From equation (2.1) it becomes apparent that the speed of the machine must change since there is power imbalance between the input P_m and the output $P_e = P_{tr} = 0$ during the period of the fault. The speed of the synchronous machine therefore increases, under the influence of the positive accelerating power, from the initial operating point and the generator rotor angle increases from δ_1 to δ_{cl} (the angle at which the fault is cleared) as shown in Fig. 2.2. Once, the fault is cleared, V_r is assumed to return to its pre-disturbance value, and from equation (2.2) the electrical power transmitted by the line is now higher than the pre-disturbance value since the rotor angle has advanced to δ_{cl} (see Fig. 2.2). The power imbalance $P_a = P_m - P_e$ is now negative and the machine starts to decelerate. However, although the machine decelerates, its rotor angle continues to increase (up to δ_m in Fig. 2.2), as long as the rotor speed remains greater

than the synchronous speed. For the extreme case considered in Fig. 2.2, the rotor angle reaches a maximum value of δ_m. If the rotor angle swings past this maximum value δ_m, the electrical power output of the generator P_e will become lower than the mechanical power input P_m resulting in re-acceleration of the rotor, and pole slipping occurs (the generator loses synchronism). The equal area criterion can be used to determine whether following a severe disturbance, the rotor angle will swing beyond this maximum angle δ_m.

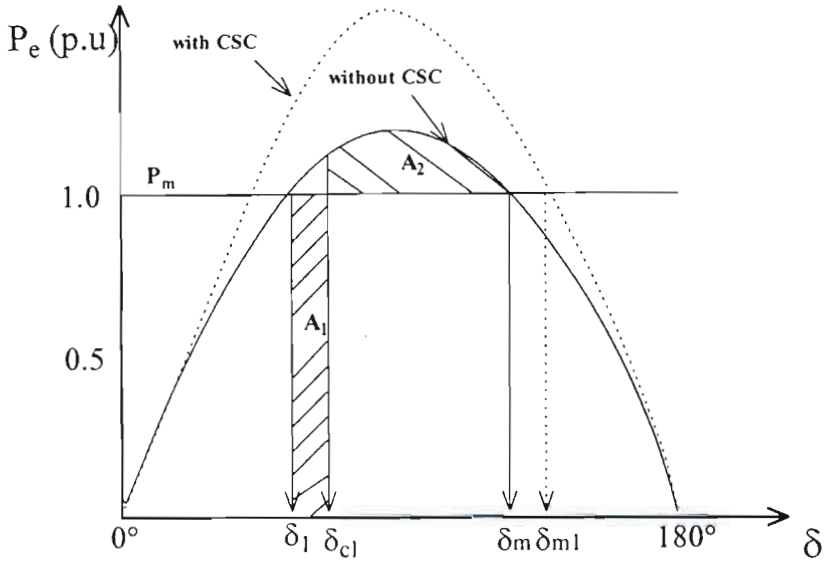

Fig. 2.2: Power-angle curves with and without CSC.

In Fig. 2.2 the area A_1 represents the kinetic energy gained by the rotor during the fault and area A_2 represents the kinetic energy lost from the rotor after the fault is cleared. If all energy gained is not returned to the power system, synchronism is lost. Hence, $A_2 = A_1$ is a criterion for stability. In the extreme case considered in Fig. 2.2, where the generator rotor angle δ swings up to δ_m, δ_{cl} is called the *critical clearing angle* and the time taken by δ to reach this critical clearing angle is called the *critical clearing time* (CCT). Thus, if the fault is not cleared before the CCT, the generator rotor will not survive the first swing and makes *asynchronous rotation* [16]. Hence, the CCT is an important transient stability index.

Considering the case when the series compensation is introduced into the transmission line as shown in Fig 2.1, the effect is to increase the amplitude of the generator output power at all the values of rotor angle δ. This is represented in Fig. 2.2 by the dotted curve. This means that the available post fault area (i.e. the capacity to decelerate the rotor) has increased by an amount A_3 (see Fig. 2.3).

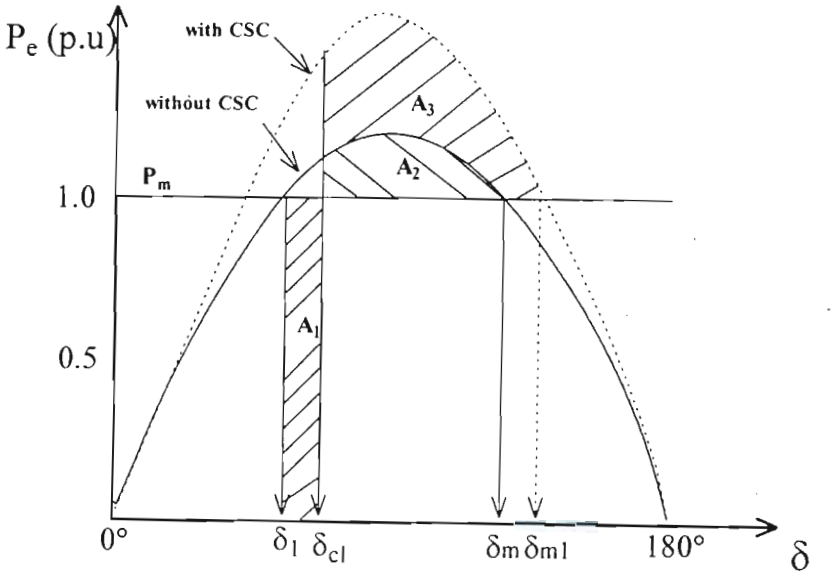

Fig. 2.3: Increase in post-fault decelerating area with CSC.

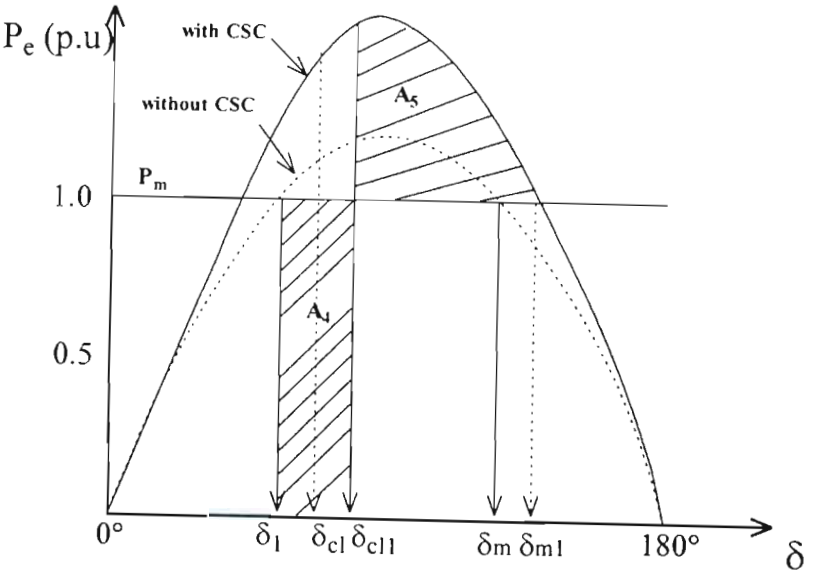

Fig. 2.4: Increase in critical clearing angle with CSC.

As a result of this additional *capacity* to decelerate the rotor, the system can survive a longer period of initial acceleration before stability is lost. This is illustrated in Fig.

2.4 which shows the same system subjected to the same fault, but for a longer period. The pre-fault area (now shown as A_4 in Fig. 2.4) is greater than in Fig. 2.3 but, because of the larger amplitude of the $P-\delta$ curve, it can still be matched by an equal post-fault area (A_5 in Fig. 2.4).Consequently, the critical clearing angle increases and hence the CCT of the system increases. The transient stability is increased with a new maximum angle of excursion δ_{m1}. The above method of fixing the operating condition for the generator with a certain active power output, and then examining the duration of fault that can be tolerated before instability results, is very useful to show theoretically the effect of series compensation on the transient stability limit of the system. In this method the CCT value is then the means of gauging the transient stability limit. Another means of gauging the stability limit is to determine, for a given fault type and clearing time, the maximum power output of the generator before pole slipping will occur. This latter method is a more realistic approach as normally faulted elements in a power system are removed by circuit breakers with a certain clearing time.

In its simplest form, *variable* compensating reactance control for transient stability enhancement is simply an extension of the above concept. Again consider a three phase short-circuit fault at the receiving end (point F) of Fig. 2.1. While this fault is applied, V_r is zero and from eqn. (2.2) $P_e = P_{tr} = 0$. From eqn. (2.2) it is apparent that until such time as the short circuit fault is cleared (that is, while V_r remains zero), the impedance of the line has no influence on the accelerating power of the machine for this particular fault type. However, once the fault is cleared the controllable capacitive reactance X_{CSC} can be used to influence the transmitted power P_{tr}, and hence the accelerating power imbalances in the generator as explained below.

In simple terms eqn. (2.2) shows what action can be taken in order to influence the power flow and hence the generator rotor angle swing during transient conditions following a fault. When the generator rotor has excess kinetic energy (that is, its speed deviation $\Delta\omega > 0$) *increasing* the magnitude of the controlled capacitive series reactance X_{CSC} in the transmission line acts to *increase* the power transfer out of the generator (by increasing the area A_2) hence reducing the amplitude of the excursion

of the generator rotor angle δ from δ_1 towards the critical point δ_m; conversely, when the generator rotor's kinetic energy is too low ($\Delta\omega < 0$) *reducing* the magnitude of the variable series capacitance X_{CSC} acts to decrease the power transfer out of the generator, thus reducing the amplitude of the return swing of the generator rotor angle along the path from δ_m back through δ_1 towards zero degrees.

From the above discussion it is apparent what the basic control action should be in order for a controlled compensating reactance to enhance a generator's transient stability: whenever the generator speed deviation is positive, an additional amount of compensating reactance X_{CSC} can be inserted, and subsequently removed whenever the generator speed deviation is negative [3, 5, 14]. Later in this chapter various other control algorithms that have been proposed for varying X_{CSC} are reviewed.

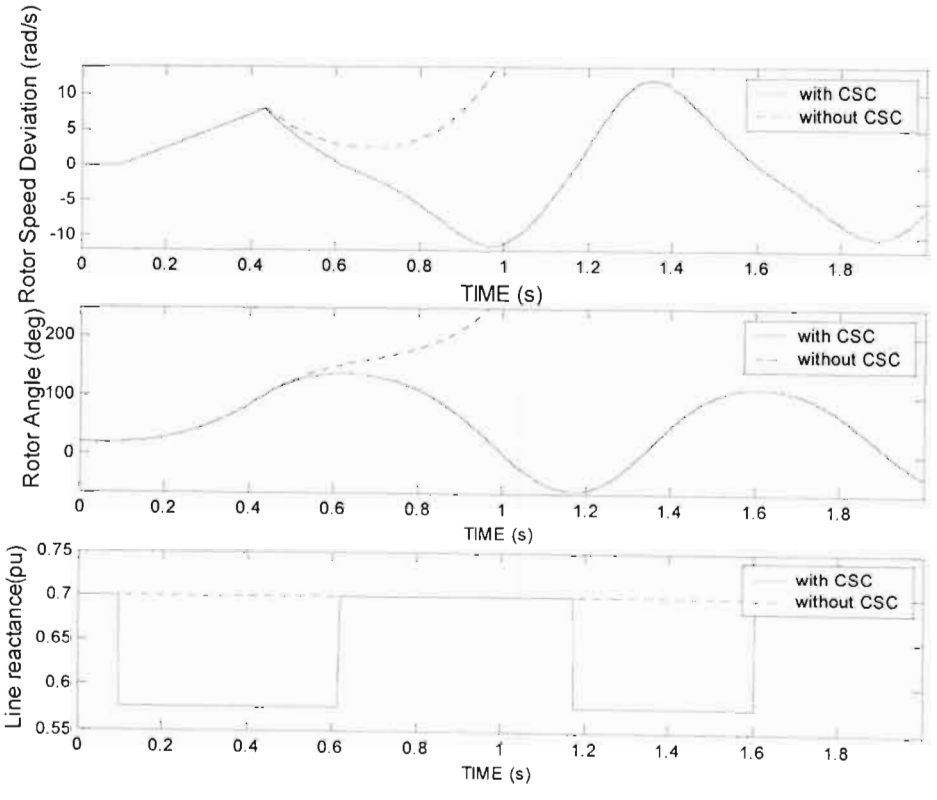

Fig. 2.5: Simulation results illustrating the improvement in the first swing behaviour of a generator which can be obtained by dynamically controlled series compensation.

Fig. 2.5 now shows an example of this basic technique, whereby the improvement in transient stability is obtained by changing X_{CSC} dynamically according to the

generator speed deviation as proposed in [3]. The dotted curves show the behaviour of an uncontrolled system following a three-phase short circuit fault; the generator rotor performs an asynchronous rotation and does not survive the first swing. The solid curves show the behaviour of the same system when a small (18% of $X_L + X'_d$) amount of controlled series capacitive reactance X_{CSC} is used. Following the disturbance, whenever the generator speed deviation $\Delta\omega$ is positive, the controlled reactance X_{CSC} is switched into the line thus reducing the total line reactance of the system; whenever the generator speed deviation is negative, the controlled reactance X_{CSC} is switched out of the line. This control action causes the generator to survive the first swing following the same disturbance in the system.

The purpose of the simple example shown in Fig. 2.5 is to explain the fundamental operating principles of variable series reactance control to enhance the transient stability of the power system which may be summarised as:

(i) to decrease the overall line impedance (by increasing the magnitude of the dynamically controlled series capacitive reactance) so as to transfer excess accelerating power out of the affected generators; and

(ii) to increase the overall line impedance (by decreasing the magnitude of the dynamically controlled series capacitive reactance) so as to minimise excess decelerating power in the affected generators.

This fundamental principle has been shown using the example of dynamic series compensation varied in a discrete fashion between maximum and minimum values, the so-called bang-bang type of control. In practice, a variety of approaches have been proposed for varying the compensating reactance and for synthesising input signals to the controller which contain information (directly or indirectly) about accelerating power. The following section reviews these proposed control approaches for enhancing the transient stability of power systems.

2.4 Transient Stability Enhancement by Variable Impedance Control in the literature

As explained earlier, the original idea for improving the transient stability of power systems using variable impedance control was based on switching the series capacitor in a capacitor bank in and out of the transmission line. Kimbark's control scheme in [4] was a simple single switching in of a series capacitor upon occurrence of a disturbance after the faulted line is switched out. The input signal to this simple control scheme was the trip signal from the protective relay system used to detect the fault and initiate the opening of the circuit breakers to isolate the faulted line. The same trip signal was also used to open the circuit breaker installed in parallel to the series capacitor to switch the latter into the line.

Wnile the control scheme in [4] proposed a single switching in of a series capacitor, Smith [13] proposed a coordinated insertion and removal during transient power swings for transient stability control. Smith showed for a two machine system, it is possible to achieve a dead-beat, non-oscillatory response during transients, with a proper choice of switching sequence of the capacitor. The switching sequences were based on the sign reversal of a decision function, which was derived from the equal area criterion and required a knowledge of the final steady states of the power system. By applying optimal control theory, the control scheme proposed the insertion of the series capacitor when the fault is detected and its removal when the time rate of change of power flow through the capacitor is zero or the rate of change of phase angle between line terminations is zero. The capacitor should then be reinserted when the kinetic energy due to speed deviations equals the amount of kinetic energy that can be removed during the remaining swing to the target state, independent of whether or not the line is restored to service. The input signals required for the controller are the machine velocity ω, transmitted power P_{tr}, a knowledge of which line has been lost as well as pre-transient information. The use of local input variables was also proposed, namely frequency deviation and the associated inertia of the group of machines most strongly affected. Despite the complexity of the control scheme involving complicated decision functions, Smith concluded that even simple switching based on angle excursions (X_{CSC} switched *in* for increasing angle

differences and X_{CSC} switched *out* for decreasing angle differences) will greatly improve the transient stability.

RamaRao and Reitan [15] used optimal theory to propose an approach with two-intermittent-duty series capacitors to improve the transient stability of a SMIB system. The proposed optimal control is bang-bang in nature and results from the application of Pontryagrin's maximum principle; a switching function is described as the product of an adjoint variable (obtained using the maximum principle) and sin δ.

The dead-beat control proposed in [13] is complicated and is likely to be impractical; indeed the author himself adopted a far simpler and more practical control approach in a subsequent paper [14]. The control law adopted in [14] was to insert and bypass a series capacitor based on the speed deviation $\Delta\omega$. The proposed bang-bang algorithm was as follows:

insert X_{CSC} if $\Delta\omega > 0$

bypass X_{CSC} if $\Delta\omega < 0$.

The only input to the controller is the speed deviation. This control scheme later appears in [3, 5] for variable impedance control of transmission line with FACTS devices. However it is the degree of compensation which is varied with respect to $\Delta\omega$ in these latter papers:

$$X_{CSC} = X_{CSC\,max} \quad \text{if } \Delta\omega > 0$$

$$X_{CSC} = X_{CSC\,min} \quad \text{if } \Delta\omega < 0.$$

In [3, 5] the author explains that the above bang-bang approach is most effective for transient stability control following large-signal disturbances. However, for damping of small-signal oscillations, particularly with a relatively large series compensator, continuous variation of the degree of compensation in sympathy with the generator angle or output power may be a better alternative.

Wang [17] considers the improvement of transient stability by employing nonlinear variable structure control (VSC) technique for series capacitor control. The VSC is based on the state – space representation of the single machine infinite bus (SMIB) system.

$$[\dot{X}] = [A][X] + [B]U \tag{2.4}$$

The series capacitance is controlled by a scalar input signal U,

$$U = \frac{1}{X'_{d\Sigma} - X_c} - \frac{1}{X'_{d\Sigma}} \tag{2.5}$$

where $X'_{d\Sigma}$ is the sum of the d-axis transient reactance, transformer reactance and the transmission line reactance and

X_C is the reactance of the series capacitor.

The components of matrices [X] [A] and [B] are fully defined in [17] by using a 4th order model of an SMIB system. By simplifying the 4th order model of the system to a 2nd order model, the following equation for U is derived by determining the sliding mode equation and using the reaching condition for sliding control,

$$U = -\frac{1}{b_3 \sin(X_1 + \delta_0) + b_4 \sin(2X_1 + 2\delta_0)} \left[b_1 + b_2 X_2 + b_3 \sin(X_1 + \delta_0) + b_4 B \sin(2X_1 + 2\delta_0) + \frac{C_1}{C_2} X_2 + e^S + kS \right]$$

where $X_1 = \delta - \delta_0$, $X_2 = \omega$,

$$b_1 = \frac{\omega_0}{H} P_m ,$$

$$b_2 = -\frac{D}{H} ,$$

$$b_3 = -\frac{\omega_0}{H} V_s E'_{q0} ,$$

$$b_4 = -\frac{1}{2} V_s^2 \left(\frac{X'_d}{X_d} - 1 \right) \frac{\omega_0}{H} ,$$

$e^S + kS$ is the controller's exponential switching surface,

D is the damping ratio,

E'_q is the transient q-axis voltage,

X_d is the d-axis reactance,

X'_d is the d-axis transient reactance,

V_s is the amplitude of the infinite bus voltage.

By constructing a Lyapunov function V, the range of values for C_1 and C_2 are determined such that the rate of change $\dot{V}$ is negative, i.e. the sliding mode equation of the system is asymptotically stable.

Kosterev [18] considers a bang-bang control switching algorithm by the use of a time-optimal switching policy for a second-order swing equation model to provide a robust transient stability controller for interconnected power systems. The scheme is based on the phase-plane trajectory of the SMIB system. Following a disturbance, as the system's trajectory leaves a defined region R_o on the phase-plane, the CSC's reactance is switched on. The CSC's reactance is then switched off when the trajectory of the system reaches a time-optimal switching line to force the system to the stable equilibrium point. The input signals to the controller are the rotor speed and the rotor angle.

Kosterev [19] considers a transient stability controller (TSC) that provides a compensation policy which fully uses the TCSC *transient* overload capabilities (10 seconds) to maximize the device effectiveness for transient stability enhancement. At the end of the control time interval, the TCSC's reactance X_{TCSC} has to be adjusted to a value within the device's *temporary* overload capabilities at the post-disturbance current loading.

A robust static controller is designed in the following form:

$$u = h(\delta - \delta_{ref}) + g(\omega) + X_{TCSC0} \tag{2.6}$$

where u is the X_{TCSC} request,

$h(\delta - \delta_{ref})$ and $g(\omega)$ are monotonic gain functions and

X_{TCSC0} is the X_{TCSC} set-point.

The compensation policy determined by the above eqn. (2.6) should use the full transient capabilities of the TCSC capacitors. The gain function g should provide positive damping. The gain function h and reference δ_{ref} are selected using results of power flow studies in such a way that for post-disturbance steady-state $(\omega = 0)$, the X_{TCSC} request determined by eqn. (2.6) stays within the temporary overload capabilities of TCSC capacitors. Such a control scheme maximizes effectiveness for the first swing stability and provides positive damping. It also minimizes the transients related to the TSC disconnection and the X_{TCSC} adjustment at the end of the control interval. Both local and remote signals are used for the controller. Phasor Measurement Units are used to obtain the synchronized phasors from which δ and Δω are estimated. Additional signals provided to the controller are the status of the circuit breakers on the intertie and the scheduled power transfer.

Padiyar [20], [21] presents the use of energy functions to devise a suitable control strategy for the controlling the TCSC for enhancing the stability of a SMIB system. The switching strategy is as follows:

(i) The TCSC switches to maximum compensation level as soon as the disturbance is detected.

(ii) The TCSC switches to minimum compensation level when $\frac{dW_{PE}}{dt} = 0$ and $\frac{d\delta}{dt} \leq 0$ where W_{PE} is the potential energy of the SMIB system given by the following equation:

$$W_{PE} = \int_{\delta_s}^{\delta} (P - P_0) d\delta \qquad (2.7)$$

where P is the power transfer, P_0 is the steady state power and δ_s is the stable equilibrium point.

(iii) The TCSC switches to maximum compensation level when $\frac{d\delta}{dt}$ is maximum provided $\left(\frac{d\delta}{dt}\right)_{\max} \geq \varepsilon$.

The paper then describes an extension of the control strategy to a multi-machine system. The change in the energy of the transmission line is given by the following equation:

$$W_{line} = \int_{t_0}^{t} (P - P_0) \frac{d\phi}{dt} dt \tag{2.8}$$

where P is the power flow in the line, P_0 is the steady state power and ϕ is the voltage angle difference between the sending bus and receiving bus.
The control strategy is analogous to the SMIB control strategy:

(i) The TCSC switches to maximum compensation level as soon as the disturbance is detected.

(ii) The TCSC switches to minimum compensation level when $\frac{dW_{line}}{dt} = 0$ and $\frac{d\phi}{dt} \leq 0$.

The input signals to the controller are the voltage angle between the sending bus and the receiving bus, and the power flow in the transmission line.

Chang [22] proposes a time optimal switching control scheme to enhance the transient stability of power systems similar to the approach proposed by Kosterev in [18], but extending the scheme to use the TCSC in inductive mode. In the proposed scheme in [22] the TCSC operates in both inductive and capacitive mode. The scheme is based on the phase-plane trajectory of the SMIB system. Following a disturbance as the system trajectory leaves a defined region R_{cs} on the phase-plane, the TCSC is switched to maximum level in the *capacitive* mode. The TCSC is then switched to maximum level in the *inductive* mode when the trajectory of the system reaches a time-optimal switching line to force the system to the stable equilibrium point. The

input signals to the controller are the rotor speed and rotor angle. A nonlinear observer is proposed to estimate the states of the SMIB system based on the line power locally measured at the position of the TCSC.

Based on the second order swing model of the SMIB system:

$$\dot{\delta} = \Omega_0 \omega \tag{2.9}$$

$$2H\dot{\omega} = P_m - \frac{V_1 V_2}{X}\sin\delta = P_m - k\sin\delta \tag{2.10}$$

where δ is the machine angle (rad);

ω is the machine speed in (p.u.);

Ω_0 is the system frequency (rad/sec);

H is the machine inertia;

P_m is the mechanical input power (p.u.);

V_1 is the generator internal voltage;

V_2 is the infinite bus voltage;

X is the reactance from the generator to the infinite bus;

and the local measurement of line power:

$$P_e = k_e \sin\delta \tag{2.11}$$

where k_e depends on V_1, V_2 and X;

the nonlinear observer can be expressed as:

$$\dot{\hat{\delta}} = \Omega_0\hat{\omega} + k_e l_1\left(\sin\delta - \sin\hat{\delta}\right) \tag{2.12}$$

$$2H\dot{\hat{\omega}} = P_m - k\sin\hat{\delta} + k_e l_2\left(\sin\delta - \sin\hat{\delta}\right) \tag{2.13}$$

where l_1 and l_2 are the observer gains.

The nonlinear observer provides better angle estimates compared to the synthesized method based on equivalent impedances [22].

Jiang [23] considers a nonlinear control scheme for the TCSC to improve the transient stability and dampen power oscillations of the power system. Based on the swing equation model, the state – space representation of the SMIB system is determined. By using feedback linearisation, the affine nonlinear equations of the state – space equations are linearised to give the control variable $\tilde{X}_{TCSC}$ as follows:

$$\tilde{X}_{TCSC} = -\frac{(X_T) + E'_q V_s \sin\delta}{P_e + H\dfrac{(\Delta\delta + \sqrt{2}\Delta\omega)}{\omega_0} + H\dfrac{\Delta\dot{\omega}}{\omega_0}} \tag{2.14}$$

The firing angle α is determined by solving the equation

$$X_{TCSC}(\alpha) = \tilde{X}_{TCSC} \tag{2.15}$$

where

$$X_{TCSC}(\alpha) = \frac{k^2}{\pi\omega C(k^2-1)}(\pi - 2\alpha + \sin 2\alpha) - \frac{1}{\omega C} - \frac{4k^2}{\pi\omega C(1-k^2)^2}\left[k\sin^2\alpha\tan k\left(\frac{\pi}{2}-\alpha\right) - \frac{\sin 2\alpha}{2}\right] \tag{2.16}$$

Thus, using the input signals ω, δ and P_e, the output firing angle α can be determined using the above equations. The estimations of these input signals adopt local measurements by using the technique developed in [24].

Wang [25] proposes a robust nonlinear co-ordinated generator excitation and TCSC controller to enhance the transient stability of power systems. Based on a dynamic equation model of the a generator and TCSC system, a direct feedback linearization (DFL) technique is employed to determine the DFL model of the generator and TCSC model described by the following equations:

$$u_f(t) = \frac{X_{ad} I_f(t)}{k_c P_e(t)}\left\{v_f(t) - T'\left[Q_e(t) + \frac{V_s^2}{X_{ds}}\right]\omega(t)\right\} - \frac{(X_d - X'_d)}{k_c} T'_{d0}\omega(t)\frac{P_e(t)}{X_{ad} I_f(t)} \tag{2.17}$$

$$u_c(t) = -K_{C1}\Delta x_{TCSC}(t) - K_{C2}\omega_L(t) \tag{2.18}$$

where: $u_f(t)$ is the input of the SCR amplifier of the generator,

$u_c(t)$ is the input signal to the TCSC regulator,

$X_{ds} = X_d + X_{transfo} + X_{Txline1} - X_{TCSC}(t)$,

and K_{C1} and K_{C2} are obtained from the solution of Ricatti equation for the robust controller.

The input signals to the generator exciter controller are $P_e(t)$, $Q_e(t)$, $\omega(t)$ and $I_f(t)$ and the input to the TCSC controller is the relative speed $\omega_L(t)$ at the TCSC busbar.

Yu [26] extends the DFL technique for transient stability control of a multi-machine interconnected power system. Via a self-correction two-machine equivalent model, the DFL technique is adopted as the control law to the following equation for the TCSC's equivalent impedance:

$$X_{TCSC} = \frac{V_1 V_2 \sin(\theta_1 - \theta_2)}{(P_{spec} - \Delta P_{spec}) + M_T K \omega_{COI}} \tag{2.19}$$

where $V_1\angle\theta_1$ is the voltage at the sending bus,

$V_2\angle\theta_2$ is the voltage at the receiving bus,

P_{spec} is the desired real-power transmitted between the interconnected systems,

ΔP_{spec} is the unmodelled real power deviation,

M_T is the resultant inertia of the two groups of machines and

ω_{COI} is the center of inertia (COI) rotor speed between the two groups of machines.

The ω_{COI} is the differential value of the COI power angle which is computed via the bus voltage. Hence, all the input signals in the above controller are available from the Phasor Measurement Units (PMUs) at the respective buses and hence can be easily applied to real-time applications.

Zhou [2], [27] proposes open-loop control similar to the control scheme in [19] such that, following a disturbance the TCSC operates at a maximum compensation level $X_{TCSCmax}$ during a certain fixed duration T_{forced}. The control is then transferred to the damping loop to suppress the subsequent power oscillations. The author subsequently in [28] proposes an alternative control scheme to the conventional control method

used in [2, 27] which proposes rapid insertion of control loops for transient stability and then for damping of low frequency oscillations. These control schemes have low adaptability and cannot correctly reflect the complexity and nonlinearity of power systems because of their linearisation at a specific operating point. Also, the operation of switching the different loops is inconvenient. In particular, the insertion time that is arbitrarily fixed has great influence on the stability control. Thus, to reflect the nonlinearity of the power system and adapt to a large range of operating states, a nonlinear adaptive control scheme based on differential geometry is proposed that can execute both transient stability control and damping control simultaneously, that doesn't need to switch different control loops and is expected to acquire good performance at any operating condition. With the theory of differential geometry applied to the power system, the nonlinear system can be linearised through coordinate transformation. The following control scheme is then derived using linear optimal technique (LQR):

$$X_{TCSC} = \frac{V_1 V_2 \sin\delta^*}{P_{L0} + \frac{H}{\omega_0}\left(K_1\Delta\delta^* + K_2\Delta\omega^*\right)} - X_L \tag{2.20}$$

where δ^* is the power angle between the sending and receiving buses, V_1 and V_2 are the magnitudes of the voltages at the sending and receiving buses, P_{L0} is the initial active power of the lines. V_1, δ^*, ω^* are derived from the local variables V_2, P_2 and Q_2 at the receiving bus where the TCSC is located.

Dai [29] focuses on the use of neural network (NN) α^{th}-order inverse control strategy in the control of the TCSC for enhancing the transient stability of power systems. The NN α^{th} - order inverse system control has a simple structure that does not require the mathematical model of the original system and can be easily implemented. By combining linear and NN α^{th} - order inverse system control to form a composite controller that uses the error between the reference value of δ and the actual δ value, the output of controller is used to control the equivalent reactance X_{TCSC}, so as to force the rotor angle of the generator δ to track the reference value. The input to the controller is the actual rotor angle and the given or targeted rotor angle of the generator.

Dai [30] later proposes an improved structure of artificial neural network (NN) α^{th}-order inverse and its application as a TCSC controller in a real power system consisting of 49 equivalent buses and 19 equivalent machines, to increase transient stability. The structure is an improved version of the TCSC's controller in [29] to further increase the adaptability of the inverse system for various loads and different operating states (double lines or single line) by adding two additional signals to the static NN to form an improved NN α^{th}-order inverse. The first signal is an invariant power P_{L0} ($P_{L0} \approx P_m$), while the other one is a state signal (1 or 0) relevant to double or single line operation mode. Thus, the input signal to the composite TCSC's controller is the error signal δ_{given}-δ_{actual}, P_{L0} and state (1 or 0) and the output of the controller is the desired TCSC reactance X_{TCSC}. The improved control scheme enhances not only the first swing stability but also damps subsequent oscillations for both SMIB systems and also in a multi-machine power system.

Mei [31] proposes a nonlinear, multi-target, H_∞ controller for the TCSC to improve the transient stability and the dynamic performance of a multimachine power system and to enhance the power transfer capability of long transmission lines. The direct feedback linearisation (DFL) technique is employed to transform the nonlinear power system model with a TCSC into a linear system. Then, by means of H_∞ theory, a multi-target controller is designed as follows:

$$X_{TCSC} = \frac{\left(\frac{\omega_{10}}{H_1} - \frac{\omega_{20}}{H_2}\right) E'_{q1} E'_{q2} \sin\delta^*}{K_1\left(\delta^* - \delta_0^*\right) + K_2\left(\omega^* - \omega_0^*\right) + \left(\frac{\omega_{10}}{H_1} P_{e10} - \frac{\omega_{20}}{H_2} P_{e20}\right)} - X_\Sigma \qquad (2.21)$$

where ω_{10} and ω_{20} are the synchronous speed of the machines in area 1 and area 2,

and $X_\Sigma = X_{Transfo1} + X_{L1} + X'_{1d} + X_{Transfo2\Sigma} + X_{L2} + X'_{2d}$.

This designed control has the property of independence of the parameters of networks since the variables in the control are locally measured.

Tan [32] presents a fuzzy control scheme for a TCSC for enhancing first-swing stability as well as providing effective damping. A Takagi – Sugeno (T-S) model of a

SMIB system containing a TCSC is proposed. The speed deviation is used as the only premise variable in the T-S fuzzy model where each rule has the following form:

IF $\Delta\omega$ is M_i

THEN $\dot{X} = A_i X + B_i \Delta u, \quad i = 1, 2, \ldots\ldots, r$

where $X = [\Delta P_e, \Delta\omega, \Delta X_{TCSC}]^T$

The fuzzy controller of the TCSC has r rules:

Controller rule i:

IF $\Delta\omega$ is M_i

THEN $\Delta u_i = F_i X, \quad i = 1, 2, \ldots\ldots, r$

F_i is obtained using linear optimal control theory. In deriving F_i, an appropriate weight matrix Q_i for the state variables and an appropriate weight coefficient R_i for the control variable is proposed. By keeping the weight coefficient R_i constant, Q_i was chosen such that when the power system is under fault conditions, Q_i is relatively large so as to increase the feedback gains: enhancing the influence of the feedback signals to provide prompt compensation and hold back the power angle's first swing. When the system is experiencing power swings, Q_i should be relatively small to decrease the feedback gains to reduce the impact of noise and provide effective damping.

The final control Δu is inferred using sum-product reasoning method:

$$\Delta u = \frac{-\sum_{i=1}^{r} w_i F_i X}{\sum_{i=1}^{r} w_i} \tag{2.22}$$

where w_i is the activating degree of the i-th rule. The overall controlled system is:

$$\dot{X} = \frac{\sum_{i=1}^{r} w_i (A_i X + B_i \Delta u)}{\sum_{i=1}^{r} w_i} \tag{2.23}$$

The only input signal used is $\Delta\omega$. Since in the proposed installation, the TCSC is far away from the generator, $\Delta\omega$ is not a local signal. A practical approach is presented to compute ΔP_e using the local voltages and currents. The $\Delta\omega$ is then computed as follows:

$$\Delta\omega = \frac{\omega_0}{H}\int(\Delta P_m - \Delta P_e - \Delta P_D)dt \tag{2.24}$$

The fuzzy controller is optimized using a gradient descent method to update truth factors of the fuzzy control rules.

Rajkumar [33] proposes a bilinear self-tuning controller of a variable series capacitor for multi-machine transient stability enhancement. When faults of concern are large and de-stabilising, it is proposed that nonlinear model-based controllers can enhance the region of stability of the power system, and return the states to their stable equilibrium. A simple predictive nonlinear self-tuning controller using local measurements of relative rotor angles is examined. The relative rotor angle measurements from N machines of interest is assumed to be available and the N bilinear sub-systems, one for each machine under study is given as follows:

$$y_{j,k} = \sum_i a_{j,i}y_{j,k-i} + \sum_i b_{i,j}u_{k-i} + \sum_i c_{j,i}y_{j,k-i}u_{k-i} \tag{2.25}$$

where $i = 1,2,.....,n$, n = order of each bilinear subsystem;

$J = 1,2,.....,N$, N = number of machines from which measurements are available;

$y_{j,k-1}$ is the latest output measurement from machine j;

u_{k-1} is the incremental series capacitor.

The unknown model parameters $a_{j,i}$, $b_{j,i}$, $c_{j,i}$ are determined using N parallel recursive least-squares identifiers. A global controller is designed by using an integrated one-step-ahead cost function J_k which includes all available subsystems.

By minimising the criterion function with respect to u_{k-1}, by setting $\frac{dJ_k}{du_{k-1}} = 0$,

$$u_{k-1} = -\frac{\sum_j \left[E_j - \tilde{y}_{j,k}\right] b_{j,0}}{\rho + \sum_j b_{j,0}^2} \tag{2.26}$$

where $E_j = \sum_{i=1}^{n} a_{j,i} y_{j,k-i} + \sum_{i=2}^{n} b_{j,i} u_{k-i} + \sum_{i=2}^{n} c_{j,i} y_{j,k-i} u_{k-i}$;

$b_{j,0} = b_{j,1} + c_{j,1} y_{j,k-1}$;

$j = 1, 2, \ldots\ldots, N$;

$\tilde{y}_{j,k}$ is the reference output which is normally fixed at the desired post-fault equilibrium value of the chosen output and

ρ is the weighing constant imposed on the controller to ensure bounded values of control.

Rajkumar [34] proposes a time-series generalised predictive control of the TCSC for enhancing the transient stability of power systems as well as damping power oscillations. The control scheme is a simplified version of eqn. (2.25) to illustrate that the bilinear control can also be used on a TCSC in a SMIB system as follows:

$$y_k = \sum_i a_i y_{k-i} + \sum_i b_i u_{k-i} + \sum_i c_i y_{j,k-i} u_{k-i} \tag{2.27}$$

The TCSC controller based on bilinear self-tuning feedback of generator armature current is compared to the feedback of generator speed. Both of those signals provides good self-tuning control.

Yu [35] proposes an improved optimal aim strategy (OAS) for the design of a TCSC controller to enhance the inter-area transient stability of interconnected power systems. A reduced order model of an interconnected multi-machine system is proposed for the controller design. The reduced order model involves only the tie line terminal bus voltage phasors which can be measured by PMUs. The OAS TCSC controller has the following structure for a SMIB system:

$$\bar{U} = x_L + x_{TCSC} = \frac{V_s V_r \sin\delta}{P_m + M(\omega - D\omega)} \tag{2.28}$$

The improved OAS TCSC controller has the following structure for a SMIB system:

$$\bar{U} = x_L + x_{TCSC} = \frac{2V_s V_r \sin\delta}{2P_m + M(K_d\omega + K_p(\delta - \bar{\delta}) + \omega - 2D\omega)} \tag{2.29}$$

The improved OAS TCSC controller as opposed the OAS controller doesn't give steady-state errors. The main reason for the existence of the steady state errors is that the OAS TCSC controller command has no feedback information of δ. The parameters K_p and K_d can be chosen by using pole placement methods or linear quadratic optimal methods.

Venkatasubramaniam [36] proposes a local voltage based TCSC discrete controller that varies the TCSC reactance for transient and damping support of an intertie. The simple discrete controller is designed to vary the TCSC capacitance proportionally to the local voltage input signal of the TCSC and uses the thermal overload capability of the TCSC as part of the control design. The TCSC consists of six 4Ω capacitor banks. The voltage based controller operates on the following scheme:

X_{TCSC} => 8 Ω (nominal value)

If the TCSC voltage > 545 kV then X_{TCSC} => -1.2 Ω (inductive as all caps are off)

If the TCSC voltage > 540 kV then X_{TCSC} => 4Ω

If the TCSC voltage < 530 kV then X_{TCSC} => minimum of 16Ω for Timer < 6 sec;

=> minimum of 12Ω for Timer > 6 sec.

When the TCSC voltage is < 530 kV, the Timer counts the TCSC operation at its 10 seconds capacitive limit for up to 6 seconds. After 6 seconds that is, when 60% of the overload capacity is reached, the TCSC is kept at 12Ω which is the 30 minute overload limit. An upper limit is included on the number of switchings over a specified time period to prevent the possibility of hunting between different controller settings.

From the review of the literature presented, it is apparent that the bang-bang approach of controlling series compensating reactance is considered by many researchers to be most suitable for enhancing transient stability following a severe disturbance in the power system. However, this approach can be detrimental to the small-signal behaviour of the system due to the so-called controller chatter problem which has been reported in [14]. Near steady state, small speed deviations can introduce unwanted operation of the controller and is a disadvantage of this control approach since it can introduce negative damping. The authors of [14] avoid this problem by including a time-based, exponentially-decreasing override function: this approach enables the full benefit of the bang-bang control when the system is far away from steady state and gradually phases out the control as the system approaches steady-state. In [38] the problem of chatter was avoided by introducing a small dead-band ε into the basic switching algorithm of bang-bang control such that the series compensating reactance is not altered for small deviations in the generator speed. The control algorithm then is as follows:

insert X_{CSC} if $\Delta\omega > \varepsilon$

bypass X_{CSC} if $\Delta\omega < -\varepsilon$.

Another approach as proposed in [3, 5] is to vary the degree of compensation in a continuous approach after the system has survived the transient condition and is approaching steady-state. Based on this idea, along with the control schemes proposed in [2, 27] the bang-bang control scheme was selected for study in this thesis as a good candidate for the transient stability control loop, and the linear proportional control scheme in [38] was selected for the damping control loop. The coordination of the two control loops is based on the number of switchings that the transient stability control loop performs prior to transferring the control to the damping loop. Two other good candidates were also identified for enhancing the transient stability of power systems as well as damping of power oscillations. Those control schemes are based on locally-measured signals synthesised for use as the controller input.

With phasor measurement units (PMUs), it is technically feasible to measure angles between remote bus voltages. PMU measurements are expensive compared to local measurements (i.e. measurements at the site of the TCSC) but they are seriously being

considered in modern power systems. However, measurement of angles between remote bus voltages is still considered more feasible than measuring remote generator quantities such as speed-deviation. The switching strategy based on energy functions [20, 21] and the nonlinear adaptive control approach [28] were both selected as they don't require the rapid insertion of control loops for transient stability and then for damping of power system oscillations. Thus, those three schemes were selected for study in this thesis. The performance of each control scheme is also compared by evaluating the amount by which it extends the transient stability margin of the power system. The performance in terms of damping of power system oscillations is also compared.

2.5 Conclusion

This chapter has presented an overview of the strategies suitable for enhancing the transient stability of power systems using controllable series compensators. The review has shown that the bang-bang control approach is considered most effective for transient stability control but that it can be inappropriate for small-signal behaviour of the system.

The review has also identified some promising approaches for control of series compensators, notably those of Padiyar in [20, 21] and Zhou [28], that can be used for both transient stability enhancement as well as the damping of small-signal oscillations, and that use locally-measured input signals to synthesise the controller input. The performance of each of these schemes is compared in subsequent chapters of the thesis.

In order to analyse these control approaches, simulation models are needed. The following chapter now presents and develops the mathematical models of the SMIB power systems used in the analyses and simulation studies of this thesis.

CHAPTER THREE

MATHEMATICAL MODELLING FOR TRANSIENT STABILITY STUDIES

3.1 Introduction

Chapter Two of this thesis has provided the background theory to enhancing transient stability of power systems using controllable series compensators. By using the equal area criterion, it has been shown how controllable series compensation can extend the transient stability limit of a power system.

Chapter Two also presented a literature survey that was carried out in order to identify the particular approaches to be considered for transient stability control. From the review, it was found that the bang-bang approach of controlling series compensating reactance is considered most effective. Two other control approaches were identified for enhancing the transient stability as well as damping small-signal oscillations. Those switching strategies use locally-measured signals to synthesise the controller inputs. In order to study the influence of the TCSC and its control on transient stability, it is necessary to have suitable simulation models of both the power system and of the TCSC itself. Although a number of studies have been conducted on the TCSC for power system stability enhancement, few have modelled the TCSC itself in detail.

This chapter presents the mathematical models that have been developed for simulation and analysis in the thesis: a simple swing-equation model and a detailed nonlinear model of a SMIB system. The latter model represents the TCSC's power electronics and internal control in some detail. The theory and operation of the TCSC is also briefly presented and the effect of short-circuit faults on the TCSC's internal control is examined. The chapter will show that a detailed representation of the TCSC is necessary to predict the performance of the device itself under transient conditions.

3.2 Swing Equation Model

As explained in the previous chapter, the dynamics of the two area power system of Fig. 2.1, can be represented by the swing equation model, eqns. (2.1-2.3). This swing equation model of the SMIB system has been developed for use in the analyses of this thesis in the Matlab programming language [8]. In this swing equation model, the TCSC itself is assumed to be an ideal capacitive reactance whose magnitude can be changed instantaneously. The full Matlab code for the swing equation model is shown in Appendix B.

The swing equation model has been used in the thesis to illustrate the fundamental concepts of variable impedance control and to test control algorithms prior to their implementation on a more detailed system model. Indeed, the swing equation model was used to generate the results shown in Fig. 2.6 of Chapter Two. Fig. 2.6 showed the response of the SMIB system with and without bang-bang control of the CSC following a 3-phase fault at the generator terminals for a particular clearing time of 440ms; the size of X_{CSC} used is 25% of the transmission line reactance X_L. The simulation results in Fig. 2.6 showed that, following the fault, while the speed deviation of the rotor is positive, the total line reactance is reduced as the CSC is inserted. This causes the rotor to survive the first swing. Hence the generator is transiently more stable. Although the swing equation model is useful for understanding the fundamental concepts behind variable impedance control, it is not detailed enough for actual transient stability studies. The following section describes a more detailed simulation model of a SMIB power system.

3.3 Detailed Nonlinear Simulation Model in PSCAD

This section describes a detailed nonlinear simulation model of the SMIB power system that has been developed in the power system simulation package PSCAD [9]. The PSCAD (Power System Computer Aided Design) program has been designed to help simulate power systems; a graphical diagram of the system is built in PSCAD using pre-coded building blocks. Fig. 3.1 shows a single line diagram of the SMIB study system modelled in PSCAD; Fig. A.2 in Appendix A shows the PSCAD model itself for this system.

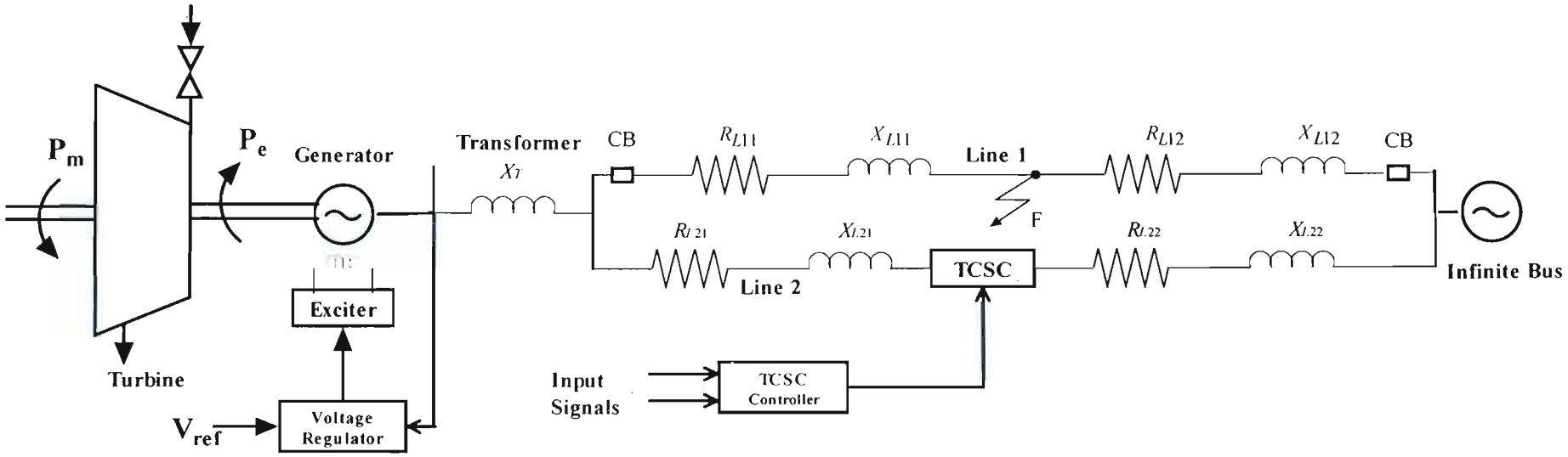

Fig. 3.1: Single-line diagram of the detailed SMIB study system model developed in PSCAD.

Fig. 3.1 shows that the model comprises at the sending end, a synchronous generator, a transformer represented by a lumped impedance, synchronised through a transmission line to an infinite bus (ideal three-phase voltage source) at the receiving end. The synchronous machine is represented using a full two-axis model which accounts for the generator electrical and mechanical dynamics and includes an automatic voltage regulator (AVR). The model has the facility of having two parallel transmission lines each of lumped impedance $R_L + jX_L$. The dynamic behaviour of the lumped-impedance transmission lines is represented in the model, that is the transmission line circuits are no longer represented simply as fundamental frequency (50Hz) impedances (as is the case in the swing-equation model) but rather by means of differential equations in the PSCAD simulation model.

In the detailed system model, a 3-phase short-circuit fault component is placed in transmission line 1 and the TCSC is placed midway in line 2 ($R_{L21} = R_{L22}$ and $X_{L21} = X_{L22}$). Once the fault has been applied in the simulation model, it is cleared by permanently opening the circuit breakers at each end in line 1. The circuit breakers are controlled by timers, allowing the duration of fault on the power system to be varied from one simulation study to another. The model also offers the facility for positioning faults at different distances along the line: this is accomplished by adjusting the ratio of the line impedances to the left ($R_{L11} + jX_{L11}$) and right ($R_{L12} + jX_{L12}$) of the fault position in line 1. Hence, the position of the fault in a particular simulation study is expressed as a percentage of the total reactance X_L of line 1 from the sending bus to the infinite bus ($X_{L11} + X_{L12} = X_L$). The effect of the turbine-governor dynamics in these studies is ignored such that the mechanical input power P_m to the turbine is assumed to be constant over the time frame of the investigation. The parameters of the SMIB system used in the thesis are based on the parameters of Machines Research Laboratory at the University of KwaZulu – Natal because of the intention within the research group to compare these studies to practical measurements in the future. The full details of these parameters can be found in Appendix A. In the PSCAD model of the power system in Fig. 3.1, the TCSC itself is modelled in detail [50]. The following section describes briefly the operating principles of the TCSC and the detailed model of the device developed in PSCAD.

3.4 The TCSC Model in PSCAD

3.4.1 Introduction

One of the first FACTS compensators to be designed and implemented was a TCSC at the Bonneville Power Administration (BPA). The basic TCSC scheme (see Fig. 3.2) was proposed in 1986 by Vithayathil and others as a method of rapid adjustment of network impedance [5]. It consists of an inductor connected in series with a pair of back-to-back thyristors, which is then connected in parallel with a fixed capacitor protected by a metal oxide varistor (MOV). The branch containing the thyristors and the inductor is known as a Thyristor Controlled Reactor (TCR). The TCR branch is the part of the TCSC that makes variable impedance control possible. The net value of the TCSC reactance X_{TCSC} can be adjusted in magnitude and can be made either inductive or capacitive depending on the value of the firing angle α in the TCR branch. In this thesis, only the net capacitive operating region of the TCSC is considered for study and analysis.

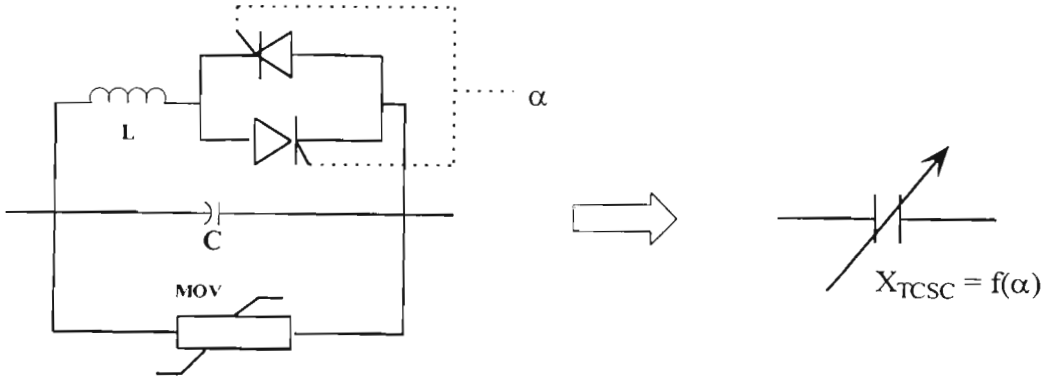

Fig. 3.2: Single-line diagram of the basic TCSC module

3.4.2 Operating Principles of a TCSC

The variable reactance of the TCSC is achieved by varying the firing angle α of the TCR. Fig. 3.3 shows the characteristic of the TCSC's net reactance as a function of the firing angle α.

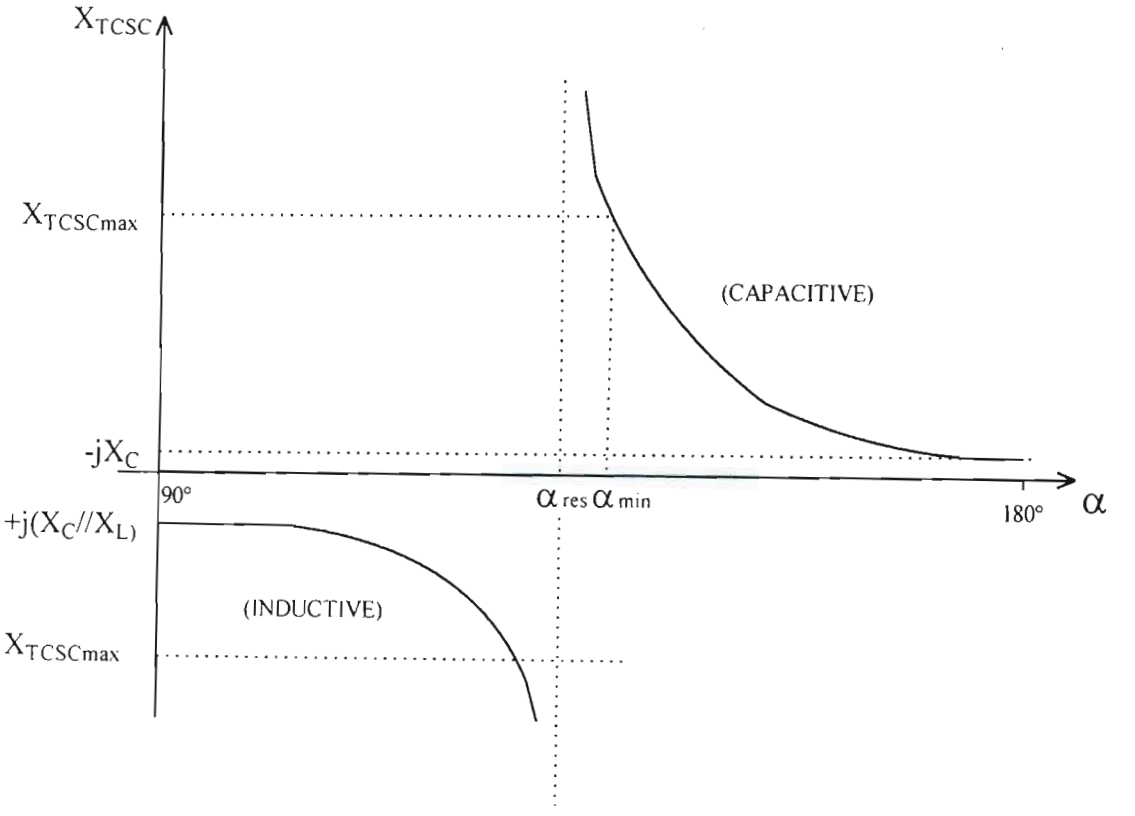

Fig. 3.3: The TCSC reactance vs firing angle

The characteristic of the TCSC reactance can be explained by considering the three basic operating modes of the TCSC [39]:

- Thyristor blocked,
- Thyristor bypassed and
- Vernier operation.

Thyristor Blocked

When the thyristor valve is not triggered and the thyristors are kept in the non-conducting state the TCSC is operating in blocking mode. The TCSC's net reactance is then simply the capacitive reactance of the internal capacitor, $-jX_C$. This mode occurs when the firing angle is 180° as shown in Fig. 3.3. In this mode the TCSC performs like a fixed series capacitor. Figure 3.4 shows that no current passes through the thyristors, hence $I_{line} = I_{TCSC}$ and $I_{TCR} \cong 0$.

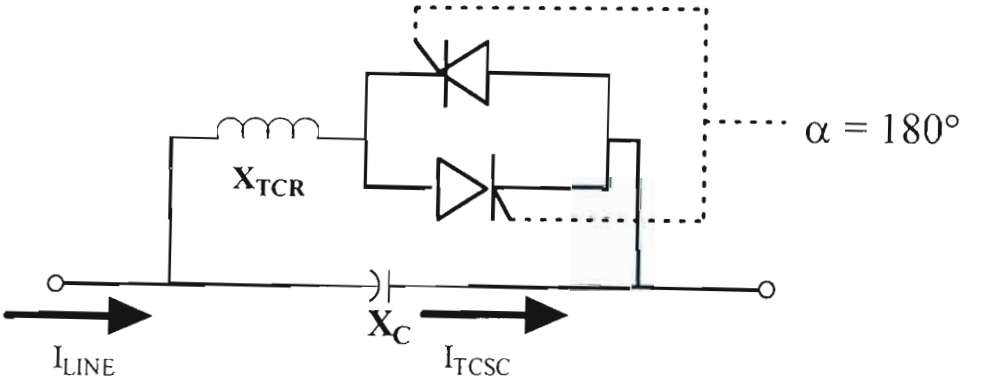

Fig. 3.4: Diagram of the TCSC operating under thyristor blocked mode

Thyristor bypassed

If the thyristor valve is triggered continuously the valve stays conducting all the time and the TCSC behaves as a parallel connection of the series capacitor bank with the TCR inductor. Hence, the net TCSC reactance is $+j(X_C // X_L)$ and this mode occurs when the firing angle is 90° as shown in Fig. 3.3. Figure 3.5 shows the flow of current under this mode. Depending on the design of the TCSC, most of the line current flows through the TCR branch and hence $I_{line} = I_{TCR}$ and $I_C \cong 0$.

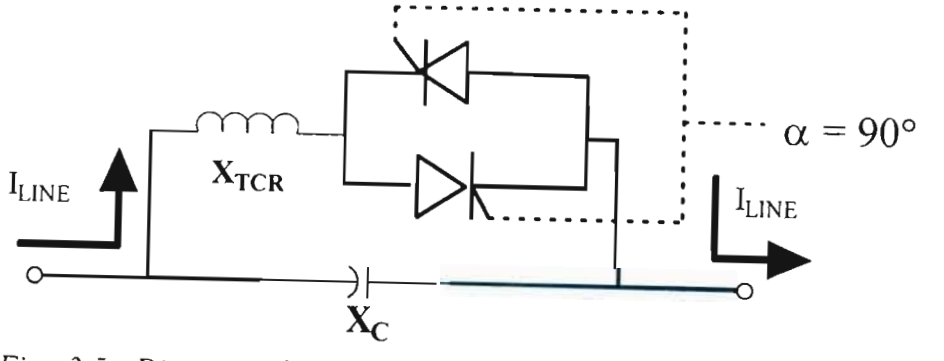

Fig. 3.5: Diagram of the TCSC operating under thyristor bypassed mode

Vernier operation

This is the most common mode of operation. If a trigger pulse is supplied to the thyristor having forward bias voltage just before the capacitor voltage reaches zero, a capacitor discharge current pulse will circulate through the parallel inductive branch. This discharge current pulse adds to the line current through the capacitor bank. The current pulse causes a component of voltage across the TCSC's capacitor that adds to the voltage caused by the line current. The capacitor peak voltage thus will be increased in proportion to the charge that passes through the TCR branch. The fundamental voltage also increases almost proportionally to that charge.

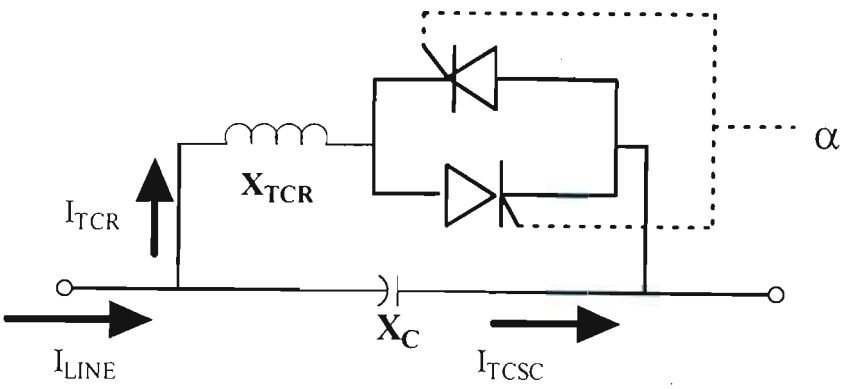

Fig. 3.6: Diagram of the TCSC operating under capacitive vernier operation mode

The vernier mode is subdivided into two categories, namely: inductive vernier mode $\left(90^\circ < \alpha < \alpha_{res}\right)$ and capacitive vernier mode $\left(\alpha_{res} < \alpha < 180^\circ\right)$ (see Fig. 3.3). Under the vernier mode, the net TCSC reactance can be calculated based on the following equation [39]:

$$X_{TCSC} = X_c\left\{1+\frac{2}{\pi}\frac{\lambda^2}{\lambda^2-1}\left[\frac{2\cos^2\beta}{\lambda^2-1}\left(\lambda\tan\lambda\beta-\tan\beta\right)-\beta-\frac{\sin 2\beta}{\beta}\right]\right\} \qquad (3.1)$$

where $\lambda = \sqrt{\frac{|X_c|}{|X_L|}}$ is a parameter of the TCSC,

$\beta = \pi - \alpha$ is the conduction angle.

Figure 3.6 shows the distribution of currents under capacitive vernier mode which is the mode considered in this thesis. The operating range of the TCSC's firing angles in the capacitive region is from 180 degrees to α_{min} (see Fig. 3.3). However, if the firing angle is any angle below α_{min}, the TCSC will be in the resonant part of the operating region. The exact resonance point of the TCSC is reached when the capacitive reactance equals the inductive reactance of the TCR, $|X_{TCR}| = |X_C|$. At this point (where $\alpha = \alpha_{res}$ in Fig. 3.3), the TCSC reactance becomes infinitely large and the voltages and currents internal to the device become prohibitively high. Hence the TCSC is always operated far from this point in practice, and the range of the firing angles is $\left[\alpha_{min}, 180^\circ\right]$. This limitation in the firing angle sets an upper bound for the value of X_{TCSC} to $X_{TCSC\,max}$ as shown in Fig. 3.3.

3.4.3 The Reactance Order

The reactance order (X_{ORDER}) (also known as the boost factor K_B) of the TCSC is defined as the ratio of its capacitive reactance to the capacitive reactance of its internal capacitor [39]:

$$X_{ORDER} = \frac{X_{TCSC}}{X_C} \tag{3.2}$$

Hence, when the TCSC is operating in blocked mode $(X_{TCSC} = X_C)$, then from eqn. (3.2) $X_{ORDER} = X_{ORDER\,min} = 1$; when the firing angle is α_{min}, $X_{TCSC} = X_{TCSC\,max}$ and hence $X_{ORDER} = X_{ORDER\,max}$. One of the limiting factors of $X_{ORDER\,max}$ is the resonant region as discussed in the previous section.

3.4.4 Operating Capability of the TCSC

The operating range of the TCSC is dictated by a number of application requirements. This section describes these limits in terms of typical capability curves for the TCSC in the capacitive vernier mode. The main circuit of the TCSC is designed for a certain

maximum X_{ORDER} available at a certain line current. When the line current exceeds a certain value, the X_{ORDER} thus must be reduced along a hyperbola giving constant capacitor voltage as shown in Fig. 3.7. An important consideration of this voltage constraint is duration. The maximum voltage constraint is typically given for three durations: continuous, 30-minutes and 10-seconds as illustrated in Fig. 3.7.

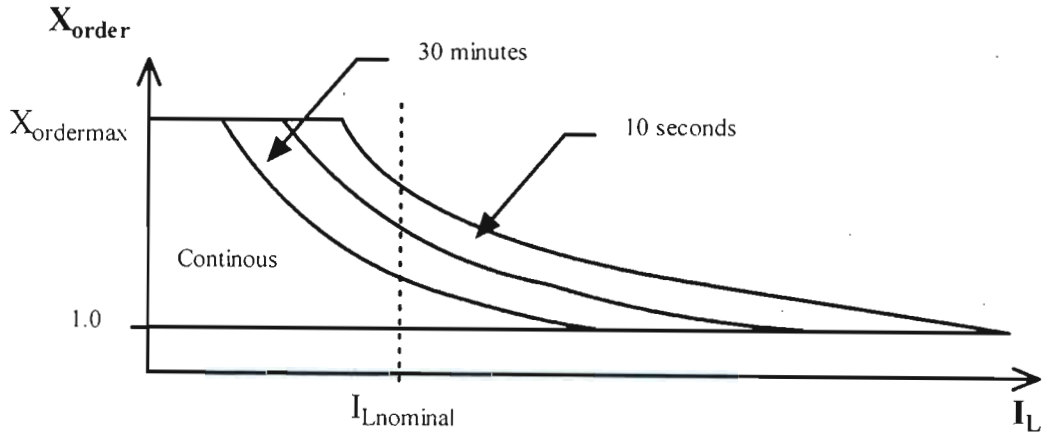

Fig. 3.7: TCSC Operating area for capacitive vernier operation mode

3.4.5 Internal control scheme of the TCSC

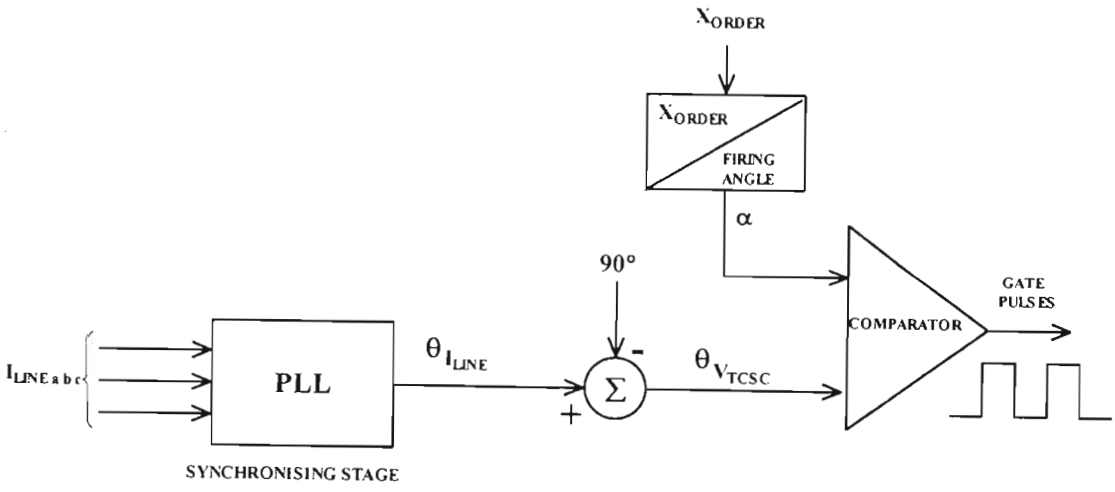

Fig. 3.8: Simplified block diagram of the TCSC's internal control scheme

Fig. 3.8 shows a simplified block diagram of the elements in a TCSC's internal control scheme. The function of the internal control scheme of the TCSC is to provide appropriate gate drive for the thyristors to produce the compensating reactance (or reactance order X_{ORDER}) defined by a reference input. The first basic function of this internal control is synchronous timing. This is done by using a three-phase PI-controlled Phase-Locked Loop (PLL) in PSCAD that tracks the positive sequence component of the line currents. Although the firing angle is measured from the zero crossing of the capacitor voltage (Fig. 3.9), the line currents are used for synchronisation. The PLL tracks the line current phasor to give $\theta_{I_{LINE}}$ and by adding an offset of -90°, the angle of the TCSC's voltage phasor $\theta_{V_{TCSC}}$ can be determined (see Fig. 3.8). This is because the capacitor voltage phasor lags the line current phasor by 90°. The main reason for using the line currents for synchronisation is because the TCSC voltage gets distorted by harmonics caused by the TCR pulses [69]. The second function of the internal control scheme is the TCSC reactance order X_{ORDER} to firing angle α conversion, which is achieved by using eqns. (3.1) and (3.2). The third function is the generation of suitable turn-on and turn-off pulses for the thyristors using the tracking angle from the PLL and the firing angle α. Here, the angle $\theta_{V_{TCSC}}$ is compared to the required firing angle α and when ($\theta_{V_{TCSC}} > \alpha$), the appropriate SCR is turned ON, else it is turned OFF. This is achieved using the interpolated gate pulse generator in PSCAD so that accurate firing angle resolution can still be obtained even if the simulation time step is not very small [9].

In order to illustrate the internal firing control of the TCSC, the TCSC model was simulated in PSCAD. Fig. 3.9 shows the time domain behaviour of the TCSC circuit variables in one phase of the TCSC circuit at a particular firing angle α = 151° ($X_{ORDER} = 1.5$). As can be observed, the thyristors are fired by the internal control of the TCSC on each half cycle of the capacitor voltage allowing the TCR current to flow. The firing angle is measured from the zero-crossing of the capacitor voltage on each half cycle. The current pulses driven along the TCR path of the TCSC circuit are alternately positive and negative as the thyristors in the anti-parallel pair become forward biased (and gated) on alternate half cycles of the capacitor voltage. The effect of these alternate current pulses is to increase the amplitude of the capacitor voltage

waveform on both cycles by alternately adding positive and negative offset voltages to the capacitor [57].

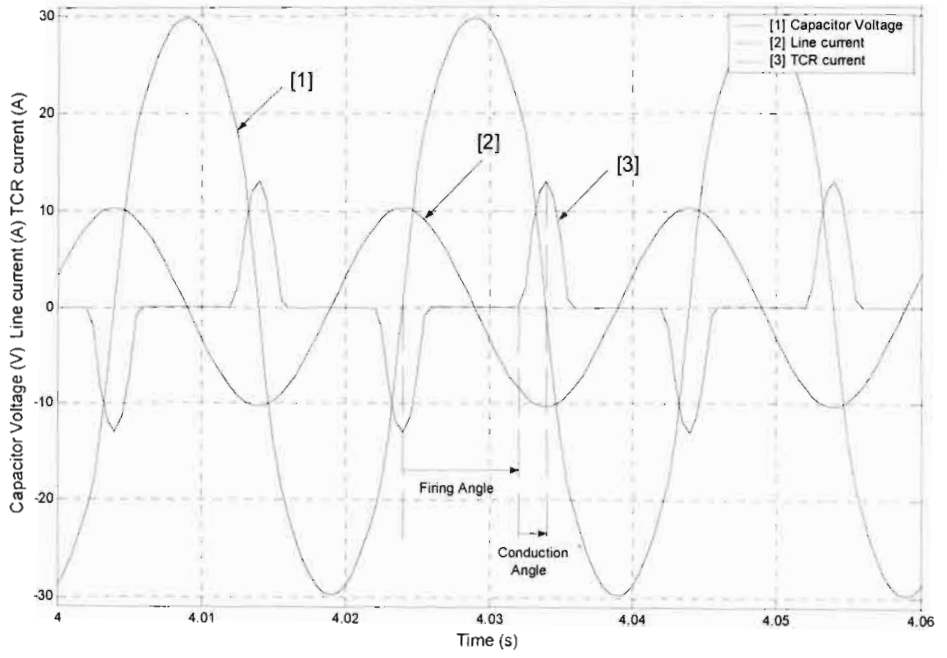

Fig. 3.9: Simulated TCR current pulses, capacitor voltage and line current with $X_{order} = 1.5$

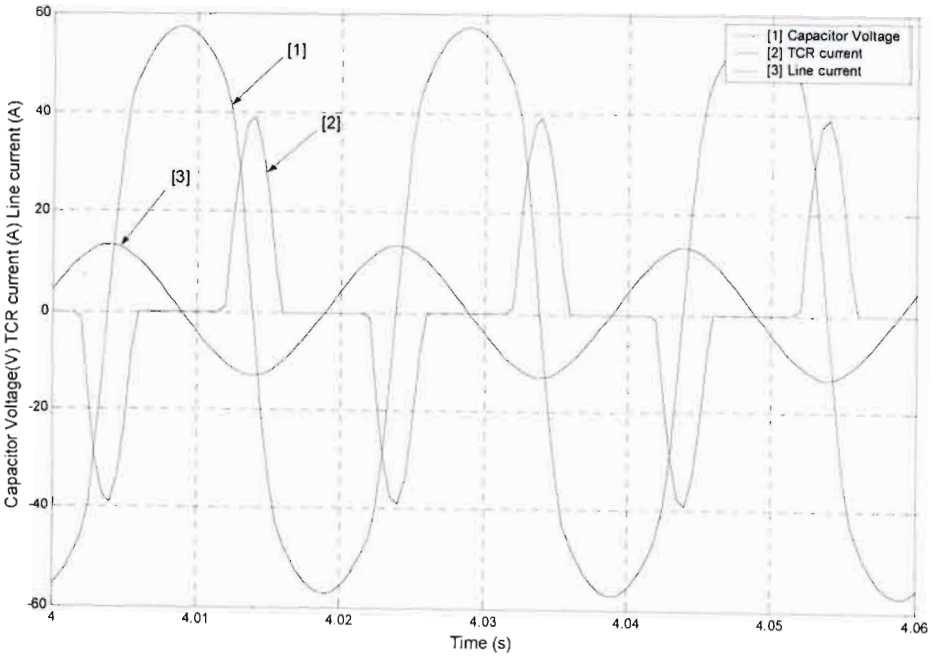

Fig. 3.10: Simulated TCR current pulses, capacitor voltage and line current with $X_{order} = 2.5$

To illustrate the effect of these current pulses, the TCSC model has been simulated again, but with a higher compensation level of $X_{ORDER} = 2.5$ that corresponds to a firing angle α = 146° as shown in Fig. 3.10. As can be observed, by comparison of Fig. 3.8 and Fig 3.9, the amplitude of the capacitor voltage is increased when the compensation level of the TCSC is increased. Thus, by gating the thyristors for a short period at the end of each half cycle, the capacitor voltage is increased for a given transmission line current passing through the TCSC as a whole, and hence the TCSC presents a capacitive reactance larger than that of its internal capacitor alone.

TCSC under transient conditions

Since the principal objective of the using the TCSC in this thesis is to improve the transient stability of power systems, the device needs to be able to operate satisfactorily under transient conditions. During the course of the research in the thesis, it was found that the TCSC's internal firing control scheme in the detailed simulation model could suffer a loss in synchronism, with resulting misfiring of the TCSC thyristors, following the application of short circuit faults in the transmission line. The reason for this misfiring of the TCSC under certain fault conditions was found to be large changes in the phase of the line currents, particularly for faults located between the TCSC and the sending end of the transmission system. Under such fault conditions, the large change in the magnitude and phase of the line currents causes a significant disturbance to the angles $\theta_{I_{LINE}}$ and $\theta_{V_{TCSC}}$ in the PLL control of Fig.3.8 causing misfiring of the thyristors. Although attempts were made to re-design the response of the PLL firing control to be immune to such disturbances, it was found that this resulted in the degradation of the performance of the firing controls under normal (un-faulted) conditions. Ultimately, it was found that the solution to the problem was to include in the detailed TCSC simulation model the Metal Oxide Varistors (MOV) that are actually included in practical TCSC installations.

To illustrate the effect of these MOVs on the internal control of the TCSC under transient conditions, the study system shown in Fig. 3.1 was simulated for a fault in transmission line 1 and the TCSC circuit variables were observed as shown in Fig

3.11 and Fig. 3.12. For the purposes of these tests, the X_{ORDER} value of the TCSC was kept constant in each case.

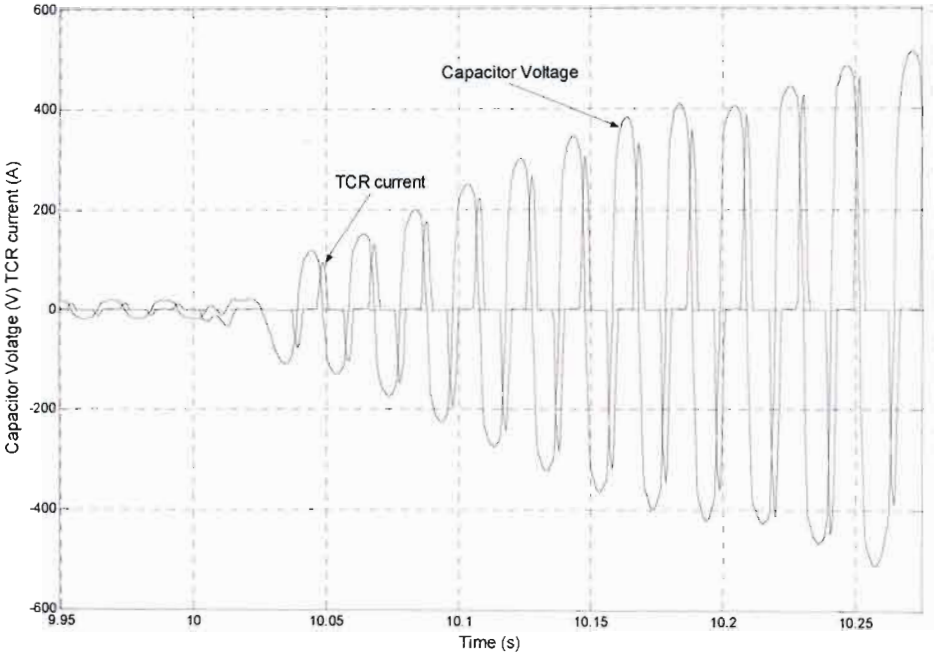

Fig. 3.11: Simulated TCR current pulses, capacitor voltage under fault condition without MOVs included

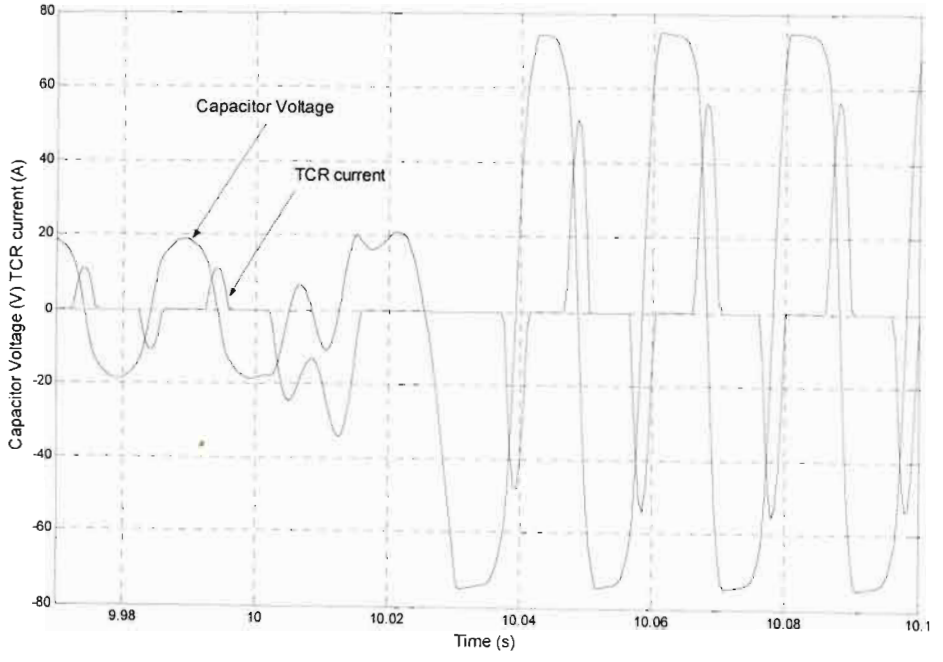

Fig. 3.12: Simulated TCR current pulses, capacitor voltage under fault condition with MOVs included

Consider first the results in Fig. 3.11, in which the TCSC model does not include MOVs. It can be observed that prior to the short circuit fault on the transmission line (at t = 10s), the magnitude of the capacitor voltage is constant, since the X_{ORDER} is kept constant. Then, at the instant the fault is applied, the PLL loses its synchronisation with the line current for two cycles. However, once this initial transient is over, although the PLL appears to have re-synchronised with the line current, the capacitor voltage V_C and TCR current I_{TCR} monotonically increase, showing that the device is not correctly following the constant X_{ORDER} reference command (due to misfiring of its thyristors). In fact, V_C and I_{TCR} attain prohibitively high values that exceed the rated values used in the practical TCSC in the research laboratory ($V_{C\ RATED}$ = 400V and $I_{TCR\ RATED}$ = 55A) [48]. This shows that without MOV protection across the capacitors of the practical laboratory TCSC, in practice, the device could be damaged under transient conditions as a result of loss of synchronism of the PLL.

The TCSC model was then simulated with MOV protection across the capacitors as shown in Fig. 3.12. It can be observed that there is still a transient disturbance to the firing controls at the moment the fault is applied. However, proper synchronisation is recovered after two cycles of V_C as the magnitudes of I_{TCR} and V_C settle to a higher, and new constant value associated with the increased line current. Note that this approximates the correct behaviour of the TCSC during the fault: the TCSC voltage is expected to be larger as a result of the larger (faulted value) of the line current flowing through the (in this case) constant reactance of the device, but it should remain constant in amplitude after the application of the fault since X_{ORDER} is being kept fixed in this test. Although the TCSC is attempting to maintain a constant compensating reactance, its capacitor voltage is actually clamped to a value of 80V which is the protective level voltage (V_{PL}) of the MOVs in this case. Thus although the actual value of the TCSC reactance during the fault will be lower than the X_{ORDER} command when the MOVs begin limiting the TCSC voltage, the TCSC does at least behave as a constant reactance as required, and there is no catastrophic loss of internal control. In practice, the duration of faults in a power system are limited to a

few cycles, and hence the ability to maintain control of the TCSC is more important than a brief deviation from the commanded X_{ORDER} value during a short circuit.

In the case of the TCSC in this thesis, the value of V_{PL} for the MOVs was designed using the relationship [70]:

$$V_{PL} = \sqrt{2} I_C X_{TCSC\max} \tag{3.3}$$

where I_C is the rated continous rms current of the TCSC's capacitors (Appendix A). It should also be pointed out that the practical ratings of the TCSC equipment in the research laboratory were deliberately over designed so as to be very conservative. Thus, while the laboratory TCSC's capacitors are rated to 400V, the value of V_{PL} = 80V is actually reasonable since at rated line current and $X_{ORDER\max}$, the laboratory TCSC's voltage is approximately 50Vrms.

3.5 Conclusion

This chapter has presented an overview of the simulation models that have been developed for analysis of the SMIB study system of this thesis. A simple swing equation model was presented to illustrate the fundamental concepts behind variable impedance control. A detailed simulation model, developed in PSCAD, that is more appropriate for actual transient stability studies, was then presented. The basic theory and operation of the TCSC and the TCSC model used in the detailed representation of the SMIB study system were also presented.

Chapter Four of the thesis now presents the results of a study of the performance of the SMIB study system when the TCSC is equipped with an external transient stability control loop.

CHAPTER FOUR

BANG – BANG CONTROL OF THE TCSC FOR POWER SYSTEM STABILITY ENHANCEMENT

4.1 Introduction

The earlier chapters of this thesis have described the basic theory of enhancing the transient stability of power systems using the TCSC. Chapter Two also presented a literature survey that was carried out in order to identify the particular approaches to be considered for transient stability control. From the review, it was found that the bang-bang approach of controlling series compensating reactance is widely considered to be the most effective. Two other control approaches were identified for enhancing the transient stability as well as damping small-signal oscillations. Those switching strategies use locally-measured signals to synthesise the controller inputs.

Chapter Three presented a simplified swing equation model that can be used to explain the fundamental concepts behind variable impedance control. Chapter Three then presented a detailed model of a SMIB power system developed in PSCAD that included a TCSC model with its internal controls. The theory and operation of the TCSC was briefly described and the internal control of the TCSC was investigated under transient conditions. Time-domain simulations have shown the influence of MOVs in the detailed TCSC simulation model on the response of the PLL under transient conditions. It was observed that MOVs across the capacitors help the PLL to keep synchronisation with the line currents and hence maintain the proper firing angle of the thyristors under fault conditions.

This chapter now presents the results of a study where a transient stability control loop is implemented around the TCSC in the detailed study system model in PSCAD. The transient stability control loop in this chapter varies the TCSC compensating reactance in a bang-bang manner following severe disturbances in the power system. The options of deactivating the transient stability control loop or transferring the impedance control of the TCSC to a damping control loop after a limited number of

TCSC switchings are also both considered. Finally, this chapter considers the effect of the size of the TCSC's controllable reactance range, as well as the severity of the fault, on the transient stability limit of the power system.

4.2 Transient Stability Control loop of the TCSC

In order to investigate the performance of the bang-bang approach for controllable series compensation that has been identified in the literature review of Chapter Two, an external transient stability control loop was implemented around the TCSC (see Fig. 4.1). The aim of this transient stability control loop is to allow dynamic variations in the TCSC's compensating reactance in response to post-fault excursions in the generator rotor speed: the output of this bang-bang controller is designed to vary the commanded value of the TCSC reactance order between an upper ceiling value $(X_{orderMAX})$ when the rotor speed deviation is positive, and a lower floor value $X_{orderMIN}$ when the rotor speed deviation is negative. In addition, it is possible to adjust the permissible amplitude of the excursion in the reactance order $(\Delta X_{order} = X_{orderMAX} - X_{orderMIN})$ at the output of this bang-bang impedance controller in the simulation model for comparative purposes. The following section shows the response of the power system when the TCSC is fitted with this external transient stability loop.

4.3 Response of the Variable Impedance Controller

The detailed study system model shown in Fig. 4.1 is simulated with a 3-phase fault on transmission line 1 for a particular clearing time of 200ms. Fig. 4.2 shows the response of the system with and without bang-bang control of the TCSC's reactance. As expected, following the fault, while speed deviation of the rotor is positive, the transient stability control loop operates the TCSC at maximum compensation level and when the speed deviation is negative, it operates the TCSC at minimum compensation level. This control action causes the rotor to survive the first swing, whereas without the bang-bang impedance control the system is transiently unstable for this fault (see dotted curves in Fig. 4.2).

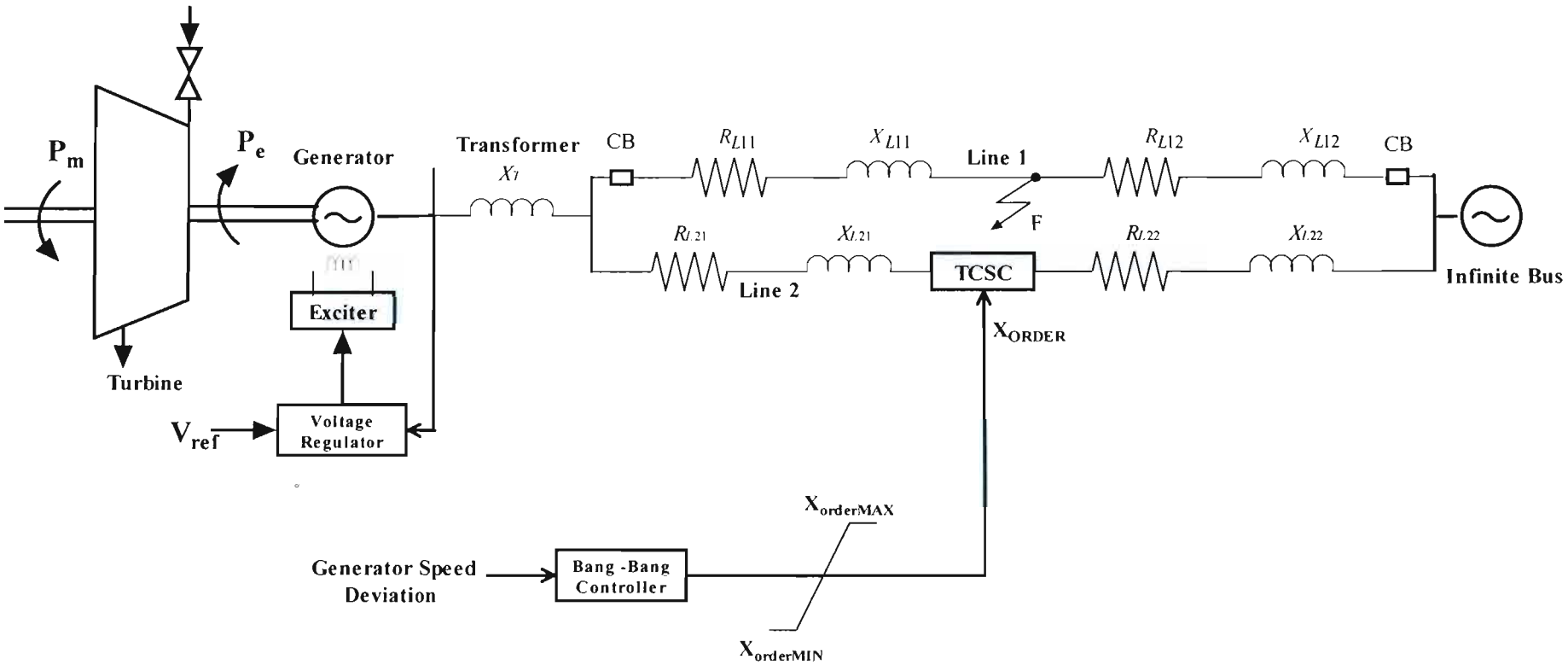

Fig. 4.1: Bang-bang TCSC controller in PSCAD.

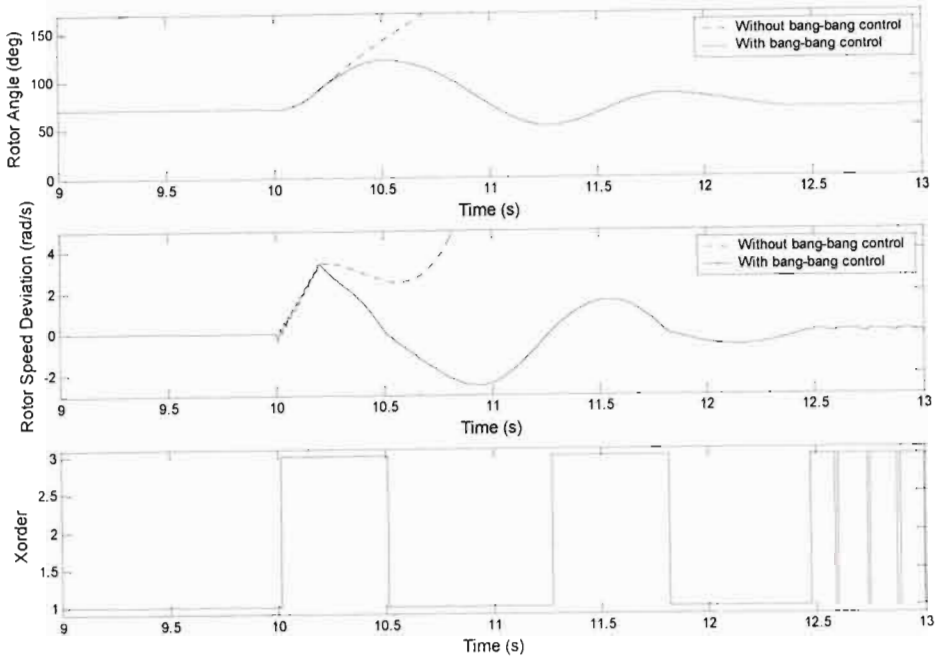

Fig. 4.2: Transient response of the rotor angle, rotor speed deviation, and TCSC X_{order} value with and without the transient stability control loop enabled.

Fig. 4.2 has shown the impact on the generator's first swing stability of switching a certain amount of TCSC reactance in bang-bang mode following a short circuit fault on transmission line 1. A range of similar simulation studies was then carried out, but each time adjusting the amplitude of excursion ΔX_{order} at the output of the bang-bang impedance controller. The base case for comparison is the SMIB system without a TCSC, and operating on the margin of stability for a particular fault with a clearing time of 200ms.

The SMIB system was then simulated at the same value of active power transfer but with *fixed* TCSC impedance (i.e. constant $X_{order} = 1.0$) for the same fault clearing time. Finally, the simulation was then repeated with the bang-bang impedance control enabled, for two different amplitudes of impedance variation $\Delta X_{order} = 1.0$ and $\Delta X_{order} = 2.0$ at the output of the controller, once again for the same fault clearing time. Fig. 4.3 compares the results of these various simulation studies.

From Fig. 4.3 it can be observed that for the same operating condition (same generator power output), the generator rotor angle has a lower value, which is further away from the margin of the first swing stability, when the fixed TCSC impedance is included in the SMIB system. Furthermore, the amplitude of the first swing in the rotor angle is reduced with the fixed-impedance TCSC, and this in itself improves the transient stability of the SMIB power system. Finally, the addition of bang-bang control of the TCSC's reactance further reduces the amplitude of the rotor angle's first swing, further enhancing the transient stability of the system. However, it is observed that increasing the amplitude of the impedance variation in bang-bang control mode from $\Delta X_{order} = 1.0$ to $\Delta X_{order} = 2.0$, results in only a small additional improvement in the amplitude of the first swing for this fault scenario.

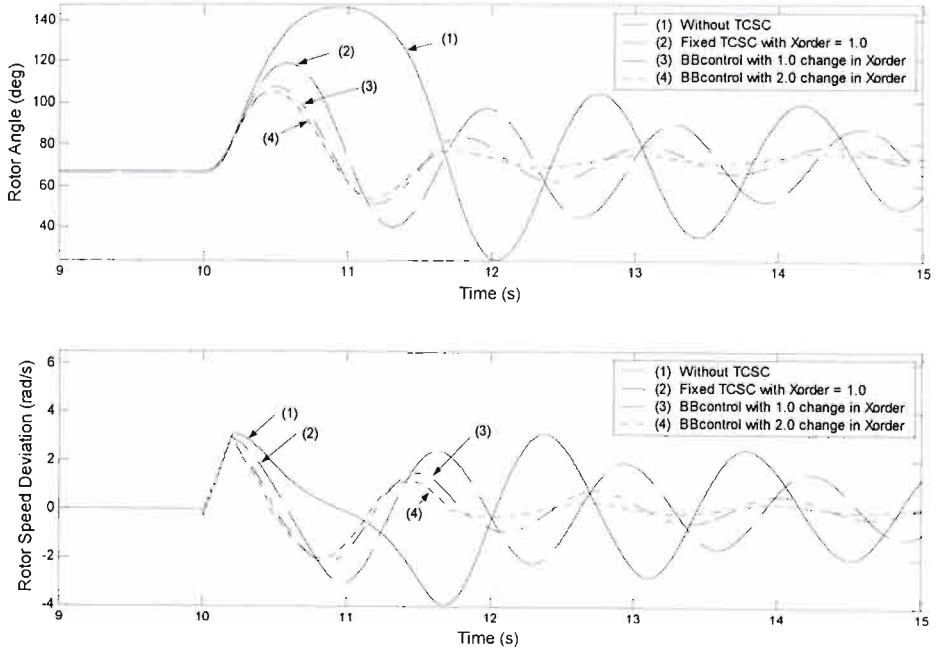

Fig. 4.3: Effect of different compensation regimes on the response of the rotor angle and rotor speed deviation.

Although the bang-bang approach to impedance control gives significant improvement in the first swing behaviour of the generator, it can however be detrimental to the small-signal behavior of the power system. For example, Fig. 4.2 shows that, instead of the generator returning to steady state after surviving the first post-fault swing, as its speed deviation $\Delta\omega$ approaches zero (after $t = 12.5$ seconds),

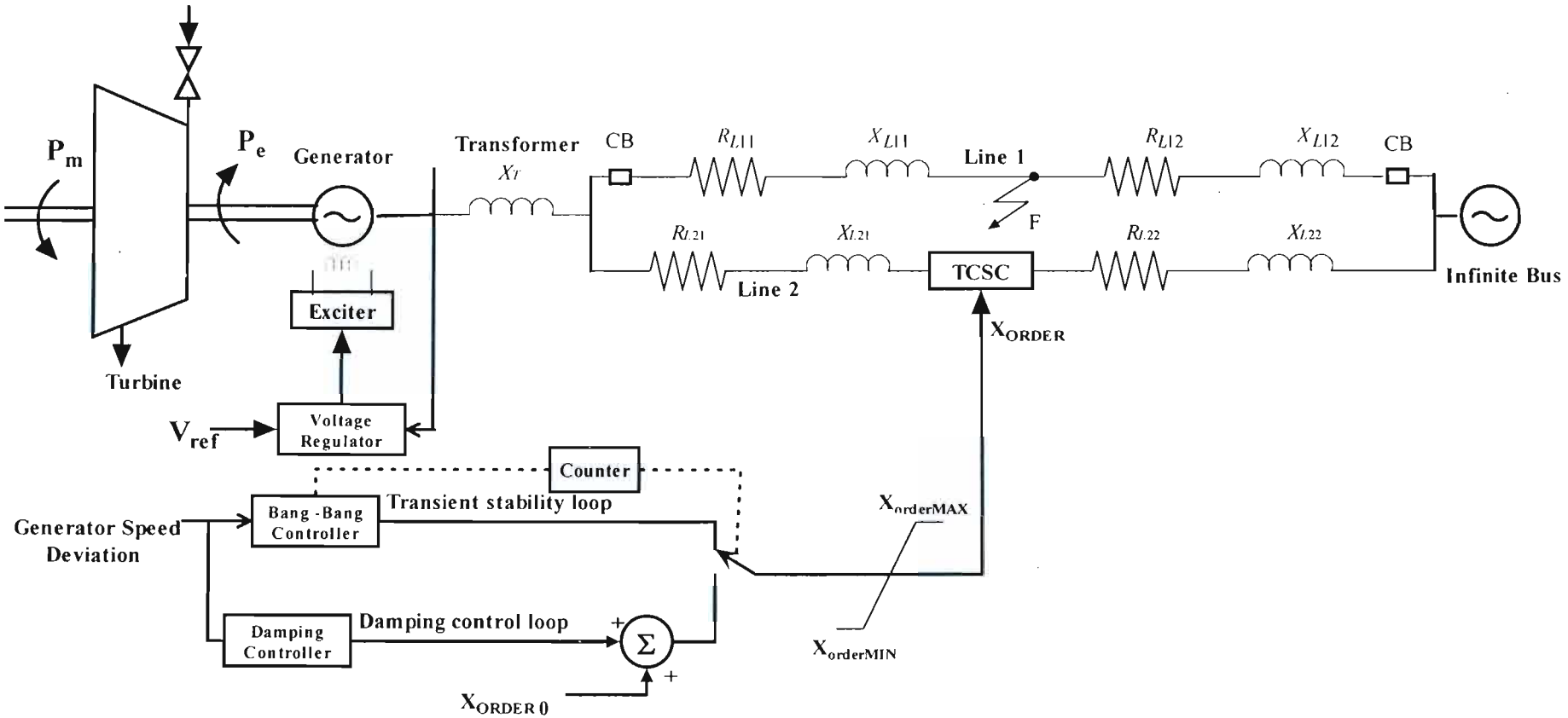

Fig. 4.4: Two-tier control of the TCSC in PSCAD.

there is successive operation of the transient stability control loop to raise and lower the TCSC's impedance. This so-called chatter of the bang-bang impedance controller has been reported in [14] and is a disadvantage of this control approach since it can introduce negative damping.

There are many ways to avoid the chatter problem as explained in the literature review. In this thesis, two such methods are considered for comparison: firstly the TCSC's impedance control is transferred from the transient stability control loop to a small-signal damping control loop after a limited number of switchings; secondly, the bang-bang control is simply deactivated after a number of switchings [2, 27]. In order to damp relatively small power oscillations with a relatively large series compensator, continuous variation of the degree of compensation is considered to be a better alternative than the bang-bang approach [3, 5]. Thus, when considering the first of these two options, a separate small-signal power oscillation damping control loop (see Fig 4.4) was implemented in such a way that the degree of compensation of the TCSC is varied linearly with respect to the generator speed deviation after the transfer of control from the transient stability loop [38]. The approach used to design the damping control loop in this thesis was based on that described in [47].

Two simulation studies were conducted to compare the performance of each of these methods of avoiding the chatter problem. In each case, the SMIB system was simulated with the same disturbance previously considered in the study of Fig. 4.2, but the number of switchings of the transient stability control loop was limited to two. In the first simulation, following these two switchings in the transient stability control loop, control was transferred to a constant $X_{order} = 1.0$ input; in the second simulation, control was transferred to the small-signal damping control loop. Fig. 4.5 compares the system response obtained in each of these two simulation studies.

It can be observed in Fig. 4.5 that in both of the schemes under comparison the chatter problem is avoided by limiting the number of switchings: after only two positive switchings of the TCSC's reactance, as the generator returns to steady state, there is no chatter of the controller in either case. However, by transferring the bang-bang impedance control to the small-signal power oscillation damping control loop, the

generator oscillations exhibit better small signal damping than when the TCSC's X_{order} is kept constant under small-signal conditions. In all the simulations shown so far, an initial value of $X_{order0} = 1.0$ has been used as the set-point for the TCSC's control loops. However, $X_{order} = 1.0$ corresponds to the lowest available value of reactance in the TCSC's control range. Consequently, when the TCSC's impedance control is transferred to the damping control loop in Fig. 4.5, the control action of this loop is limited during the negative excursions in the rotor speed deviation, at which times the output value of X_{order} remains constant at 1.0. The effect of increasing the set-point value of the controller to $X_{order0} = 2.0$ is investigated in Fig. 4.6.

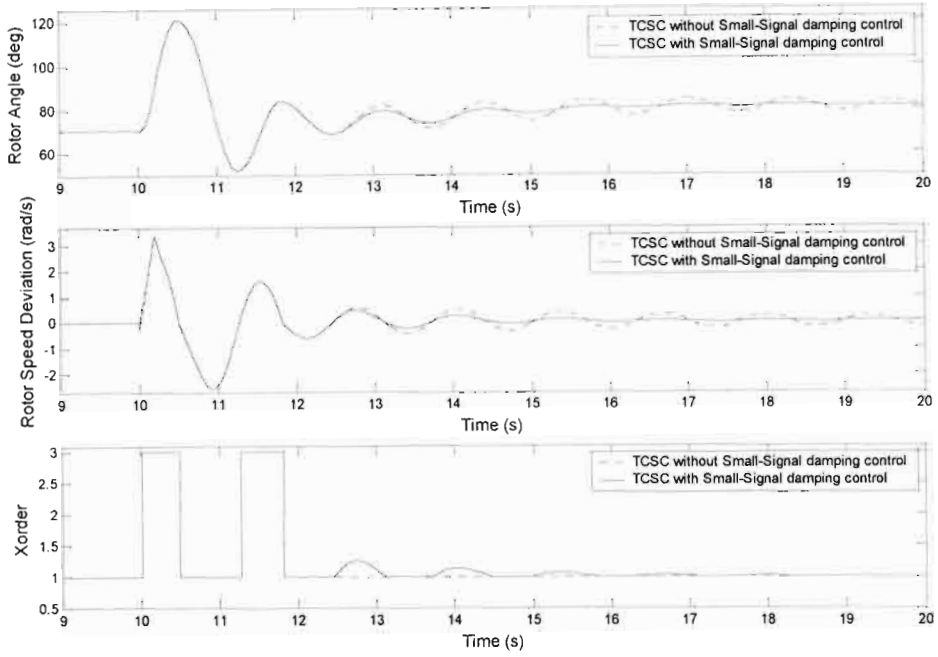

Fig. 4.5: Response of the SMIB system with limited bang-bang controller switching and with and without additional small-signal damping control.

Fig. 4.6 compares the response of the power system with a fixed TCSC reactance ($X_{order} = 2.0$) to that when there is two-tier control of the TCSC impedance around a controller set-point $X_{order0} = 2.0$. In each case the disturbance is a 3-phase fault on transmission line 1 with a particular clearing time of 200ms. As expected, following the fault, while the speed deviation is positive, the transient stability control loop operates the TCSC at its maximum compensation level, and when the speed deviation is negative, it operates the TCSC at its minimum compensation level. This control action causes the rotor to survive the first swing, whereas with a fixed TCSC of

$X_{order} = 2.0$, the system is transiently unstable for this fault (dotted curves in Fig. 4.6). The number of switchings of the transient stability control is limited to two: the control is then transferred to the small-signal power oscillation damping control loop. However, in this case, it can be observed that the control action of the damping control loop during the negative swings in the rotor speed deviation is no longer hampered. As a result of this, the post-fault generator oscillations exhibit good small signal damping.

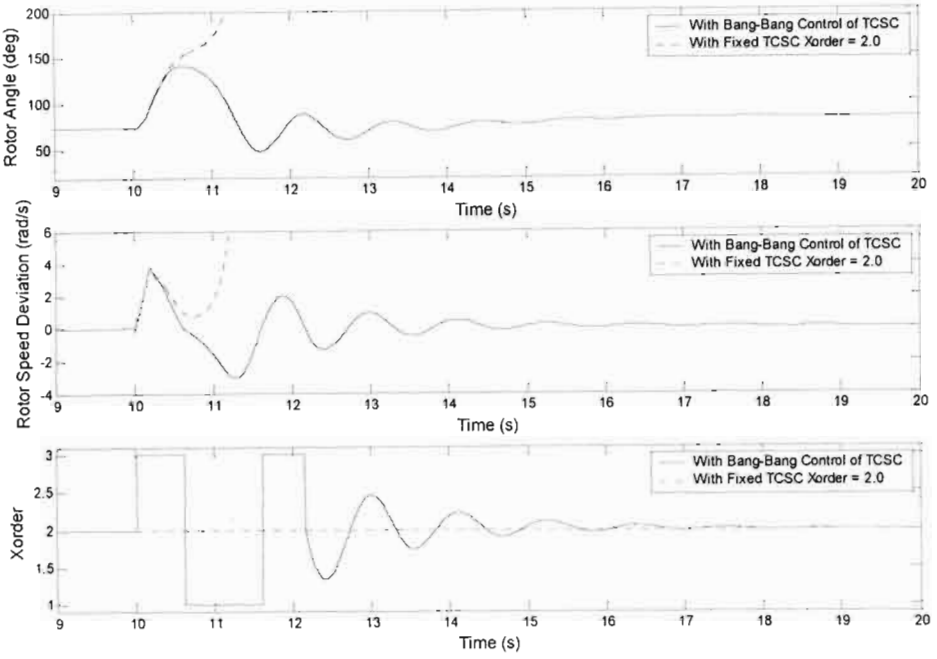

Fig. 4.6: Response of the SMIB system with the two-tier control scheme with an initial value of $X_{order0} = 2.0$.

4.4 Effect of Variable Impedance Control on the Transient Stability Limit

The previous section showed visually how a fixed series compensator improves the first swing stability of a generator, and then how this stability can be improved even further by varying the amount of compensating reactance following a disturbance. This improvement in the first swing behavior means that the generator is further from its transient stability limit, for a given fault condition. This section now presents the results of repeated simulation studies conducted in order to quantify the extent of the

improvement in the transient stability of the study system as a result of the bang-bang variable impedance control.

There are various ways to measure the improvement in transient stability of a system. One way is to set a fixed operating condition for the generator with a certain active power output, and then to examine what duration of fault can be tolerated before instability results. As discussed in Chapter Two, in this method the CCT value is then the means of gauging the transient stability limit. Another method is to apply a fault with a fixed clearing time, and then to determine the maximum power output of the generator for which transient stability can just be maintained for this particular duration of disturbance. This latter method is employed in the studies presented here. In the studies to be discussed, the transient stability of the system in Fig. 4.1 was examined for four different fault locations along line 1: 0% of X_L, 16.8% of X_L, 33.2% of X_L, and 50% of X_L. Physically, this represents positioning a 3-phase fault at different distances along the transmission line, starting at the generator bus (corresponding to 0% of X_L) and moving up to half way along the total length of the transmission line (50% of X_L). For each of these fault locations, the maximum power output of the generator at which stability is maintained, was determined for the following conditions: without compensation; with fixed compensation of different sizes; and with the bang-bang impedance control approach for different amplitudes of control range ΔX_{order}. The results obtained from these studies are summarised in Tables 4.1 – 4.8. The first set of these tables (Tables 4.1 – 4.4) compares the transient stability limits of the SMIB study system with and without a fixed-impedance TCSC compensation (i.e with no bang-bang control considered). The second set of tables (Tables 4.5 – 4.8) compare the transient stability limits without a TCSC, with fixed-impedance TCSC, and with a bang-bang controlled TCSC for different amplitudes of the variable impedance control range ΔX_{order}.

Consider firstly, Tables 4.1 – 4.4. It can be observed that the general horizontal trend in all these tables (i.e. the behaviour for a given fault clearing time) is that the transient stability limit of the SMIB system increases when the fixed TCSC is added; moreover as the size of this fixed TCSC compensation is increased, there is a further increase in the stability limit. These enhancements in the first swing stability can be

Table 4.1: Transient stability limits for a 3-phase fault at 0% of X_L with and without fixed TCSC compensation.

Fault Duration (ms)	Maximum Power Output (p.u)			
	Without TCSC	X_{ORDER} = 1.0 TCSC	X_{ORDER} = 2.0 TCSC	X_{ORDER} = 2.5 TCSC
100	0.78	0.90	1.01	1.02
200	0.67	0.75	0.81	0.82
300	0.56	0.61	0.65	0.66

Table 4.2: Transient stability limits for a 3-phase fault at 16.8% of X_L with and without fixed TCSC compensation.

Fault Duration (ms)	Maximum Power Output (p.u)			
	Without TCSC	X_{ORDER} = 1.0 TCSC	X_{ORDER} = 2.0 TCSC	X_{ORDER} = 2.5 TCSC
100	0.82	0.94	1.08	1.10
200	0.75	0.84	0.94	0.95
300	0.67	0.75	0.82	0.83

Table 4.3: Transient stability limits for a 3-phase fault at 33.2% of X_L with and without fixed TCSC compensation.

Fault Duration (ms)	Maximum Power Output (p.u)			
	Without TCSC	X_{ORDER} = 1.0 TCSC	X_{ORDER} = 2.0 TCSC	X_{ORDER} = 2.5 TCSC
100	0.83	0.96	1.11	1.13
200	0.78	0.89	1.02	1.03
300	0.72	0.81	0.92	0.93

Table 4.4: Transient stability limits for a 3-phase fault at 50% of X_L with and without fixed TCSC compensation.

Fault Duration (ms)	Maximum Power Output (p.u)			
	Without TCSC	X_{ORDER} = 1.0 TCSC	X_{ORDER} = 2.0 TCSC	X_{ORDER} = 2.5 TCSC
100	0.84	0.97	1.13	1.15
200	0.80	0.92	1.06	1.09
300	0.76	0.85	0.98	0.99

understood in terms of the equal area criterion as being due to the increase in the size of post-fault area from A2 to (A2 +A3) (see Fig. 2.3), caused by the increase in the compensation level of the TCSC. It can also be observed that the vertical trend in all the tables is that, for a given fixed value of TCSC compensation, the transient stability limit decreases as the fault duration increases. This trend can also be also understood in terms of the equal area criterion. As the fault duration is increased, the size (width) of area A1 of Fig 2.2 increases, thus reducing the transient stability limit.

It can also be observed in Tables 4.1 to 4.4 that as the 3-phase fault in line 1 is moved further away from the generator (i.e. comparing one table to another) there is a general increase in the transient stability limit of the SMIB system. For example, for the same size of fixed compensation ($X_{order} = 2.5$) and a fault duration of 100ms, the maximum power output increases from 1.02 pu with the fault at 0% of X_L to 1.15 pu with the fault at 50% of X_L. This is due to the decrease in the severity of the fault on the generator terminal voltage as the fault moves further away from the generator. The further a fault is located from the generator terminals, the less severe is the reduction caused in the generator terminal voltage during the fault; consequently, there is more power transfer from the generator during the fault and the transient stability limit is greater for faults further from the generator.

The results in Tables 4.1 – 4.4 are therefore consistent with the well-known influence of conventional fixed series capacitor compensation on the transient stability limits of a power system. However, a confirmation of these trends for fixed TCSC compensation is nevertheless important, since it serves to establish confidence in the mathematical modeling of the study system and in the approach used to gauge transient stability limits. As a result of this confirmation, the same approach can then be used with confidence to assess the impact of variable impedance control on the system stability in the remaining Tables 4.5 – 4.8.

Tables 4.5 – 4.8 show that for each fault location, and for all the fault durations considered, there is a further improvement obtained in the transient stability limit of the system when bang-bang control of the TCSC is introduced with $\Delta X_{order} = 0.5$. Furthermore, the tables show that when the size of the bang-bang controller's output

Table 4.5: Transient stability limits for a 3-phase fault at 0% of X_L without TCSC, with fixed TCSC and with bang-bang control of TCSC.

Fault Duration (ms)	Maximum Power Output (p.u)					
	Without TCSC	Fixed TCSC X_{ORDER} = 1.0	BBcontrol TCSC ΔX_{ORDER} = 0.5	BBcontrol TCSC ΔX_{ORDER} = 1.0	BBcontrol TCSC ΔX_{ORDER} = 1.5	BBcontrol TCSC ΔX_{ORDER} = 2.0
100	0.78	0.90	0.98	1.02	1.04	1.05
200	0.67	0.75	0.79	0.81	0.82	0.83
300	0.56	0.61	0.64	0.65	0.66	0.66

Table 4.6: Transient stability limits for a 3-phase fault at 16.8% of X_L without TCSC, with fixed TCSC and with bang-bang control of TCSC.

Fault Duration (ms)	Maximum Power Output (p.u)					
	Without TCSC	Fixed TCSC X_{ORDER} = 1.0	BBcontrol TCSC ΔX_{ORDER} = 0.5	BBcontrol TCSC ΔX_{ORDER} = 1.0	BBcontrol TCSC ΔX_{ORDER} = 1.5	BBcontrol TCSC ΔX_{ORDER} = 2.0
100	0.82	0.94	1.04	1.08	1.10	1.10
200	0.75	0.84	0.92	0.95	0.96	0.97
300	0.67	0.75	0.80	0.82	0.83	0.84

Table 4.7: Transient stability limits for a 3-phase fault at 33.2% of X_L without TCSC, with fixed TCSC and with bang-bang control of TCSC.

Fault Duration (ms)	Maximum Power Output (p.u)					
	Without TCSC	Fixed TCSC X_{ORDER} = 1.0	BBcontrol TCSC ΔX_{ORDER} = 0.5	BBcontrol TCSC ΔX_{ORDER} = 1.0	BBcontrol TCSC ΔX_{ORDER} = 1.5	BBcontrol TCSC ΔX_{ORDER} = 2.0
100	0.83	0.96	1.06	1.10	1.11	1.11
200	0.78	0.89	0.98	1.02	1.04	1.05
300	0.72	0.81	0.88	0.92	0.94	0.94

Table 4.8: Transient stability limits for a 3-phase fault at 50% of X_L without TCSC, with fixed TCSC and with bang-bang control of TCSC.

Fault Duration (ms)	Maximum Power Output (p.u)					
	Without TCSC	Fixed TCSC X_{ORDER} = 1.0	BBcontrol TCSC ΔX_{ORDER} = 0.5	BBcontrol TCSC ΔX_{ORDER} = 1.0	BBcontrol TCSC ΔX_{ORDER} = 1.5	BBcontrol TCSC ΔX_{ORDER} = 2.0
100	0.84	0.97	1.08	1.12	1.11	1.09
200	0.80	0.92	1.01	1.07	1.09	1.10
300	0.76	0.85	0.94	0.99	1.01	1.02

range is increased from $\Delta X_{order} = 0.5$ to $\Delta X_{order} = 1.0$, there is still further improvement obtained in the transient stability limit for all the fault durations considered. However, the tables also show, as already seen graphically in the response of the system shown in Fig. 4.3, that as the size of the output range ΔX_{order} of the bang-bang controller is increased, the marginal improvement obtained in the transient stability limit of the system decreases. Indeed, in the extreme, as the size of ΔX_{order} is gradually increased, the transient limit can even begin to decrease at high values of ΔX_{order}: Table 4.8 shows that for a 100ms fault located half way down line 1, the transient stability limit is smaller for bang-bang control with $\Delta X_{order} = 2.0$ than is the case with $\Delta X_{order} = 1.5$ (cf. two shaded cells in Table 4.8). This observation has also been reported in [14], where it was explained that there is a restriction on the amount of switched reactance that can be employed in such transient stability control schemes.

The results in Tables 4.5 – 4.8 thus suggest that, while bang-bang control of the TCSC's compensation can clearly enhance the transient stability of the system, the marginal improvement obtained in the transient stability limits is greatest for a modest amount of switched compensating reactance. Furthermore, although a case could be made for using a large amount of switched TCSC reactance in response to longer-duration faults close to the generator (for example a 300ms fault in tables 4.6 and 4.7), in other scenarios a large amount of switched reactance is likely to be counter-productive (for example a 100ms fault in Table 4.8). The results thus suggest that a 'one size fits all' bang-bang impedance controller may not be appropriate, but that a bang-bang controller with the ability to adjust its output range in response to different transient scenarios may be more suitable.

The above study was then repeated, but with the set-point value of the transient stability control increased to $X_{order0} = 2.0$. The purpose of this study is to consider the effect of adding bang-bang control to the TCSC when it is initially operating at a higher compensation level. In this study, because the maximum value of X_{order} attainable from the TCSC is $X_{order} = 3.0$, the available ΔX_{order} values that can be

Table 4.9: Transient stability limits for a 3-phase fault at 0% of X_L without TCSC, with fixed TCSC and with bang-bang control of TCSC.

Fault Duration (ms)	Maximum Power Output (p.u)			
	Without TCSC	Fixed TCSC X_{ORDER} = 2.0	BBcontrol TCSC ΔX_{ORDER} = 0.5	BBcontrol TCSC ΔX_{ORDER} = 1.0
100	0.78	1.01	1.04	1.05
200	0.67	0.81	0.82	0.83
300	0.56	0.65	0.66	0.66

Table 4.10: Transient stability limits for a 3-phase fault at 16.8% of X_L without TCSC, with fixed TCSC and with bang-bang control of TCSC.

Fault Duration (ms)	Maximum Power Output (p.u)			
	Without TCSC	Fixed TCSC X_{ORDER} = 2.0	BBcontrol TCSC ΔX_{ORDER} = 0.5	BBcontrol TCSC ΔX_{ORDER} = 1.0
100	0.82	1.08	1.11	1.13
200	0.75	0.94	0.96	0.97
300	0.67	0.82	0.83	0.84

Table 4.11: Transient stability limits for a 3-phase fault at 33.2% of X_L without TCSC, with fixed TCSC and with bang-bang control of TCSC.

Fault Duration (ms)	Maximum Power Output (p.u)			
	Without TCSC	Fixed TCSC X_{ORDER} = 2.0	BBcontrol TCSC ΔX_{ORDER} = 0.5	BBcontrol TCSC ΔX_{ORDER} = 1.0
100	0.83	1.11	1.15	1.17
200	0.78	1.02	1.03	1.05
300	0.72	0.92	0.93	0.94

Table 4.12: Transient stability limits for a 3-phase fault at 50% of X_L without TCSC, with fixed TCSC and with bang-bang control of TCSC.

Fault Duration (ms)	Maximum Power Output (p.u)			
	Without TCSC	Fixed TCSC X_{ORDER} = 2.0	BBcontrol TCSC ΔX_{ORDER} = 0.5	BBcontrol TCSC ΔX_{ORDER} = 1.0
100	0.84	1.13	1.18	1.20
200	0.80	1.06	1.09	1.10
300	0.76	0.98	1.00	1.01

considered for comparison are now limited to $\Delta X_{order} = 0.5$ and $\Delta X_{order} = 1.0$. Tables 4.9 – 4.12 summarize the results of this investigation. Tables 4.9 – 4.12 show that for each fault location, and for all the fault durations considered, there is a further improvement obtained in the transient stability limit of the system when bang-bang control of the TCSC is introduced with $\Delta X_{order} = 0.5$ to a TCSC initially operating at $X_{order0} = 2.0$. Furthermore, the tables show that when the size of the bang-bang controller's output range is increased from $\Delta X_{order} = 0.5$ to $\Delta X_{order} = 1.0$, there is still further improvement obtained in the transient stability limit for all the fault durations considered. The results in Tables 4.9 – 4.12 (when compared with those in Tables 4.5 – 4.8) illustrate that even though the usable bang-bang control range is smaller when the value of X_{order0} is increased from 1.0 to 2.0, the overall impact on the transient stability limits of the controlled-impedance TCSC is better at the larger value of X_{order0}.

As explained previously, both the fixed and variable components of the TCSC's series compensation act to improve the transient stability limits of the system. However, it must be borne in mind that the set-point value of the TCSC's reactance would not in practice be chosen only with transient stability limits in mind – the steady-state value of the TCSC's impedance would also depend on other functions of the device in the transmission network such as scheduling line power flows etc.

4.5 Conclusion

This chapter has considered the impact on the transient stability limits of the SMIB study system when the TCSC's reactance is controlled by an external transient stability control loop based on the bang-bang control approach using generator speed deviation as the input signal. Time-domain simulation results were presented to compare the transient responses of the generator rotor angle and speed deviations for both fixed and bang-bang controlled TCSC reactance. The results showed the improvement in the first swing behaviour that can be achieved by adding bang-bang control to the TCSC. Two different approaches to preventing the problem of controller chatter associated with bang-bang approach were compared in the chapter:

de-activating the transient stability control loop, and switching the TCSC's impedance control to a linear damping control loop after a few bang-bang switchings.

Finally, the quantitative improvements in the transient stability limit of the SMIB study system for different fault scenarios were presented for fixed TCSC compensation of different sizes, and for bang-bang control of TCSC reactance with different output ranges of the control. It was observed that for this study system, the use of a large bang-bang control range on the TCSC's reactance ($\Delta X_{order} = 2.0$) in response to longer-duration faults close to the generator further enhances the transient stability limits. However, for other scenarios (e.g. when the fault is half way along the transmission line), a large amount of switched reactance is likely to be counter-productive. However, the results have shown that using the TCSC at a higher initial compensation level and switching moderate values of ΔX_{order} in bang-bang mode is the better option for this study system. With this latter approach, it was found there is further enhancement in the transient stability limits, even for faults positioned half way along the transmission line.

Chapter Five of the thesis now presents the results of a study into the performance of the SMIB study system when the TCSC is equipped with a different external transient stability control loop based on energy functions.

CHAPTER FIVE

DISCRETE CONTROL OF THE TCSC BASED ON ENERGY FUNCTIONS FOR POWER SYSTEM STABILITY ENHANCEMENT

5.1 Introduction

Chapter Four has considered the impact on the transient stability limits of the SMIB study system when the TCSC's reactance is controlled by an external transient stability control loop based on the bang-bang control approach using generator speed deviation as the input signal. Time-domain simulation results were presented to compare the transient responses of the generator rotor angle and speed deviations for both fixed and bang-bang controlled TCSC reactance. The results showed the improvement in the first swing behaviour that can be achieved by adding bang-bang control to the TCSC. Two different approaches to preventing the problem of controller chatter associated with bang-bang approach were compared in the chapter: de-activating the transient stability control loop, and switching the TCSC's impedance control to a linear damping control loop after a few bang-bang switchings.

Chapter Four also presented the quantitative improvements obtained in the transient stability limit of the SMIB study system for different fault scenarios with fixed TCSC compensation of different sizes, and for bang-bang control of TCSC reactance with different output ranges of the control.

This chapter now presents the results of a study into the performance of the SMIB study system when the TCSC is equipped with a different external transient stability control loop based on energy functions. The following section presents the details of the control scheme, following which time-domain simulation results are presented to show the response of the energy function controller. Finally, the performance of this energy-function controller is then compared with that of the bang-bang control approach considered in Chapter Four, again by evaluating the extent to which this method improves the transient stability limit of the power system.

5.2 Transient Stability Control loop of the TCSC

In order to investigate the performance of the energy-function approach for controllable series compensation that has been identified in the literature review of Chapter Two, a different external transient stability control loop was implemented around the TCSC in the detailed study system (see Fig. 5.1). The aim of this transient stability control loop is to allow dynamic variations in the TCSC's compensating reactance in response to post-fault excursions in the generator rotor speed and angle: the output of this energy-function controller is designed to vary the commanded value of the TCSC reactance order between an upper ceiling value $(X_{orderMAX})$ upon the detection of a disturbance in the power system, and a lower floor value X_{order0} when $\frac{dW_{line}}{dt} = 0$ and $\frac{d\phi}{dt} \leq 0$, where the transmission line energy W_{line} is evaluated by using equ. (2.8) and ϕ is the voltage angle difference between the sending and receiving bus. The TCSC's compensating reactance can be re-boosted (to $X_{orderMAX}$) for damping power oscillations when $\frac{d\phi}{dt}$ is a maximum, provided $\left(\frac{d\phi}{dt}\right)_{MAX} \geq \varepsilon$, where ε is a small dead-band value. In addition, it is possible to adjust the permissible amplitude of the excursion in the reactance order $(\Delta X_{order} = X_{orderMAX} - X_{order0})$ at the output of this energy-function impedance controller in the simulation model for comparative purposes. The controller's input signals (transmission line energy and voltage angle difference) are synthesised from measurements in the transmission lines and from the sending and receiving end buses (Appendix C includes the details of the differential filter design for $\frac{d\phi}{dt}$). The following section shows the response of the power system when the TCSC is fitted with this external transient stability loop.

5.3 Response of the Variable Impedance Controller

The detailed study system model shown in Fig. 5.1 was simulated with a 3-phase fault applied on transmission line 1 for a particular clearing time of 200ms. Fig. 5.2 compares the response of the system with fixed-impedance TCSC and with energy-

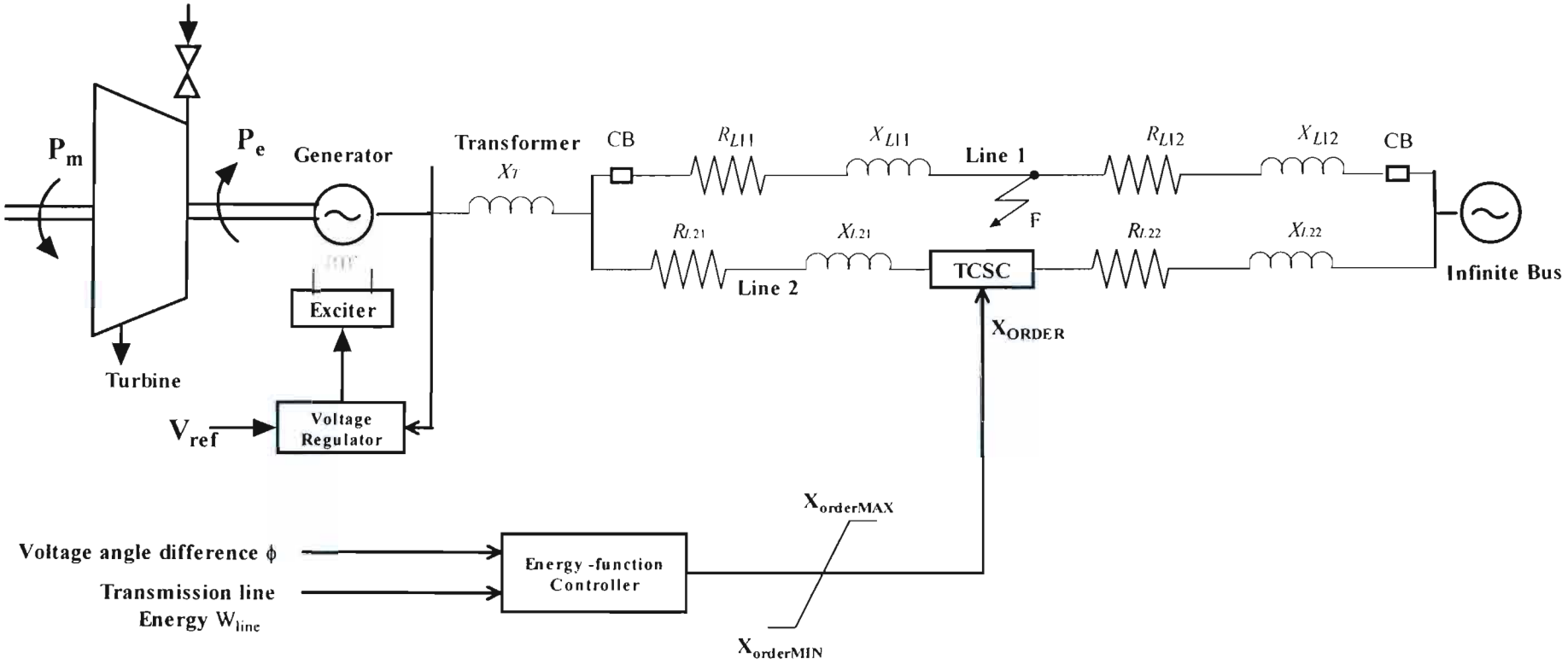

Fig. 5.1: Energy-function TCSC controller in PSCAD.

function control of the TCSC's reactance. As expected, immediately upon detection of the fault, the transient stability control loop switches the TCSC to maximum compensation level as indicated by point *a* in the results of Fig 5.2. As can also be observed, the locally synthesised signal $\frac{d\phi}{dt}$ has some noise even after filtering until some period after the fault is cleared. Consequently, the transient stability loop was designed in such a way that its subsequent switching operations following the first

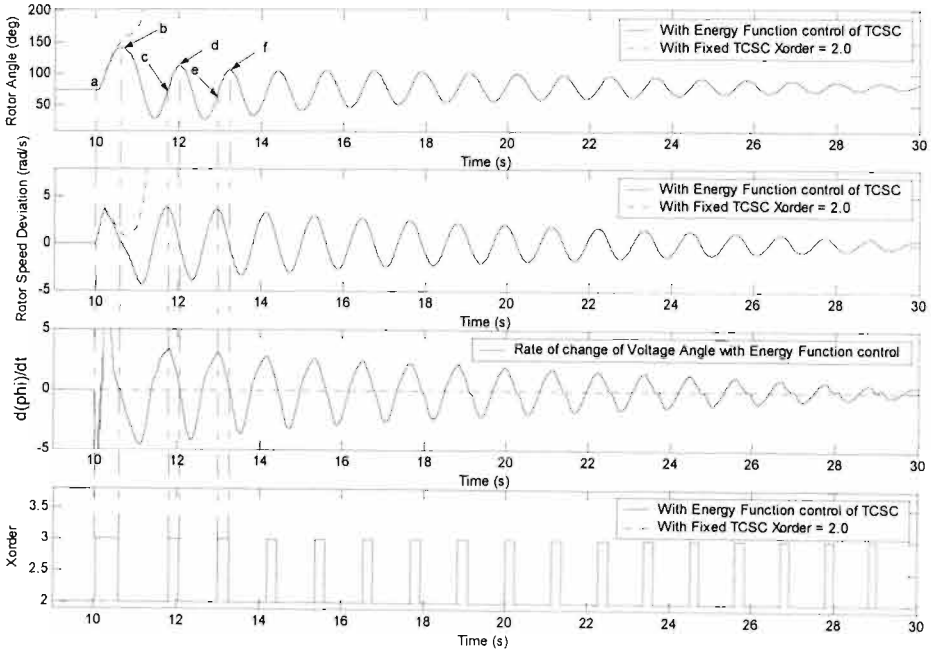

Fig. 5.2: Transient response of the rotor angle, rotor speed deviation, $\frac{d\phi}{dt}$, and TCSC X_{order} value with and without the transient stability control loop enabled.

boost to maximum TCSC compensation are enabled only once the fault has been cleared. Thus at point *b* in Fig 5.2, where $\frac{d\phi}{dt}=0$, from equ. (2.8) $\frac{dW_{line}}{dt}=(P-P_0)\frac{d\phi}{dt}$, and hence $\frac{dW_{line}}{dt}=0$ and the transient stability control loop then switches the TCSC to the lower floor value of compensation level. This control action causes the rotor to survive the first swing, whereas with the fixed-impedance TCSC the system is transiently unstable for this fault (see dotted curves in Fig. 5.2).

Following the first switching of the TCSC to the lower floor value X_{order0}, the energy-function controller once again boosts the TCSC's reactance to the maximum compensation level when $\frac{d\phi}{dt}$ reaches a maximum (point *c* in Fig. 5.2) for damping purposes. The switching algorithm then repeats itself when $\frac{d\phi}{dt} = 0$ by again operating the TCSC at its lower compensation value of X_{order0} (point *d*). This entire cycle of the control action is repeated at points *e* and *f* and so on throughout the post fault system oscillations in an attempt to enhance the damping of these oscillations. As can be observed from Fig. 5.2, once the generator has survived the first swing, there are a large number of these successive switchings of the TCSC reactance for damping purposes. The large number of these switchings was of some concern since their impact on the damping of the post fault oscillations does not appear to be significant. Thus, before investigating the impact of this energy-function controller on the transient stability limit of the study system, the following section considers the effect of de-activating the operation of the energy-function controller after a limited number of switchings.

5.4 Small-signal response of the Variable Impedance Controller

To determine the impact of the energy-function controller on small-signal damping, a further study was conducted to compare the response of the system with and without multiple post-fault switchings of the TCSC. The study system of Fig. 5.1 was simulated for the same disturbance as that in the simulation results of Fig. 5.2, but with post-disturbance TCSC switchings limited to two.

Fig. 5.3 compares the behaviour of the system with and without limits placed on the number of TCSC switchings. It can be observed that without multiple post fault switchings of the TCSC, the generator oscillations exhibit poor damping (see dotted curves). However, it can be observed that with multiple post-fault switchings, (as already seen in Fig. 5.2) there is some improvement in damping but the damping nevertheless remains poor.

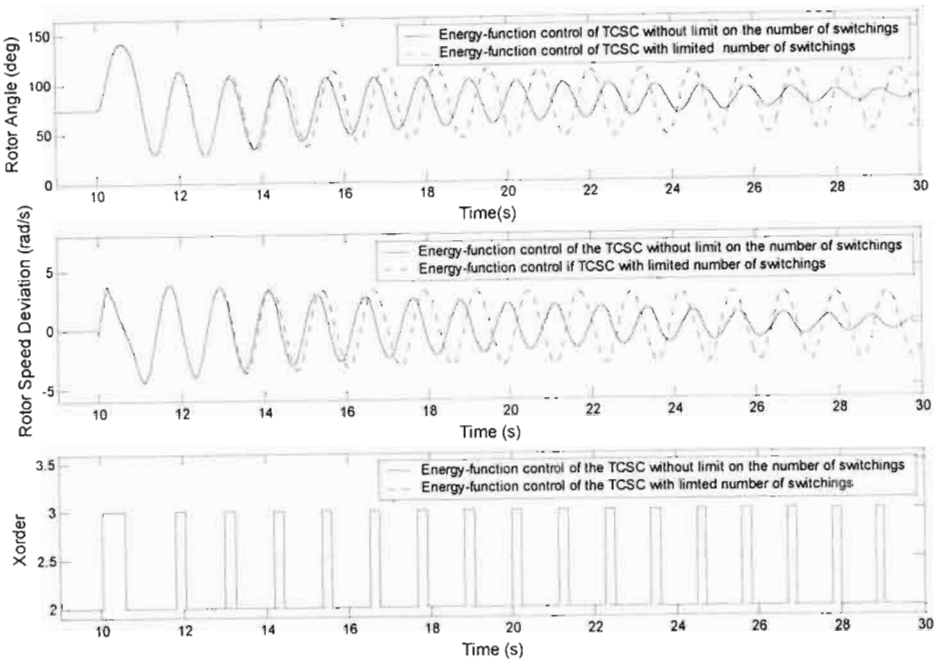

Fig. 5.3: Transient response of the rotor angle, rotor speed deviation, and TCSC X_{order} value with and without limiting the number of switchings of the energy-function transient stability control loop.

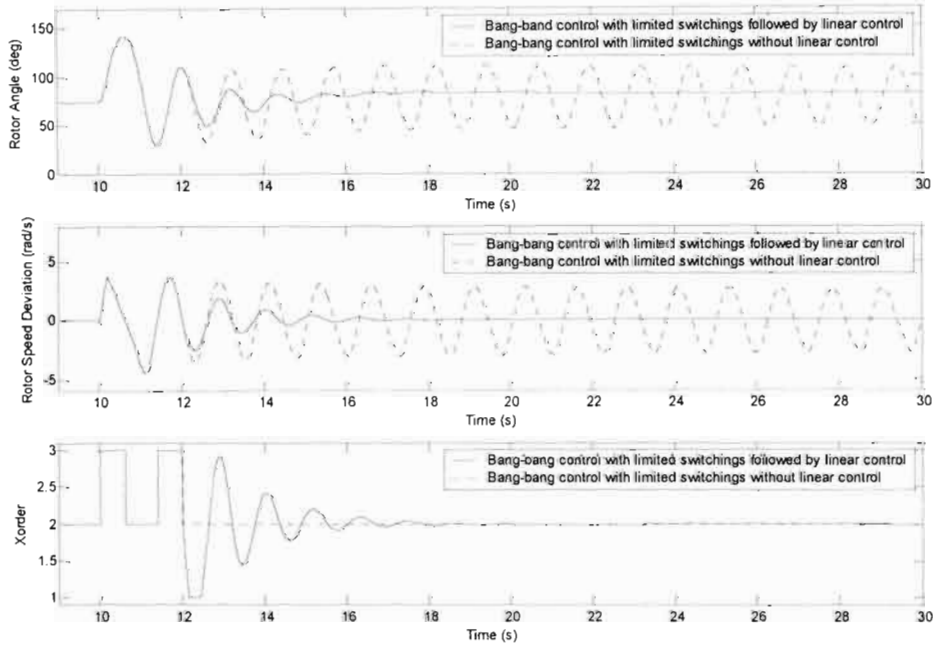

Fig. 5.4: Transient response of the rotor angle, rotor speed deviation, and TCSC X_{order} value for speed deviation based bang-bang control with and without the small-signal damping control.

In order to further assess the impact of the energy-function control approach on the small-signal response, a direct comparison to the speed-deviation based bang-bang controller of Chapter Four was conducted. The study system of Fig 4.1 was simulated with the same disturbance and operating point as that considered in the simulation results in Fig 5.3. In order to match the upper and lower values of X_{TCSC} that are commanded by the controller in the results of Fig 5.3, for the comparative speed-deviation based bang-bang controller study in Fig. 5.4, the TCSC was also set to operate at an initial value $X_{order0} = 2.0$ and a reactance order output control range of $\Delta X_{order} = 1.0$ was imposed. Fig. 5.4 compares the behaviour of the system with the same limits placed on the number of switchings of the TCSC (two), after which the TCSC X_{order} was either kept constant or transferred to a small-signal damping control loop. It can be observed that by keeping the TCSC X_{order} constant after two positive switchings, the generator oscillations also exhibit poor damping (see dotted curves). However when the control is transferred to the linear damping control loop, a significant amount of damping can be observed in the system oscillations.

When the simulation results of Fig. 5.3 are compared to those in Fig. 5.4, it can be observed that the energy-function control approach (with unlimited switchings) adds some damping to the system but not as much as the combination of speed-deviation based bang-bang control and linear damping control used in Chapter Four. As pointed out in the literature review of Chapter Two [5, 38], linear control based on speed-deviation is accepted as the most efficient method for small-signal damping control using a TCSC. However, although the damping performance with the energy-function control approach is clearly not as good as that of speed-deviation linear control, it does not require measurement and communication of the speed signal from a remote generator to the location of the TCSC. However, the energy-function method does require careful design of its filters, both the input filters used to reduce measurement noise and the filtered differentiator stage used to synthesise the signal $\frac{d\phi}{dt}$. Nevertheless, the principles of filter design for such signals in FACTS-based power oscillation damping schemes are well understood [73], and the need for such filtering is not a serious drawback for this approach.

5.5 Effect of the Variable Impedance Controller on the Transient Stability Limit

The previous section showed visually how energy-function control of the TCSC's compensating reactance improves the first swing stability of a generator following a fault in the power system. This improvement in the first swing behavior means that the generator is further from its transient stability limit, for a given fault condition. This section now presents the results of repeated simulation studies conducted in order to quantify the extent of the improvement in the transient stability of the study system as a result of the energy-function variable impedance control.

A similar study to that in Chapter Four was conducted, where the transient stability of the system in Fig. 5.1 was examined for four different fault iocations along line 1: 0% of X_L, 16.8% of X_L, 33.2% of X_L, and 50% of X_L. For each of these fault locations, the maximum power output of the generator for which stability is maintained was determined for the following conditions: without compensation; with fixed compensation; and with the energy-function impedance control approach for different amplitudes of control range ΔX_{order}. Based on the findings of Chapter Four, only smaller values of ΔX_{order} were considered for analysis in the case of the energy-function controller. The results obtained from these studies are summarised in Tables 5.1 – 5.4 to compare the transient stability limits of the SMIB study system.

It can be observed that the general horizontal trend in all these tables (i.e. the behaviour for a given fault clearing time) is that the transient stability limit of the SMIB system increases when the fixed TCSC is added. This increase in the transient stability limit can be understood in terms of the equal area criterion as previously discussed in Chapter Four. It can also be observed that the vertical trend in all the tables is that, for a given fixed value of TCSC compensation, the transient stability limit decreases as the fault duration increases. This trend can also be also understood in terms of the equal area criterion. As the fault duration is increased, the size (width) of area A1 of Fig 2.2 increases, thus reducing the transient stability limit.

Table 5.1: Transient stability limits for a 3-phase fault at 0% of X_L without TCSC, with fixed TCSC and with energy-function control of TCSC.

Fault Duration (ms)	Maximum Power Output (p.u)			
	Without TCSC	Fixed TCSC X_{ORDER} = 2.0	EFcontrol TCSC ΔX_{ORDER} = 0.5	EFcontrol TCSC ΔX_{ORDER} = 1.0
100	0.78	1.01	1.04	1.05
200	0.67	0.81	0.82	0.83
300	0.56	0.65	0.66	0.66

Table 5.2: Transient stability limits for a 3-phase fault at 16.8% of X_L without TCSC, with fixed TCSC and with energy-function control of TCSC.

Fault Duration (ms)	Maximum Power Output (p.u)			
	Without TCSC	Fixed TCSC X_{ORDER} = 2.0	EFcontrol TCSC ΔX_{ORDER} = 0.5	EFcontrol TCSC ΔX_{ORDER} = 1.0
100	0.82	1.08	1.11	1.13
200	0.75	0.94	0.96	0.97
300	0.67	0.82	0.83	0.84

Table 5.3: Transient stability limits for a 3-phase fault at 33.2% of X_L without TCSC, with fixed TCSC and with energy-function control of TCSC.

Fault Duration (ms)	Maximum Power Output (p.u)			
	Without TCSC	Fixed TCSC X_{ORDER} = 2.0	EFcontrol TCSC ΔX_{ORDER} = 0.5	EFcontrol TCSC ΔX_{ORDER} = 1.0
100	0.83	1.11	1.15	1.17
200	0.78	1.02	1.03	1.04
300	0.72	0.92	0.93	0.94

Table 5.4: Transient stability limits for a 3-phase fault at 50% of X_L without TCSC, with fixed TCSC and with energy-function control of TCSC.

Fault Duration (ms)	Maximum Power Output (p.u)			
	Without TCSC	Fixed TCSC X_{ORDER} = 2.0	EFcontrol TCSC ΔX_{ORDER} = 0.5	EFcontrol TCSC ΔX_{ORDER} = 1.0
100	0.84	1.13	1.17	1.20
200	0.80	1.06	1.09	1.10
300	0.76	0.98	1.00	1.01

Tables 5.1 – 5.4 show that for each fault location, and for all the fault durations considered, there is a further improvement obtained in the transient stability limit of the system when energy-function control of the TCSC is introduced with a controller output range of $\Delta X_{order} = 0.5$. Furthermore, the tables show that when the size of the energy-function controller's output range is increased from $\Delta X_{order} = 0.5$ to $\Delta X_{order} = 1.0$, there is still further improvement obtained in the transient stability limit for all the fault durations considered.

5.6 Comparison with speed-deviation based bang-bang control

Tables 4.9 – 4.12 in Chapter Four showed the impact on the transient stability limits of the study system of adding speed-deviation based bang-bang impedance control with different sizes of control range ΔX_{order}, to a TCSC that is initially operating at $X_{order0} = 2.0$. Similarly, Tables 5.1 – 5.4 in the previous section have shown the effect on the transient stability limits of this system of adding energy-function variable impedance control with different sizes of ΔX_{order}, to a TCSC that is initially operating at $X_{order0} = 2.0$. When these two sets of Tables (4.9 – 4.12) and (5.1 – 5.4) are compared, it can be observed that at the same fault location and for the same fault duration, the energy-function controller that uses locally synthesised input signals can extend the transient stability limit of this study system by the same extent when the same range of variable reactance ΔX_{order} is used. For example, in Table 4.9, when bang-bang control with $\Delta X_{order} = 0.5$ was added to the system having a 100ms fault positioned at 0% of X_L, the maximum power output of the generator increased from 1.01 pu to 1.04 pu. Similarly, it is observed from Table 5.1, that the same degree of improvement in the transient stability limit is achieved when energy-function control with $\Delta X_{order} = 0.5$ was added to the TCSC. Similar comparative performances can be observed in the other tables which represent faults that are positioned at distances further away from the generator along the transmission line. Moreover, in the energy-function scheme, by using a moderate amount of switched TCSC reactance ($\Delta X_{order} = 0.5$ and $\Delta X_{order} = 1.0$) on a TCSC that is initially operating at a

compensation level of $X_{order0} = 2.0$, it was again found that transient stability limits were extended even for faults positioned half way along the transmission line. Thus, the findings with respect to the amount of switched TCSC reactance that is recommended for transient stability enhancement are also the same for both speed-deviation and energy-function based bang-bang control.

5.7 Conclusion

This chapter has considered the impact on the transient stability limits of the SMIB study system when the TCSC's reactance is controlled by an external transient stability control loop based on the energy-function control approach using locally synthesised input signals. Time-domain simulation results were presented to compare the transient responses of the generator rotor angle and speed deviations for both fixed and energy-function controlled TCSC reactance. The results showed the improvement in the first swing behaviour that can be achieved by adding energy-function control to the TCSC.

The small-signal response of the system with this energy-function controller was also compared to the two-tier method of control in Chapter Four that was based on generator speed deviation. It was found that the local energy-function control scheme does have a small beneficial impact on the small signal damping, but that it requires a significant number of post-fault TCSC switching operations. Although significantly better performance is achieved with speed-deviation based linear damping control of the TCSC, the cost of transmitting the required input signal to the location of the TCSC may be of concern.

The quantitative improvements in the transient stability limit of the SMIB study system for different fault scenarios were presented for fixed TCSC compensation, and for energy-function control of TCSC reactance with different output ranges of the control. It was observed that for this study system, adding energy-function control to the TCSC's reactance further enhances the transient stability limits. The results have also shown that using the TCSC at a relatively high initial compensation level and

switching moderate values of ΔX_{order} is the also a suitable option in the case of this type of controller. With this latter approach, it was found there is further enhancement in the transient stability limits, even for faults positioned half way along transmission line.

Similar degrees of improvement in the transient stability limits with this energy-function controller were found when comparing the results in this chapter with those obtained from the speed-deviation based bang-bang control in Chapter Four. Thus, the energy-function control can be considered as an alternative approach in cases where it is difficult to get input signals such as generator speed deviation at the location of the TCSC.

Chapter Six of the thesis now presents the results of a study into the performance of the SMIB study system when the TCSC is equipped with a different external transient stability control loop based on a nonlinear adaptive control scheme.

CHAPTER SIX

NONLINEAR ADAPTIVE CONTROL OF THE TCSC FOR POWER SYSTEM STABILITY ENHANCEMENT

6.1 Introduction

Chapter Four has considered the impact on the transient stability limits of the SMIB study system when the TCSC's reactance is controlled by an external transient stability control loop based on the bang-bang control approach using generator speed deviation as the input signal. Time-domain simulation results were presented to compare the transient responses of the generator rotor angle and speed deviations for both fixed and bang-bang controlled TCSC reactance. The results showed the improvement in the first swing behaviour that can be achieved by adding bang-bang control to the TCSC. Chapter Five has considered the impact on the transient stability limits of the SMIB study system when the TCSC's reactance is controlled by an external transient stability control loop based on the energy-function control approach using locally synthesised input signals. Time-domain simulation results were presented to compare the transient responses of the generator rotor angle and speed deviations for both fixed and energy-function controlled TCSC reactance. The results showed the improvement in the first swing behaviour that can be achieved by adding energy-function control to the TCSC. The results in Chapter Four and Five also showed that either of the control schemes could improve the damping of power oscillations, although the scheme in Chapter Four has a more beneficial impact in this regard.

This chapter now looks at a single control method that combines functions of transient and small-signal stability controls into a single, nonlinear adaptive control scheme. This control approach, as outlined in the literature review, is also based on locally synthesised input signals and does not require rapid insertion of distinct control loops

for transient stability and then for damping of power system oscillations. The following section presents the details of the control scheme, following which time-domain simulation results are presented to show the response of the nonlinear adaptive controller. Finally, the performance of this controller is evaluated by determining the extent to which this method of impedance control improves the transient stability limits of the study system.

6.2 Transient Stability Control loop of the TCSC

In order to investigate the performance of the nonlinear adaptive control approach for controllable series compensation that has been identified in the literature review of Chapter Two [28], a different external transient stability control loop was implemented around the TCSC (see Fig. 6.1). The aim of this transient stability control loop is to allow dynamic variations in the TCSC's compensating reactance in response to post-fault excursions in the generator rotor according to the following equation (repeated from eqn. (2.20) in Chapter Two) :

$$X_{TCSC} = \frac{V_1 V_2 \sin\phi}{P_{L0} + \frac{2H}{\omega_0}\left(K_1\Delta\phi + K_2\frac{d\phi}{dt}\right)} - X_L \tag{6.1}$$

where V_1 is the magnitude of the voltage at the sending bus,

V_2 is the magnitude of the voltage at the receiving bus,

P_{L0} is the steady state active power transfer in the line,

ϕ is the voltage angle difference the sending and receiving bus,

and $\Delta\phi = \phi - \phi_0$ where ϕ_0 is the steady state value of the voltage angle difference prior to a disturbance.

The input signals to the control law shown in equ. (6.1) are synthesised from measurements from the transmission line and from the sending and receiving buses. The above control law, when compared to those in the previous chapters, is different in many aspects. In the controllers considered in Chapters Four and Five, a set-point

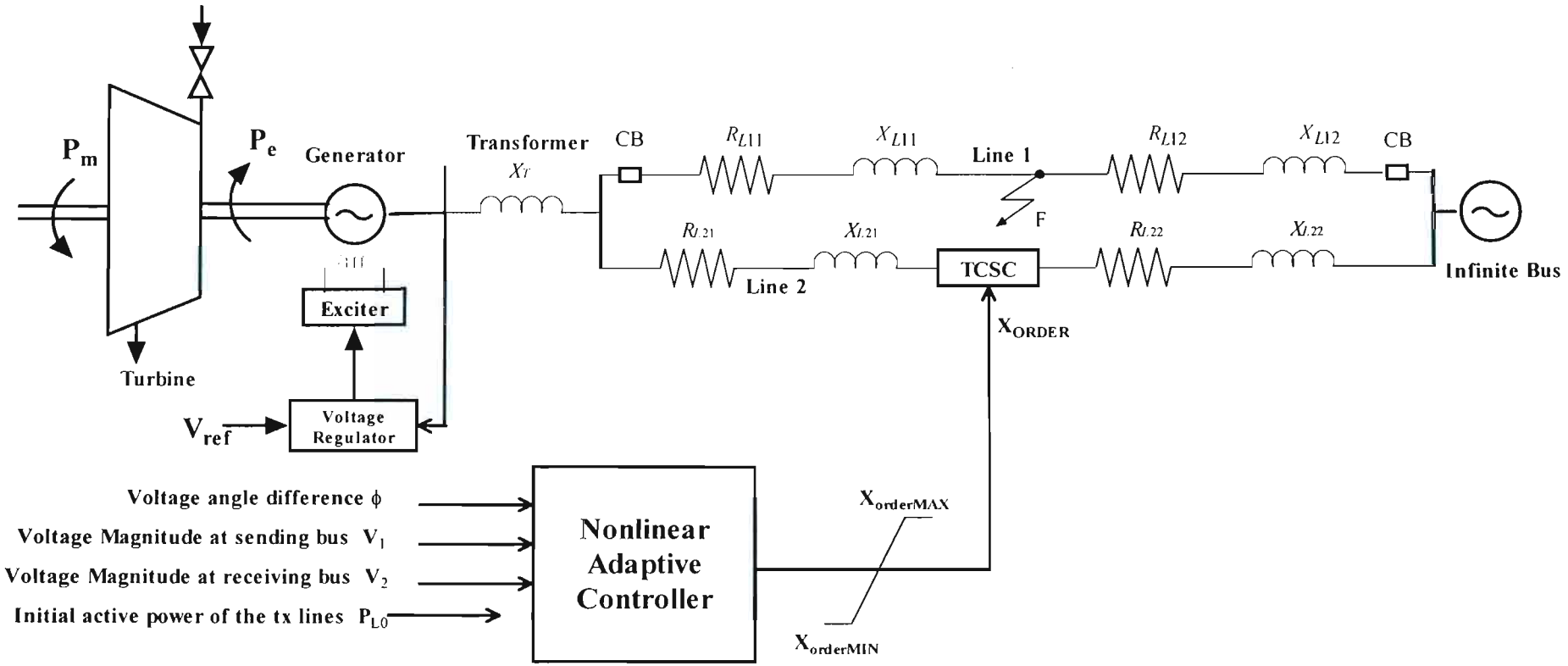

Fig. 6.1: Nonlinear adaptive TCSC controller in PSCAD.

value of the TCSC's reactance order X_{order0} was selected in each case, and the controller would vary the reactance order around this set-point value in response to some measured input signal such as speed-deviation or voltage angle difference. In this nonlinear adaptive control scheme [28], the initial set-point of the TCSC is automatically determined by the parameters of the power system and its steady-state operating point.

In the previous control schemes, it was observed that each such scheme could enhance both transient as well as small-signal stability; furthermore, with these schemes, the actual control action associated with either transient stability or damping control could be explicitly identified within the overall control approach. However, in the nonlinear adaptive control scheme considered in this chapter, the controller comprises one nonlinear function whose output varies the TCSC reactance to enhance both the transient and small-signal characteristics of the system simultaneously. The control scheme in equ. (6.1) comprises two gain values K_1 and K_2 that are not chosen independently from one another; rather, these gain values are correlated by a certain equation (see Appendix E) in such a way that specifying one gain value automatically specifies the other gain value in terms of the correlation function. Hence, the existence of the two gain terms in equ. (6.1) should *not* be taken to mean that one gain is associated with one control objective (such as transient stability) and another gain associated with some other objective such as small-signal stability. In addition, the values of K_1 and K_2 have to be selected carefully in consideration of the upper and lower limits on the TCSC's own control range $[X_{orderMAX}, X_{orderMIN}]$.

In the control scheme of equ. (6.1), the controller's input signals that act to change the TCSC reactance following a disturbance are $\Delta\phi$ and $\frac{d\phi}{dt}$. In cases where a fault in the transmission system is cleared by switching out the faulted line, the post fault transmission angle will differ from the original transmission angle prior to the disturbance when both transmission lines were in service. Thus at steady state, although the input signal $\frac{d\phi}{dt}$ in equ. (6.1) is expected to reach zero, the value of $\Delta\phi$ may not necessarily be zero and a non-zero value of $\Delta\phi$ acts to adjust the post-fault

TCSC reactance to some new compensation level in response to changes in the transmission angle. Thus, in terms of the post fault steady-state characteristics, this control scheme differs from the two previous variable impedance control approaches considered in the thesis where the post-fault steady state TCSC reactance was equal to the pre-fault compensation level, even though the post-fault system had one of the transmission lines switched out. The following section shows the simulated response of the power system when the TCSC is fitted with this external transient stability loop. The detailed design of the values of K_1 and K_2 used in the simulation studies of this chapter, and the derivation of the controller equ. (6.1) itself, can be found in Appendix E.

6.3 Response of the Variable Impedance Controller

The detailed study system model shown in Fig. 6.1 was simulated for the case of a 3-phase fault on transmission line 1 for a particular clearing time of 200ms. Fig. 6.2 shows the response of the system with fixed-impedance TCSC and with nonlinear-adaptive control of the TCSC's reactance.

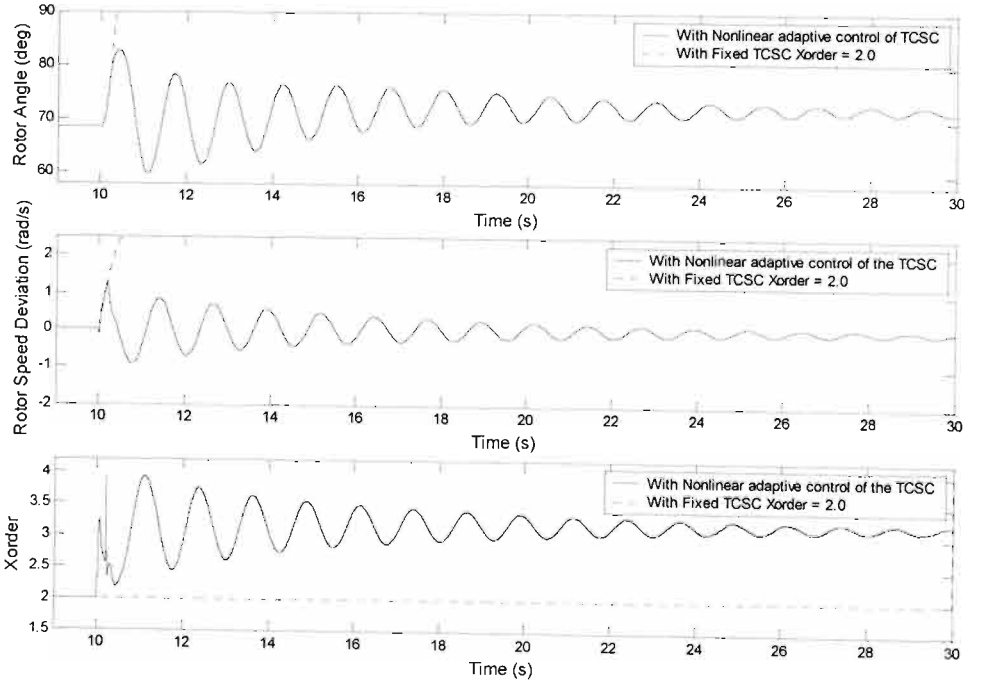

Fig. 6.2: Transient response of the rotor angle, rotor speed deviation, and TCSC Xorder value with and without the transient stability control loop enabled.

Fig. 6.2 illustrates that in a similar manner to the previous control schemes considered in Chapters Four and Five, the nonlinear adaptive control increases the TCSC's compensating reactance immediately upon occurrence of the fault in line 1. This control action causes the rotor to survive the first swing, whereas with the fixed-impedance TCSC the system is transiently unstable for this fault (see dotted curves in Fig. 6.2).

Fig. 6.2 shows that once the generator has survived the first swing, the nonlinear controller continues to vary the TCSC reactance in an attempt to damp the post-fault oscillations in rotor angle. As explained previously, because the post-fault transmission network is different to the pre-fault network (line 1 is switched out to clear the fault) the nonlinear control law changes the final steady-state operating value of the TCSC's reactance after the fault has been cleared. It can be observed that in this control scheme, the output control range is different from that in the previous chapters with a higher upper ceiling value of $X_{orderMAX} = 4.0$. This higher upper limit in the reactance order was required to avoid saturation in the control action where the reactance order would be clamped to $X_{orderMAX}$ while trying to settle at a higher post-fault value of compensation following the removal of one transmission line in the system.

Because the nature of the nonlinear adaptive controller is different from that of the bang-bang type schemes considered in Chapters Four and Five (where the size of the control range ΔX_{order} could be fixed, and the value of X_{order} was varied around a specific set-point) it is difficult to make direct quantitative comparisons between the influence of this scheme on the transient stability limits and those of the previous chapters. However, it is possible to analyse the quantitative performance of the nonlinear adaptive control scheme itself. Before investigating the impact of this nonlinear adaptive controller on the transient stability limit of the study system, the following section considers the small-signal response of the controller.

6.4 Small-signal response of the Variable Impedance Controller

To determine the impact of the nonlinear adaptive controller on the small-signal damping, a further study was conducted to compare the response of the system with and without the transient stability control loop enabled. The study system of Fig. 6.1 was simulated for a fault of shorter duration as compared to that of the simulation results of Fig. 6.2, such that the system does not lose synchronism for the case when there is no control of the TCSC reactance. Fig. 6.3 compares the responses of the system with fixed TCSC reactance and with the nonlinear adaptive control of the TCSC for this shorter fault duration of 180ms on line 1.

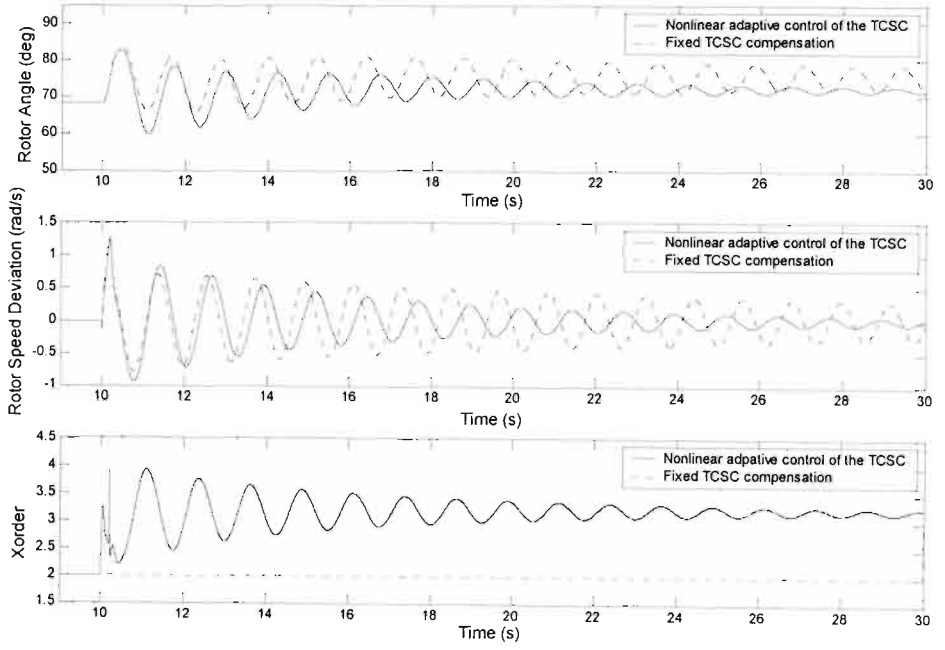

Fig. 6.3: Responses of the rotor angle, rotor speed deviation, and TCSC X_{order} value with and without the nonlinear adaptive transient stability control loop for a shorter duration fault (180ms) in line 1.

It can be observed that with the nonlinear adaptive controller, the generator oscillations exhibit better damping as compared with fixed TCSC compensation. As discussed in the previous section, the post-fault steady state load angle is different from the pre-fault steady load angle because one of the transmission lines has been

switched out. However, it can also be observed that the load angles are settling at different values at steady state in each of the two cases considered: this is because the nonlinear adaptive controller changes the TCSC's post-fault steady value of X_{TCSC} from that of fixed TCSC simulation.

6.5 Effect of the Variable Impedance Controller on the Transient Stability Limit

The previous section showed visually how nonlinear adaptive control of the TCSC's compensating reactance improves the first swing stability of a generator following a fault in the power system. This improvement in the first swing behavior means that the generator is further from its transient stability limit, for a given fault condition. This section now presents the results of repeated simulation studies conducted in order to quantify the extent of the improvement in the transient stability of the study system as a result of the nonlinear adaptive variable impedance control.

A similar study to those carried out in Chapters Four and Five has been carried out for the nonlinear adaptive controller, where the transient stability limits of the system in Fig. 6.1 have been examined for four different fault locations along line 1: 0% of X_L, 16.8% of X_L, 33.2% of X_L, and 50% of X_L. For each of these fault locations, the maximum power output of the generator that allows transient stability to be maintained was determined for the following conditions: without compensation; with fixed compensation; and with the nonlinear adaptive impedance control approach. These studies to determine the transient stability limits differ from those in the previous chapters in which different size of TCSC control range ΔX_{order} were considered in each case, because the nonlinear adaptive control scheme does not have ΔX_{order} as an adjustable setting. The results obtained from these studies are summarised in Tables 6.1 – 6.4 to show the enhancement in the transient stability limits of the SMIB study system.

It can be observed that the general horizontal trend in all these tables (i.e. the behaviour for a given fault clearing time) is that the transient stability limit of the SMIB system increases when the fixed TCSC is added. This increase in the transient

Table 6.1: Transient stability limits for a 3-phase fault at 0% of X_L without TCSC, with fixed TCSC and with nonlinear adaptive control of TCSC.

Fault Duration (ms)	Maximum Power Output (p.u)		
	Without TCSC	Fixed TCSC X_{ORDER} = 2.0	TCSC with NLcontrol
100	0.78	1.01	1.04
200	0.67	0.81	0.83
300	0.56	0.65	0.66

Table 6.2: Transient stability limits for a 3-phase fault at 16.8% of X_L without TCSC, with fixed TCSC and with nonlinear adaptive control of TCSC.

Fault Duration (ms)	Maximum Power Output (p.u)		
	Without TCSC	Fixed TCSC X_{ORDER} = 2.0	TCSC with NLcontrol
100	0.82	1.08	1.12
200	0.75	0.94	0.95
300	0.67	0.82	0.83

Table 6.3: Transient stability limits for a 3-phase fault at 33.2% of X_L without TCSC, with fixed TCSC and with nonlinear adaptive control of TCSC.

Fault Duration (ms)	Maximum Power Output (p.u)		
	Without TCSC	Fixed TCSC X_{ORDER} = 2.0	TCSC with NLcontrol
100	0.83	1.11	1.17
200	0.78	1.02	1.03
300	0.72	0.92	0.93

Table 6.4: Transient stability limits for a 3-phase fault at 50% of X_L without TCSC, with fixed TCSC and with nonlinear adaptive control of TCSC.

Fault Duration (ms)	Maximum Power Output (p.u)		
	Without TCSC	Fixed TCSC X_{ORDER} = 2.0	TCSC with NLcontrol
100	0.84	1.13	1.19
200	0.80	1.06	1.09
300	0.76	0.98	1.00

stability limit can be understood in terms of the equal area criterion as previously discussed in Chapters Four and Five. It can also be observed that the vertical trend in all the tables is that, for a given fixed value of TCSC compensation, the transient stability limit decreases as the fault duration increases. This trend can also be also understood in terms of the equal area criterion. As the fault duration is increased, the size (width) of area A1 of Fig 2.2 increases, thus reducing the transient stability limit. Tables 6.1 – 6.4 show that for each fault location, and for all the fault durations considered, there is a further improvement obtained in the transient stability limit of the system when nonlinear adaptive control of the TCSC is introduced. It can also be observed that with this control scheme, there is enhancement in the transient stability limits even for faults that are positioned half way down the transmission line. As has been observed in the other control schemes considered in the previous chapters, the marginal increase in the transient stability limits as a result of nonlinear adaptive control is quite small compared to the increase obtained by adding a fixed reactance TCSC.

6.6 Conclusion

This chapter has considered the impact on the transient stability limits of the SMIB study system when the TCSC's reactance is controlled by an external transient stability control loop based on the nonlinear adaptive control approach using locally synthesised input signals. Time-domain simulation results were presented to compare the transient responses of the generator rotor angle and speed deviations for both fixed and nonlinear adaptive controlled TCSC reactance. The results showed the improvement in the first swing behaviour that can be achieved by adding nonlinear adaptive control to the TCSC.

The impact of this nonlinear adaptive controller on small-signal damping was also investigated. Time-domain simulation results were presented to compare the transient responses of the generator rotor angle and speed deviations for both fixed and nonlinear adaptive controlled TCSC reactance. The results showed that this local

nonlinear control scheme does have a beneficial impact on small-signal damping on the post-fault generator oscillations.

The quantitative improvements in the transient stability limit of the SMIB study system for different fault scenarios were presented for fixed TCSC compensation, and for nonlinear adaptive control of TCSC reactance. It was observed that this control approach further enhances the transient stability limits of the study system over and above that obtained by using fixed TCSC reactance. In this respect, the findings are the same as for previous controllers considered. Thus, this nonlinear adaptive control scheme can also be considered as an alternative method for transient stability enhancement, with the approaches outlined in [73] being adopted to cater for the filtering requirements associated with the locally measured signals used in this particular type of controller.

Chapter Seven of the thesis now summarises and reviews the principal findings of this thesis and finally suggests further research work that could be undertaken in this area.

CHAPTER SEVEN

CONCLUSION

7.1 Introduction

This thesis has examined the specific issue of enhancing the *transient stability* of power systems using a particular form of FACTS controllable series compensation, namely the TCSC. The investigations have shown how such a FACTS device is capable of enhancing the transient stability of power systems by rapidly varying its capacitive reactance when operated in vernier capacitive mode. The investigations have shown that there are different control approaches for varying the TCSC's reactance for transient stability control. This chapter summarises and reviews the principal findings and conclusions of the thesis, chapter by chapter, and finally suggests further research work that could be undertaken in this area.

7.2 Salient Points of the Literature Review

Chapter Two presented the theory of transient stability enhancement via variable impedance control before presenting a thorough review of the technical literature on the subject of enhancing transient stability by using a variable series compensating reactance. This review highlighted that while the idea of enhancing the transient stability of power systems using variable impedance control has been around for some time, this technique did not find serious application for many years because dynamically variable series compensation could only be achieved using capacitor banks switched in and out with mechanical circuit breakers; however such devices were in practice too slow and unreliable for high-speed use demanded by dynamic control applications. Recently however, progress in the field of power electronics has led to the development of high-power electronic switches with which to implement

dynamically variable compensating reactance for the specific purpose of improving the transient stability.

The literature review in Chapter Two also presented an overview of the strategies suitable for enhancing the transient stability of power systems using controllable series compensators. The review has shown that the bang-bang control approach of controlling series compensating reactance is considered to be the most effective for enhancing transient stability following a severe disturbance in the power system, but that this approach can be detrimental to the small-signal behaviour of the system due to the so-called controller chatter problem. The review also considered the different methods of avoiding the controller chatter problem and one of these methods is to vary the degree of compensation in a continuous approach after the system has survived a transient event and is approaching steady-state. In the case of the traditional bang-bang control approach, the input signal of the transient stability controller is the generator speed deviation which may not in practice be easily obtainable at the location of the TCSC. Thus, the review has also identified two other control approaches, notably a discrete control approach based on energy-functions and a nonlinear adaptive control approach, that can be used for both transient stability enhancement as well as damping of small-signal oscillations and that use locally-measured input signals to synthesise the controller input. Both of those control schemes do not require the rapid insertion of different control loops for transient stability and then for damping of power system oscillations.

7.3 Mathematical Models for Transient Stability Studies

Chapter Three has presented an overview of the simulation models that have been developed for analysis of the SMIB study system of this thesis. A swing equation model was developed for use in the analyses of this thesis in the Matlab programming language. The swing equation model has been used in the thesis to illustrate the fundamental concepts of variable impedance control and to test control algorithms prior to their implementation on a more detailed system model.

Although the swing equation model is useful for understanding the fundamental concepts behind variable impedance control, it is not detailed enough for actual transient stability studies. Thus, Chapter Three also presented a detailed simulation model of the SMIB power system that has been developed in PSCAD, which is appropriate for actual transient stability studies. The theory and principles of operation of the TCSC, and a description of the TCSC model developed in PSCAD was also presented.

The chapter also investigated the performance of the TCSC's internal firing control scheme in the detailed simulation model under transient conditions. It has been found that the internal firing control scheme could suffer of loss of synchronism, with resulting misfiring of the TCSC thyristors, following the application of short circuit faults in the transmission line. Although attempts were made to re-design the response of the PLL firing control scheme to be immune to such disturbances, it was found that this resulted in the degradation of the performance of the firing controls under normal (un-faulted) conditions. Ultimately, it was found that the solution to the above problem was to include in the detailed TCSC simulation model the MOVs that are actually included in practical TCSC installations. The investigations subsequently carried out in the thesis made use of the detailed PSCAD models developed in Chapter Three.

7.4 Bang-bang control of the TCSC for Power System Stability Enhancement

Chapter Four presented the results of a study where a transient stability control loop was implemented around the TCSC in the detailed study system model in PSCAD. The transient stability loop considered in this chapter varied the TCSC compensating reactance in bang-bang manner following severe disturbances in the power system, by using the generator speed deviation as the input signal. Time-domain simulation results were presented to compare the transient responses of the generator angle and speed deviation for both fixed and bang-bang controlled TCSC reactance. The results showed the improvement in the first swing behaviour that can be achieved by adding bang-bang control to the TCSC.

The results also showed the problem of controller chatter associated with the bang-bang approach on the small-signal behaviour of the system. Two different approaches to preventing the problem of controller chatter were compared in this chapter: de-activating the transient stability loop, and switching the TCSC's impedance control to a linear damping control loop after a few bang-bang switchings. The results showed that with the second method of transferring control to the small-signal power oscillation damping control loop, the generator oscillations exhibit better small-signal damping than when the TCSC's reactance is kept constant under small-signal conditions.

Chapter Four also presented the quantitative improvements in the transient stability limits of the SMIB study system for different fault scenarios with and without a fixed magnitude of TCSC compensation of different sizes. It was observed that when a fixed-reactance TCSC is added, the transient stability limit increases for all the fault scenarios considered, and that as the size of the fixed TCSC compensation is increased, there is further increase in the stability limit. These enhancements in the first swing stability are consistent with the well-known influence of conventional fixed series capacitor compensation on the transient stability limits of a power system. However, a confirmation of these trends for fixed TCSC compensation was nevertheless important, since it served to establish confidence in the mathematical modeling of the study system and in the approach used to gauge transient stability limits.

Thus, the above study was then repeated without a TCSC, with a fixed-impedance TCSC, and with a bang-bang controlled TCSC that was initially operating at a $X_{order0} = 1.0$, for different amplitudes of the variable impedance control range ΔX_{order}. The results showed that when bang-bang control of the TCSC is introduced with $\Delta X_{order} = 0.5$, there is further improvement in the transient stability limit of the study system compared to the fixed-impedance TCSC with $X_{order} = 1.0$. Furthermore, the results showed that when the size of ΔX_{order} is increased from $\Delta X_{order} = 0.5$ to $\Delta X_{order} = 1.0$, there is further improvement in the transient stability limits for all the fault durations considered. However, although a case could be made for using a larger

amount of switched TCSC reactance ($\Delta X_{order} = 2.0$) in response to longer duration faults close to the generator, it was observed that the use of a large amount of switched reactance for other fault scenarios positioned half way along the transmission line is likely to be counter-productive. The conclusion was thus that a 'one-size fits all' bang-bang controller may not be appropriate, but that a bang-bang controller with the ability to adjust its output range in response to different transient scenarios may be more suitable.

The study of the impact of the bang-bang TCSC controller on the transient stability limit of the study system was further extended with the set-point of the transient stability control increased to $X_{order0} = 2.0$, to consider the effect of adding bang-bang control to the TCSC when it is initially operating at a higher compensation level. In this case, only a moderate amount of switched reactance ($\Delta X_{order} = 0.5$ and $\Delta X_{order} = 1.0$) could be used because the maximum value of X_{order} from the TCSC is $X_{order} = 3.0$. The results showed that when bang-bang control of the TCSC is introduced with $\Delta X_{order} = 0.5$, there is further improvement in the transient stability limit of the study system compared to the fixed-impedance TCSC with $X_{order} = 2.0$. Furthermore, the results showed that when the size of ΔX_{order} is increased from $\Delta X_{order} = 0.5$ to $\Delta X_{order} = 1.0$, there is further improvement in the transient stability limits for all the fault scenarios considered. It was concluded that using the TCSC at a higher compensation level and switching moderate values of ΔX_{order} in bang-bang mode is a better option for this study system. With this latter approach, it was found there is further enhancement in the transient stability limits, even for faults positioned half way along the transmission line.

7.5 Discrete Control of the TCSC based on Energy-Functions

The objective of Chapter Five was to consider the impact on the transient stability limits of the SMIB study system when the TCSC's reactance is controlled by a different external transient stability control loop based on the energy-function control approach. This energy-function controller uses locally synthesised input signals.

Chapter Five presented the details of this control scheme following which time-domain simulation results were presented to compare the transient responses of the generator rotor angle and speed-deviations for both fixed and energy-function controlled TCSC reactance. The results showed the improvement in the first swing behaviour that can be achieved by adding energy-function control to the TCSC.

Chapter Five then compared the small-signal response of the system with this energy-function controller to the two-tier method of control in Chapter Four that was based on generator speed-deviation. It was found that the local energy-function control scheme does have a small beneficial impact on the small-signal damping, but that it requires a significant number of post-fault TCSC switching operations. Although significantly better performance is achieved with speed-deviation based linear damping control of the TCSC, the cost of transmitting the required input signal to the location of the TCSC may be of concern.

Chapter Five then presented the quantitative improvements in the transient stability limit of the SMIB study system for different fault scenarios with fixed TCSC compensation, and with energy-function control of TCSC reactance for different output ranges of the control. It was observed that for this study system, adding energy-function control to the TCSC's reactance further enhances the transient stability limits. The results also confirmed that, as is the case with speed-deviation based bang-bang control, using the TCSC at a higher initial compensation level and switching moderate values of ΔX_{order} is the better option for this study system. With this latter approach, it was found there is further enhancement in the transient stability limits, even for faults positioned half way along the transmission line.

From a comparison of the results in Chapters Four and Five, it was concluded that similar degrees of improvement in the transient stability limits can be achieved with the energy-function controller to those obtained from the speed-deviation based bang-bang control in Chapter Four. Thus, the energy-function control can be considered as an alternative approach in cases where it is difficult to get input signals such as generator speed deviation at the location of the TCSC.

7.6 Nonlinear Adaptive Control of the TCSC

Chapter Six considered the impact on the transient stability limits of the SMIB study system when the TCSC's reactance is controlled by an external transient stability control loop based on a nonlinear adaptive control approach using locally synthesised input signals. Time-domain simulation results were presented to compare the transient responses of the generator rotor angle and speed deviations for both fixed and nonlinear adaptive controlled TCSC reactance. The results showed the improvement in the first swing behaviour that can be achieved by adding nonlinear adaptive control to the TCSC.

Chapter Six also considered the impact of this nonlinear adaptive controller on small-signal damping. Time-domain simulation results were presented to compare the transient responses of the generator rotor angle and speed deviations for both fixed and nonlinear adaptive controlled TCSC reactance. The results showed that this local nonlinear control scheme does have a beneficial impact on small-signal damping of the post-fault generator oscillations.

The quantitative improvements in the transient stability limit of the SMIB study system for different fault scenarios were also presented for fixed TCSC compensation, and for nonlinear adaptive control of TCSC reactance. It was observed that this control approach further enhances the transient stability limits of the study system over and above that obtained by using fixed TCSC reactance. In this respect, the findings are the same as for previous controllers considered. Thus, it was concluded that this nonlinear adaptive control method can also be considered as an alternative approach in cases where it is difficult to get input signals such as generator speed deviation at the location of the TCSC.

7.7 Suggestions for Further Work

This thesis has presented a study on the use of the TCSC for enhancing the transient stability of power systems. However, as is often the case in such research, it has not been possible to consider every aspect of the research problem in this thesis. Although some important issues have been addressed on the particular subject of enhancing the transient stability of power systems using variable impedance control of a TCSC, the thesis has uncovered further areas of concern. Therefore, the scope that exists for further research work is outlined below.

(i) This thesis has focused exclusively on the transient stability enhancement of a single-machine infinite bus power system. The investigations could be extended to examine the performance of the variable impedance control approaches of this thesis in a multi-machine power system.

(ii) In one of the variable impedance control approaches reviewed in Chapter Two, it was proposed that both the capacitive as well as the inductive regions of operation of the TCSC could be used in transient stability control. Further work could consider the impact on the transient stability limits of variable impedance controllers that more fully utilise the operating range of a TCSC in this way.

(iii) Finally, as discussed in Chapter Three, the parameters of the SMIB system as well as those of the TCSC used in this thesis are based on the parameters of the laboratory-scale power system in the Machines Research Laboratory at the University of KwaZulu – Natal. Thus, practical confirmation of the findings of this thesis could be considered by using the laboratory-scale TCSC developed by the research group.

APPENDIX A

PARAMETERS OF THE DETAILED SMIB STUDY SYSTEM IN PSCAD

This Appendix lists the parameters used in the studies of the single-machine infinite bus study system in Chapters Four, Five and Six.

A.1 Parameters of the Single-Machine Infinite Bus System

A.1.1 Generator Parameters in Per-Unit (unless stated)

R_a = 0.006

X_l = 0.11

X_d = 1.98

R_f = 0.000818

X_f = 0.1

R_d = 0.212

X_{kd} = 0.125

X_{mfd} = 0.0

X_{mq} = 1.87

R_{kq} = 0.029

X_{kq} = 0.257

H = 5.68144 MW/MVA

V_T = 1.0

Base voltage = 127.017 V_{rms} (Line to neutral)

Line current = 7.873 A_{rms}

Frequency = 50 Hz

A.1. 2 Automatic Voltage Regulator in Per-Unit (unless stated)

K_A = 17

T_C = 0.616 s

T_B = 2.266 s

T_{C1} = 0.189 s

T_{B1} = 0.039 s

A.1.3 Transformer Parameters (per phase)

X_T = 2.04 Ω

R_T = 0.0 Ω

A.1.4 Transmission Line Parameters (per phase)

Line Number 1

R_L = 0.54 Ω

X_L = 12.12 Ω

Closed CB resistance = 0.01 Ω

Opened CB resistance = 1.0×10^6 Ω

3-phase ON fault resistance = 0.01 Ω

3-phase OFF fault resistance = 1.0×10^6 Ω

Line Number 2

R_L = 0.54 Ω

X_L = 12.12 Ω

TCSC Parameters (per phase):

X_C = 2.048 Ω

I_C = 7.87 A_{rms}

X_{TCR} = 0.415 Ω

MOV rating = 67 V

A.1.5 Infinite Bus Parameters

Base apparent power = 0.003 MVA

Base voltage = 220 V_{rms} (Line to line)

Base frequency = 50 Hz

Positive sequence series resistance = 0.001 Ω

APPENDIX B

SWING EQUATION MODEL MATLAB CODE

In Chapter Three, the swing equation model was presented to describe the dynamics of the two area power system of Fig. 2.1, based on eqns. (2.1-2.3). The abbreviated MATLAB M-files which follow show the programmed swing equations; sections of the code where necessary have been omitted in the interest of conciseness.

B.1 Classical Swing Equation model Code

```
%Simulation program for the Swing Equation model
%requires accompanying files plt_swing_nl1.m ,ss_initial_swing_nl.m,
clc
clear
global Xt Jm D intvars
%Initial conditions at the generator terminals in p.u.
Pb = 0.450;
Qb = 0.049;
Vb = 1;
Wo = 100*pi;
Xdp = 0.20519;
Xe = 0.46741;
Xt = Xdp + Xe;
Xtold = Xt;
DXc = 0.05;  %Bang-bang control
%Kcsc = 0.1;   %Controller gain for continous control
H = 5.68144;
Jm = 2*H/Wo;
D = 0.0;          %Machine viscous damping coefficient
%-------------Non-linear time domain simulation---------%
%Simulation directives
delt   = 0.5e-2;
dover3 = delt/3;
tfault = 0.1;
tlift  = 0.2;
```

```
tfin   = 10.0;
nn     = 1;
ll     = nn-1;
kk     = 0;
np     = fix(tfin/delt/nn);
t=0;
%Subroutine to calculate initial values of state variables
%E = zeros(1);
[x, Tm, E] = ssinitial_swing_nl(Pb,Qb,Vb);
%Input vector in sfunc format
u(1,1) = Vb;
u(2,1) = Tm;
u(3,1) = E;
%Set up matrices for output of numerical integration
z = zeros(np,1);
xo = zeros(np,3);
intvars = zeros(1);
%-------------------------Integration loop-------------------------%
while t < tfin
if ((t >= tfault)&(t < tlift))
%system disturbance if required

%New input voltage
u(1,1) = 0.242;
elseif (t>=tlift)
%Lift system disturbance
u(1,1) = Vb;

end

   [xdot] = plt_swing_nl1(0,x,u,1);
   fk1 = xdot'*dover3;
   [ydot] = plt_swing_nl1(0,x+fk1,u,1);
   fk2 = ydot'*dover3;
   [ydot] = plt_swing_nl1(0,x+0.5*(fk1+fk2),u,1);
   fk3 = ydot'*dover3;
   [ydot] = plt_swing_nl1(0,x+(1/8)*(3*fk1+9*fk3),u,1);
   fk4 = ydot'*dover3;
   [ydot] = plt_swing_nl1(0,x+0.5*(3*fk1-9*fk2+12*fk4),u,1);
   fk5 = ydot'*dover3;
```

```
  x = x + 0.5*fk1 + 2*fk4 + 0.5*fk5;

 %continous linear control
 %DXc = Kcsc*x(1);
 %Xt = Xtold - DXc
 %Algorithm for bang-bang
 if (x(1) > 0)
    Xt = Xtold - DXc;
 elseif (x(1) <= 0)
    Xt = Xtold;
 end
 %Nonlinear control in [Zhou3]
 %Dx(2) = x(2)- delta0
 %DXc = (abs(E)*u(1,1)*sin(x(2)))/(Tm + ((H/Wo)*(K1*Dx(2) +
K2*x(1)));
 %Xt = Xtold - DXc

%time vector and output vectors for plotting

  ll=ll+1;
  if ll == nn
     ll=0;
     kk=kk+1;
     z(kk) = t;
     xo(kk,1) = x(1);instantaneous Rotor speed deviation
     xo(kk,2) = x(2);        %instantaneous Load angle(deg)
%xo(kk,3) = intvars(1);  %instantenous Electrical torque Te in pu
     xo(kk,3) = Xt;          %instantenous Line reactance in pu
 end
 t = t+delt;
end
```

```
%Steady state initialization of the state variables for the swing
model

function [x, Tm, E] = ssinitial_swing_nl(Pb, Qb, Vb)

global Xt Jm D intvars

I = (Pb - j*Qb)/Vb;
E = Vb + I*j*Xt;
x(2) = angle(E);
x(1) = 0;  %derivative of initial load angle being a constant is zero
E = abs(E);
Te = E*Vb*sin(x(2))/Xt;
Tm = Te;
```

```
%Plant equations in sfunction format for swing_nl_sim.m

function [sys,x0,str,ts] = plt_swing_nl(t,x,u,flag)

global Xt Xtold Kcsc Jm D intvars

%=============================================================================
% mdlInitializeSizes
% Return the sizes, initial conditions, and sample times for the S-
function.
%=============================================================================
function [sys,x0,str,ts]=mdlInitializeSizes

sizes = simsizes;

sizes.NumContStates  = 2;
sizes.NumDiscStates  = 0;
sizes.NumOutputs     = 2;
sizes.NumInputs      = 3;
sizes.DirFeedthrough = 0;
sizes.NumSampleTimes = 1;   % at least one sample time is needed

sys = simsizes(sizes);
% initialize the initial conditions
x0 = zeros(1,1);
% str is always an empty matrix
str = [];

% initialize the array of sample times
ts  = [0 0];

% end mdlInitializeSizes

%=============================================================================
% mdlDerivatives
% Return the derivatives for the continuous states.
%=============================================================================
function sys=mdlDerivatives(t,x,u)

global Xt Xtold Kcsc Jm D intvars
```

```
Vb = u(1,1);
Tm = u(2,1);
E = u(3,1);

DXcsc = Kcsc*x(1); %continous linear control of CSC
Xt = Xtold - DXcsc;

Te = (E*Vb*sin(x(2)))/Xt;
sys(1,1) = (Tm - Te - D*x(1))/Jm;
sys(2,1) = x(1);

% end mdlDerivatives

%=============================================================================
% mdlOutputs
% Return the block outputs.
%=============================================================================
function sys=mdlOutputs(t,x,u)

global Xt Xtold Kcsc Jm D intvars

sys(1,1) = x(1);
sys(2,1) = x(2);

% end mdlOutputs
```

APPENDIX C

FILTER DESIGN FOR LOCALLY SYNTHESISED SIGNALS

C.1 Introduction

Chapter Five and Six of this thesis considered variable impedance control approaches that are based on locally measured signals synthesised for use as controller inputs. This appendix shows the design of the filters that were used in those studies. Reference [73] provides a detailed account of the approaches to signal selection and filtering in practical systems.

C.2 Filter design

C.2.1 First-order filtering and lead compensator design

The phase difference functional block in PSCAD was used to measure the voltage angle ϕ between the sending and receiving buses of the SMIB system. In order to justify the use of the different filters that were required in synthesising the locally measured input signals, the SMIB system was simulated for a 3-phase fault cleared at a particular duration of 250ms. Fig. C.1 shows the output signal of this functional block with and without using a first-order filter $\frac{1}{1+0.1s}$. As can be observed, the first-order filter significantly removes most of the high frequency components in the signal particularly during the transient condition. However, it introduces a lagging angle to the filtered signal and this lagging angle can be read off the bode plot of the filter at the frequency of interest (5.21rad/s).

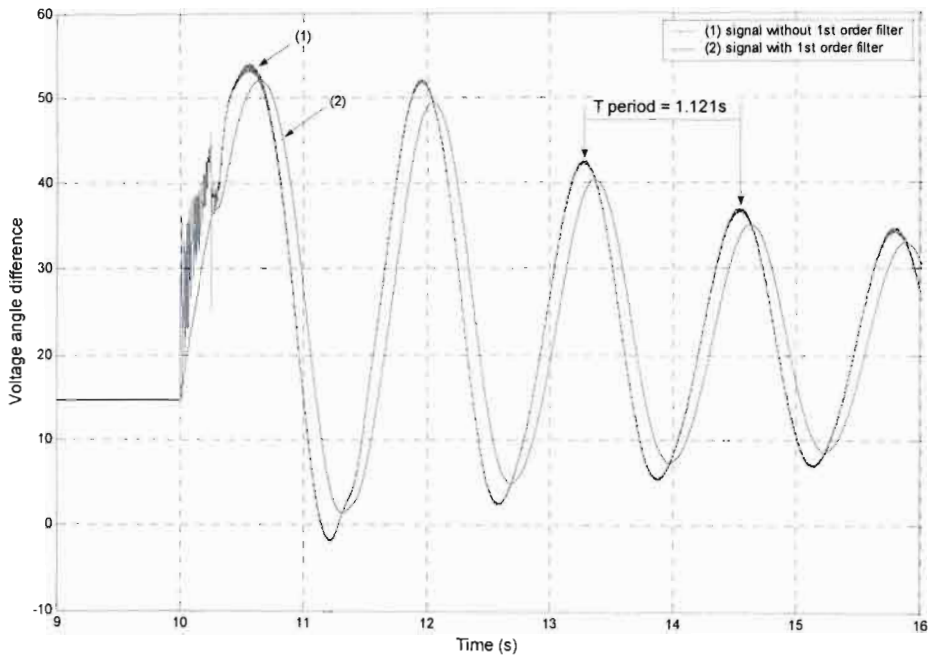

Fig. C.1: Response of the Voltage angle difference with and without 1st order filtering.

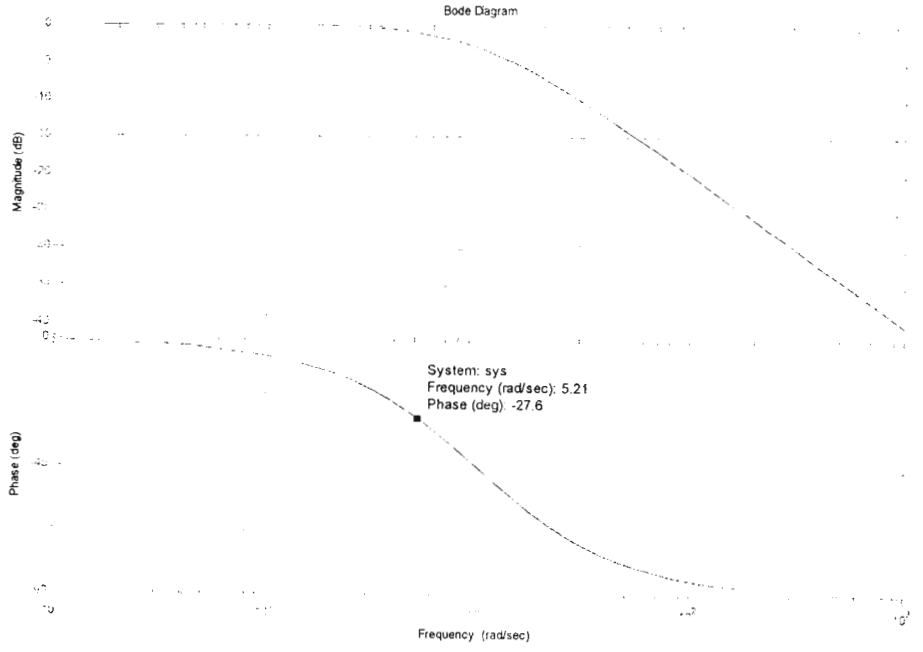

Fig. C.2: Bode plot of 1st order filter.

C.2.2 Lead compensator design

Thus, it was required to add a lead compensator to the signal to correct the lagging angle of 27.6°.

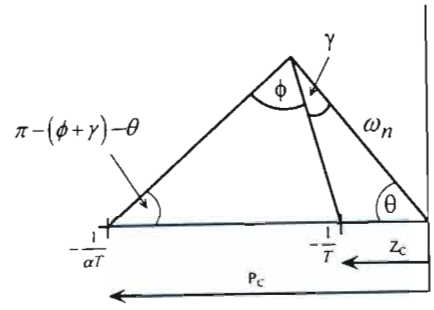

Assuming damping ratio $\xi = 0.5 \Rightarrow \theta = \cos^{-1}(0.5) = 60^o$ and $\phi = 27.6^o$ and for max k_v

$$\gamma = \frac{1}{2}(\pi - \theta - \phi) = 46.2^o$$

$(\pi - \theta) > (\gamma + \phi)$ and hence the compensation angle can be achieved using a single lead network:

$$G_C(s) = \frac{s + Z_C}{s + P_C} = \frac{s + \frac{1}{T}}{s + \frac{1}{\alpha T}} = \alpha \frac{1 + sT}{1 + s\alpha T} \qquad \text{(C.1)}$$

From the above,

$$Z_C = \frac{\omega_n \sin(\gamma)}{\sin(\pi - \gamma - \theta)} = 3.916 \text{ and} \qquad \text{(C.2)}$$

$$P_C = \frac{\omega_n \sin(\phi + \gamma)}{\sin(\pi - \phi - \gamma - \theta)} = 6.932 \qquad \text{(C.3)}$$

hence, the lead network was determined:

$$G_C(s) = \frac{s + 3.916}{s + 6.932} = 0.5648 \frac{1 + 0.2553s}{1 + 0.1442s} \qquad \text{(C.4)}$$

Fig. C.4 compares the voltage angle difference signal with both the first order filter and the lead compensator and the signal without both filters.

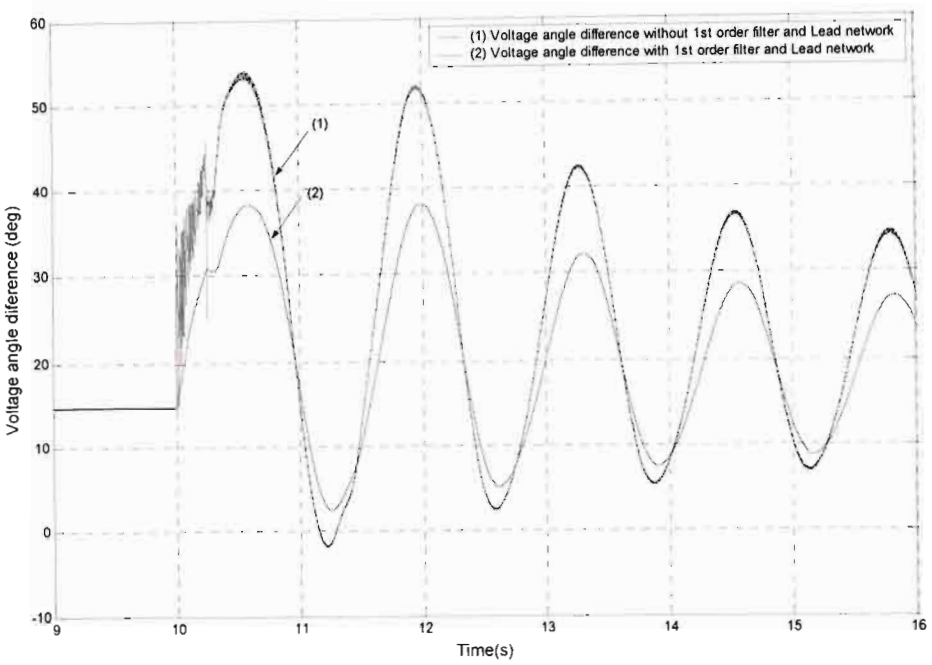

Fig. C.3: Response of the Voltage angle difference with and without both filters.

Thus as by comparing Fig. C.1 to Fig. C.3, the lagging angle introduce by the first order filter was compensated by the addition of the lead network.

C.2.3 Derivative filter design

The use of the derivative functional block sT in PSCAD has the tendency to amplify noise in the signal. A derivative filter circuit was used for that purpose to convert the voltage angle difference ϕ angle to $\frac{d\phi}{dt}$ which is a signal close to the rotor speed deviation. The proposed derivative filter [73] has the following transfer function:

$$H(s) = s\left[\frac{1}{1+sT_{DC}}\right]\left[\frac{1}{1+sT_{DC}}\right]\left[\frac{sT_{WS}}{1+sT_{WS}}\right] \qquad \text{(C.5)}$$

where $\left[s/1+sT_{DC}\right]$, $\left[1/1+sT_{DC}\right]$ are the filtered derivative circuit and

$\left[sT_{WS}/1+sT_{WS}\right]$ is a washout filter to remove any dc offset in the signal.

The design in this case was to adjust the value of T_{DC} such that a phase margin of 90° is obtained at the required frequency of 5.21rad/s. The time constant of the washout was set to 3seconds.

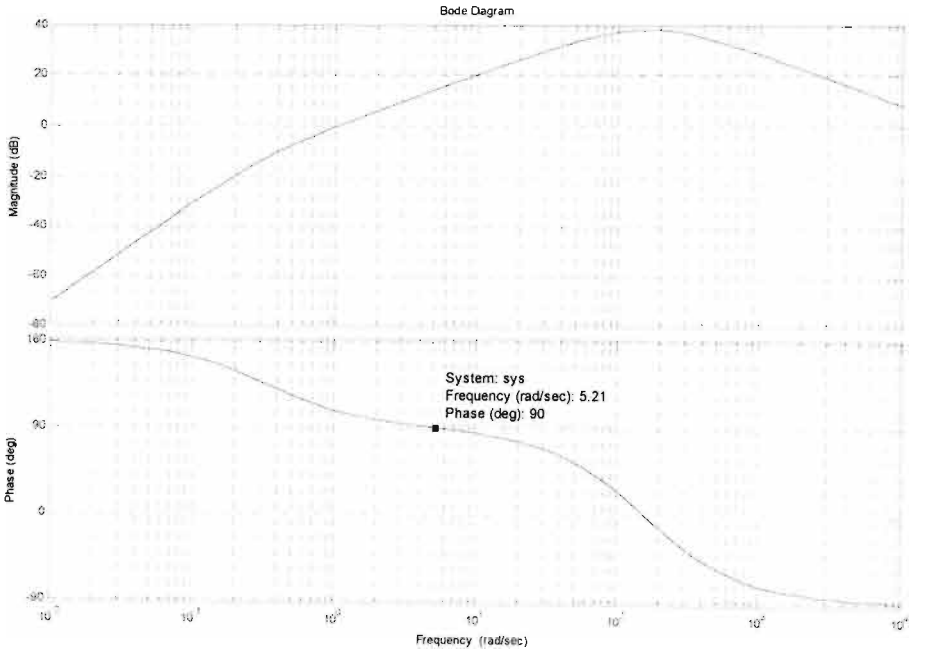

Fig. C.4: Bode plot of derivative filter circuit.

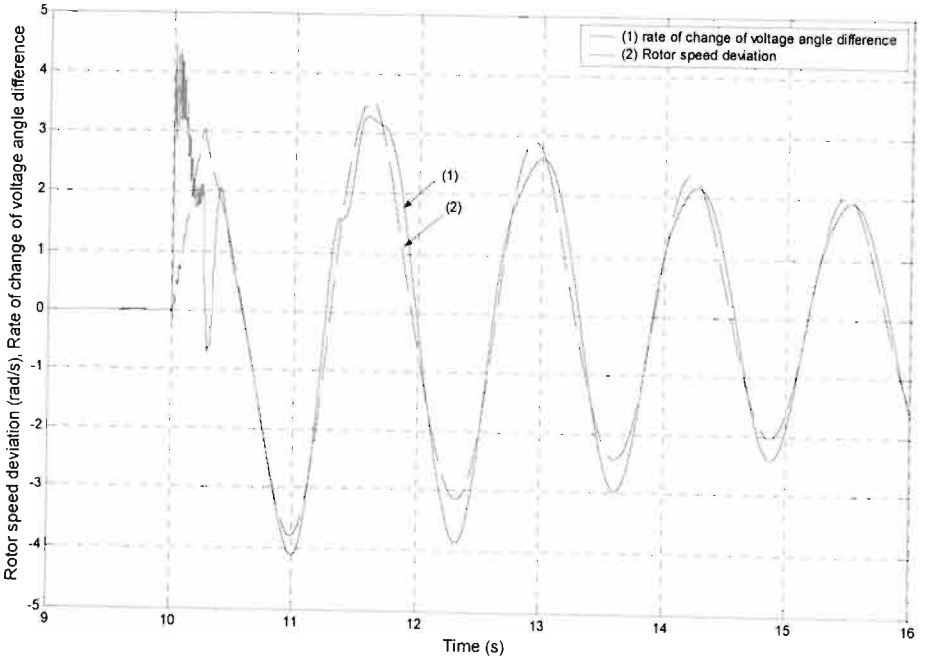

Fig. C.5: Comparison between the Rotor Speed deviation and $\frac{d\phi}{dt}$.

From the bode plot of Fig. C.4, a T_{DC} value of 0.00618 was found to give the required phase margin. The signal $\frac{d\phi}{dt}$ is compared to the rotor speed deviation in Fig. C.5. As can be observed, both signals are in phase and hence $\frac{d\phi}{dt}$ can be considered as a signal that is close to $\Delta\omega$.

APPENDIX D

PSCAD SIMULATION MODELS USED FOR TRANSIENT STABILITY STUDIES

D.1 Introduction

Chapter Four, Five and Six of this thesis showed a series of simulation results to demonstrate the improvement in transient stability of the study system that can be achieved with different control approaches of the TCSC. This appendix presents the simulation models that were used for those transient stability studies.

D.2 PSCAD simulation models

The following figures show a graphical representation of the simulation models developed for the work in this thesis. The detailed simulation model of the SMIB study system is presented followed by the detailed TCSC model in PSCAD. The appendix also shows the different transient stability control loops that were implanted around TCSC for the transient stability studies presented in this thesis.

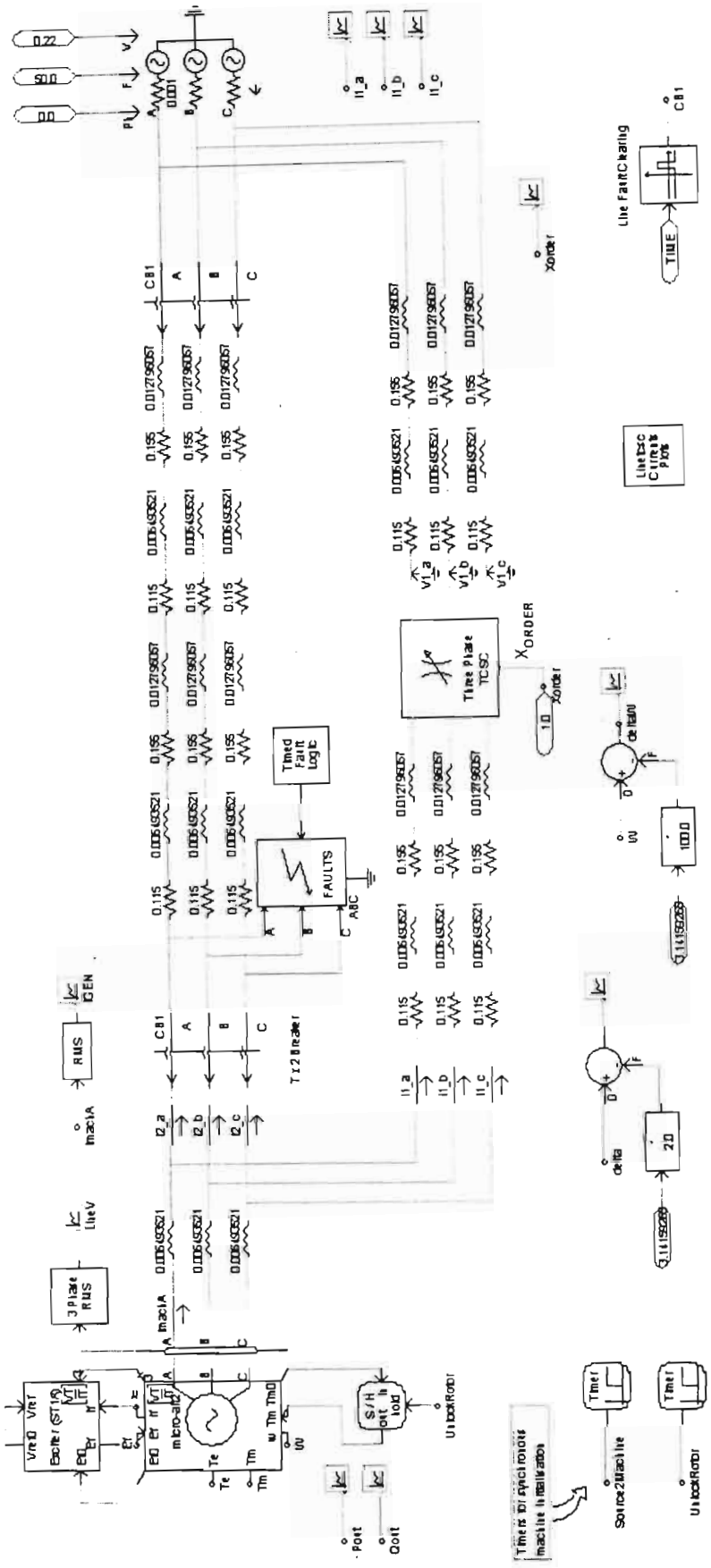

Fig. D.1: Detailed SMIB study system model developed in PSCAD.

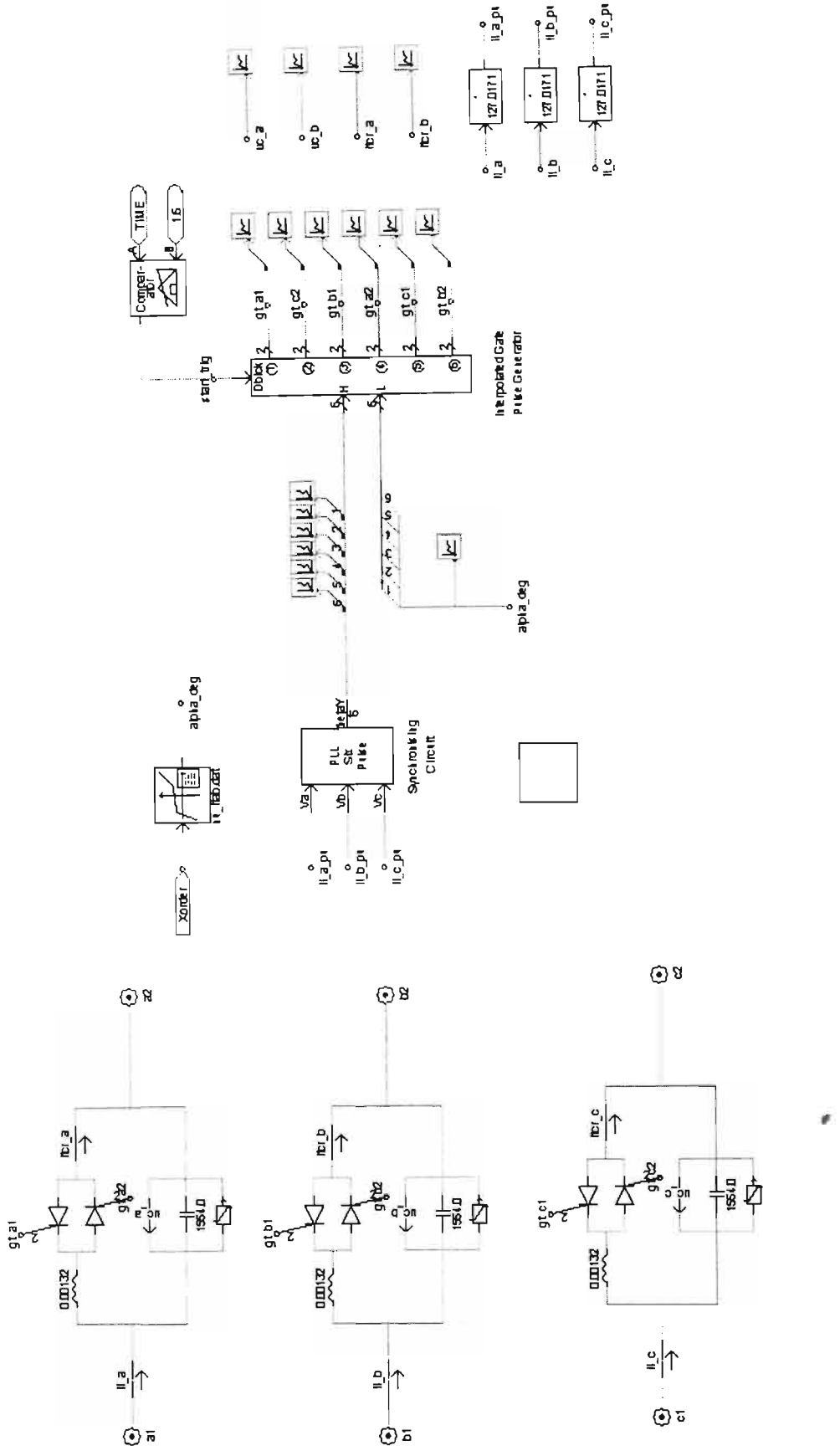

Fig. D.2: TCSC internal control model in PSCAD (subpage of Fig. D.1).

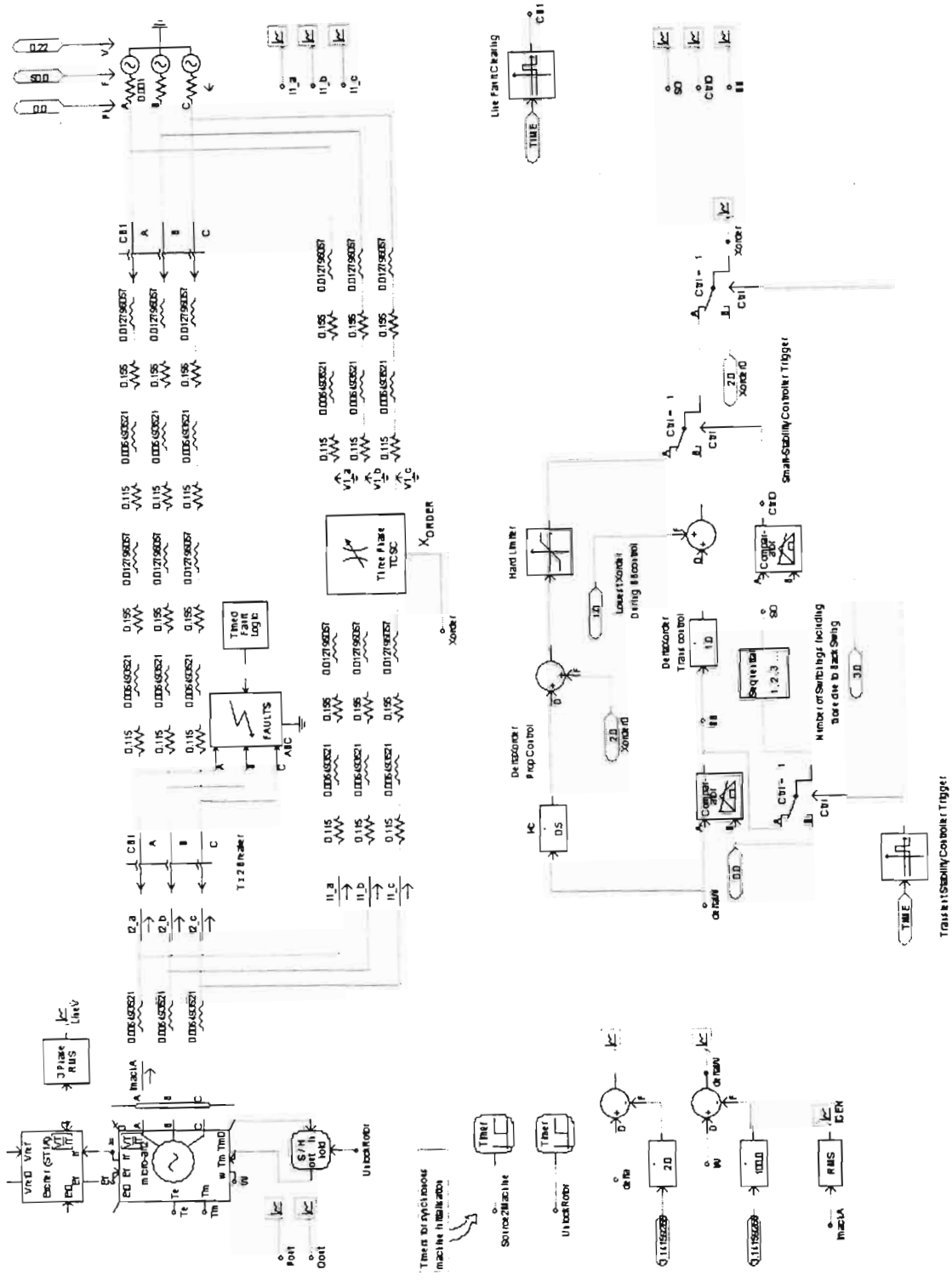

Fig. D.3: Two -tier Transient Stability Control loop for the results in Table 4.9.

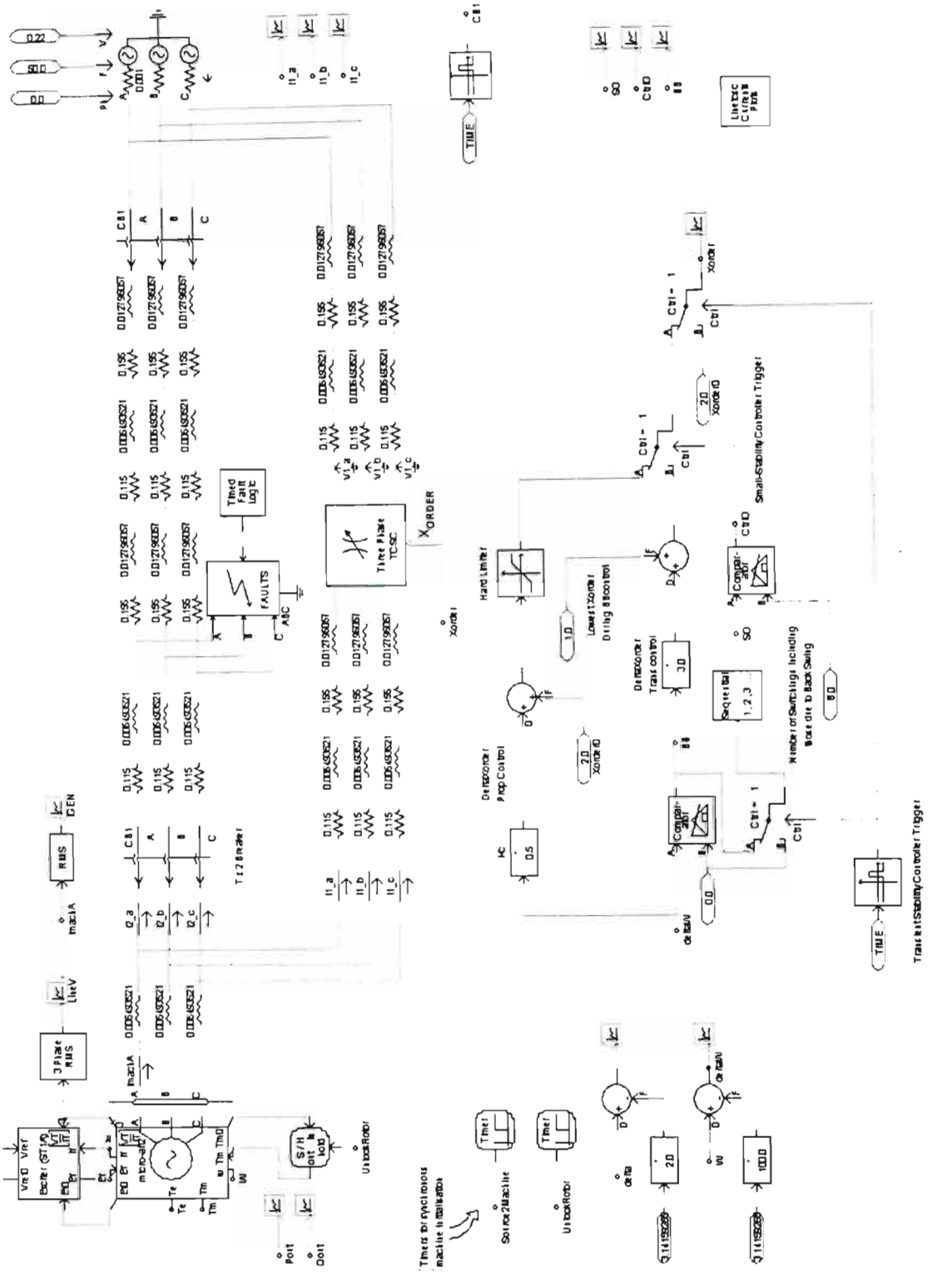

Fig. D.4: PSCAD simulation model for the results in Table 4.10.

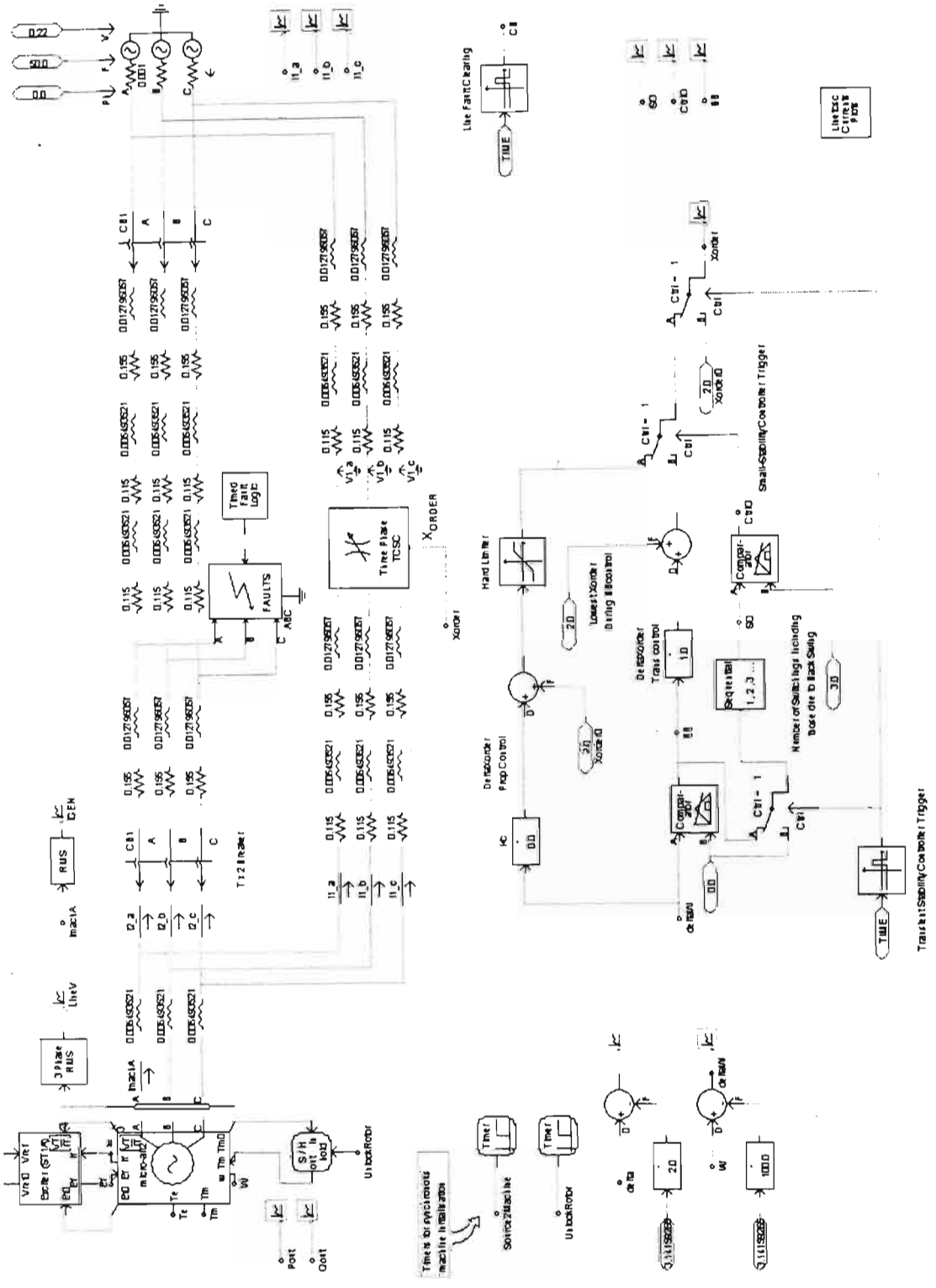

Fig. D.5: PSCAD simulation model for the results in Table 4.11.

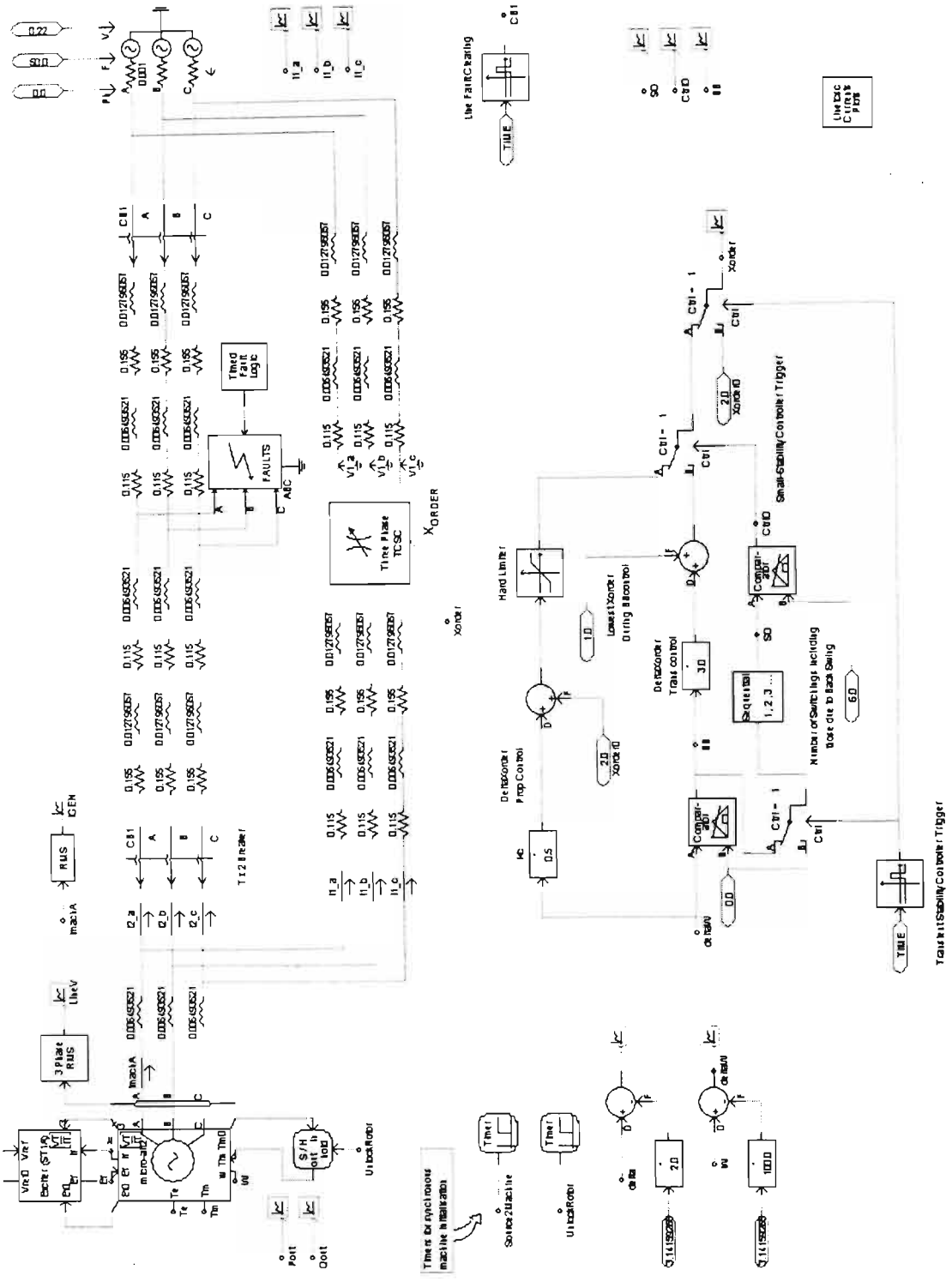

Fig. D.6: PSCAD simulation model for the results in Table 4.12.

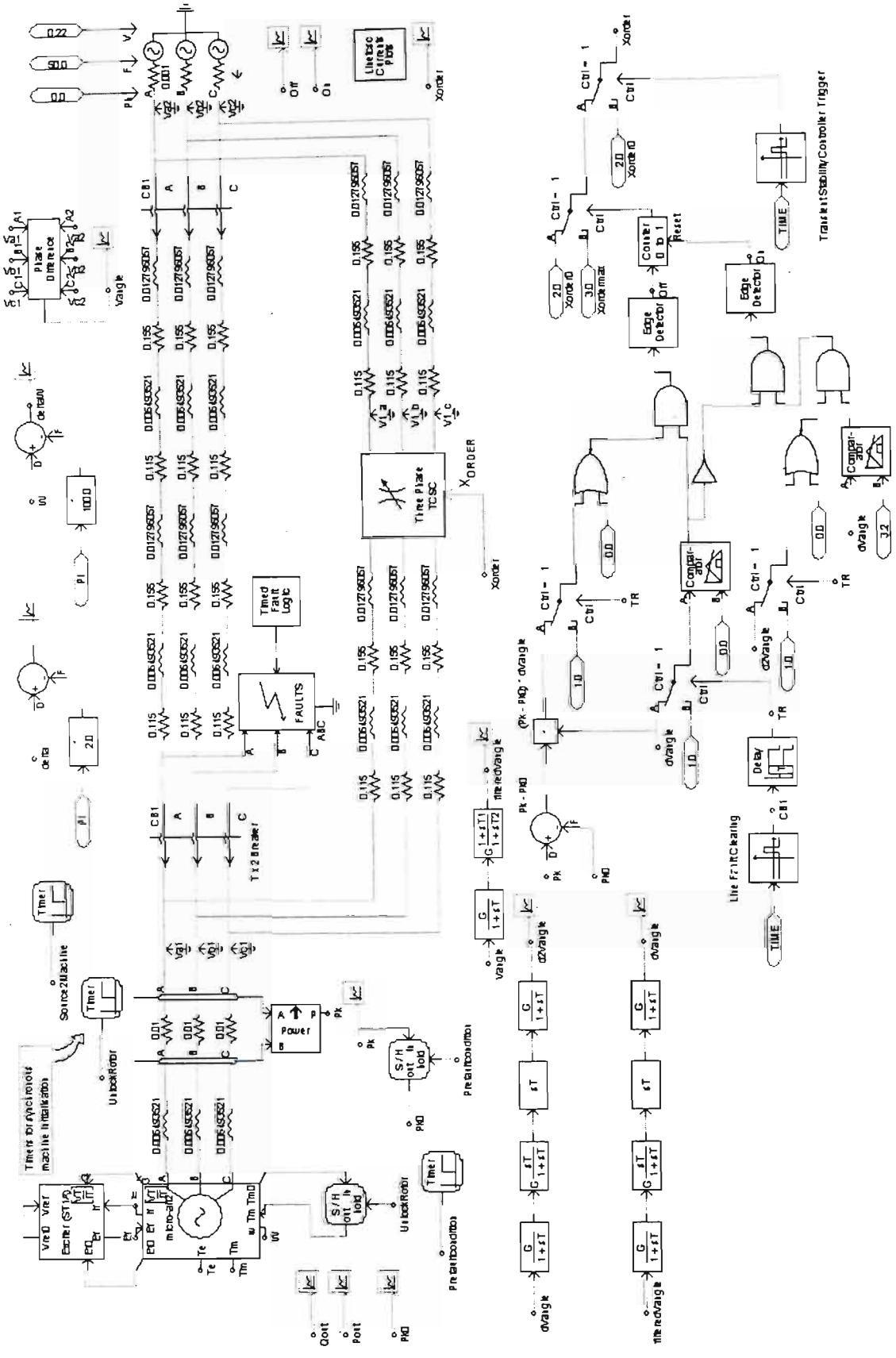

Fig. D.7: Energy-function Transient Stability control loop for results in Table 5.1.

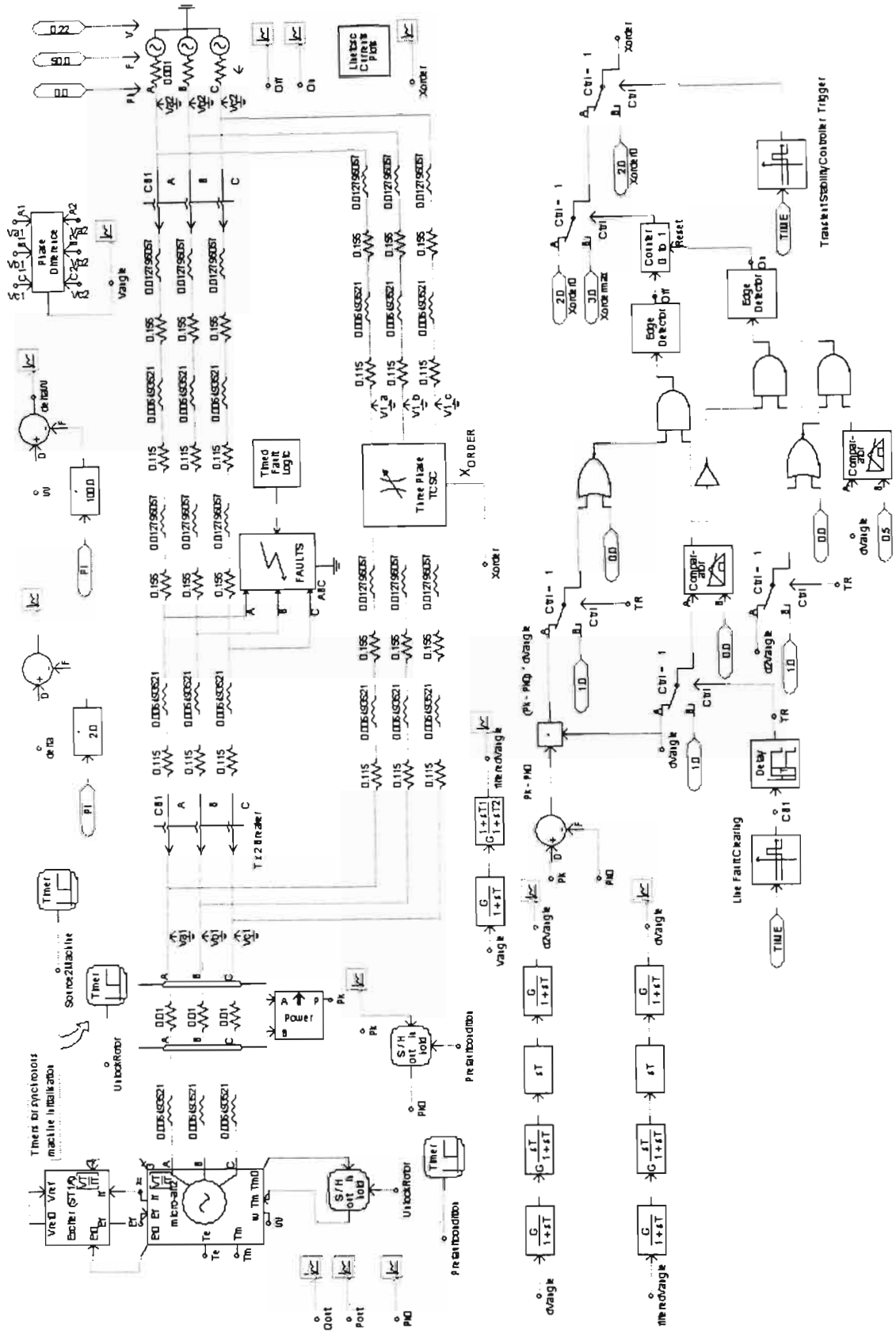

Fig. D.8: PSCAD simulation model for the results in Table 5.2.

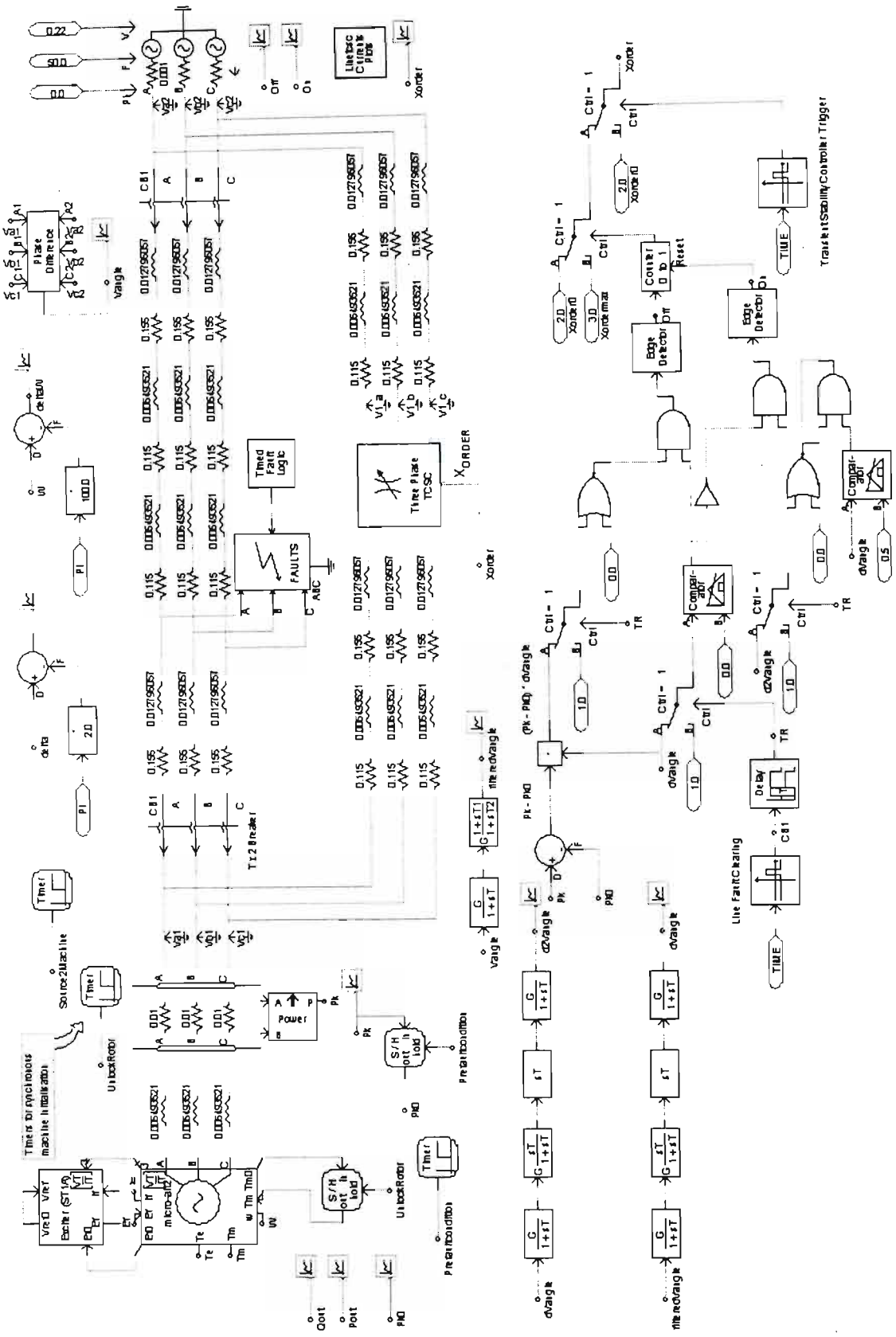

Fig. D.9: PSCAD simulation model for the results in Table 5.3.

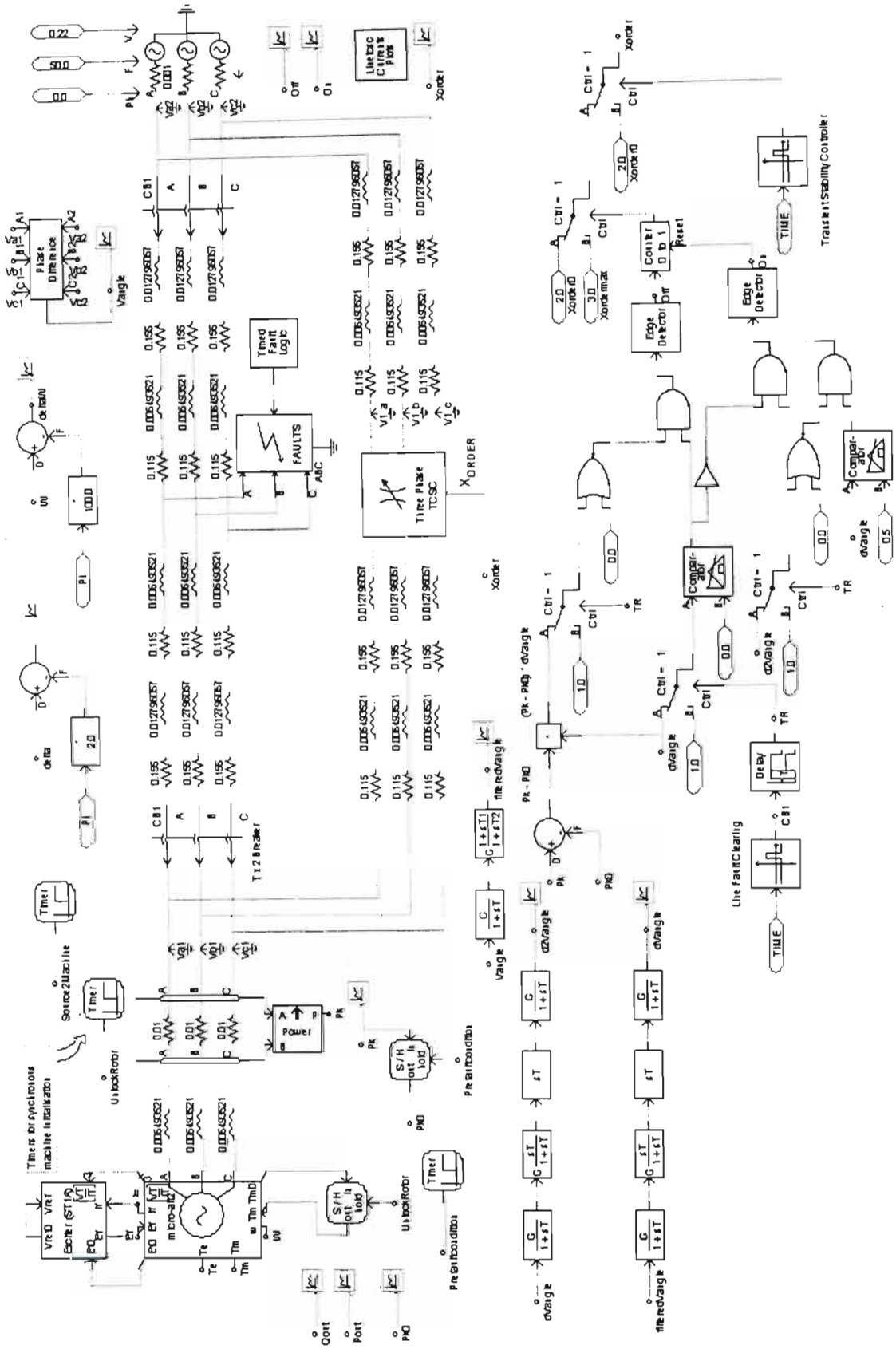

Fig. D.10: PSCAD simulation model for the results in Table 5.4.

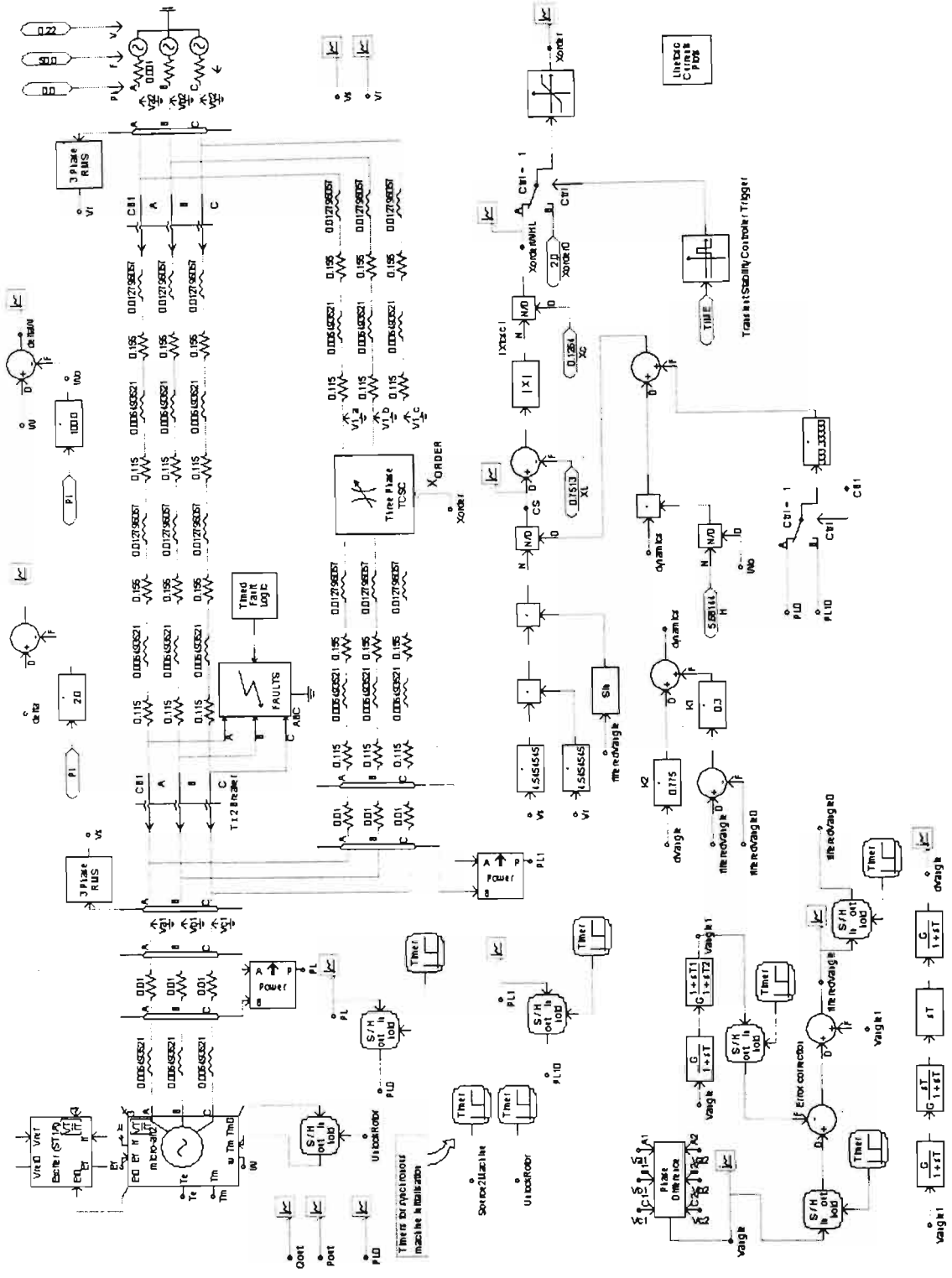

Fig. D.11: Nonlinear Adaptive Control loop for results in Table 6.1

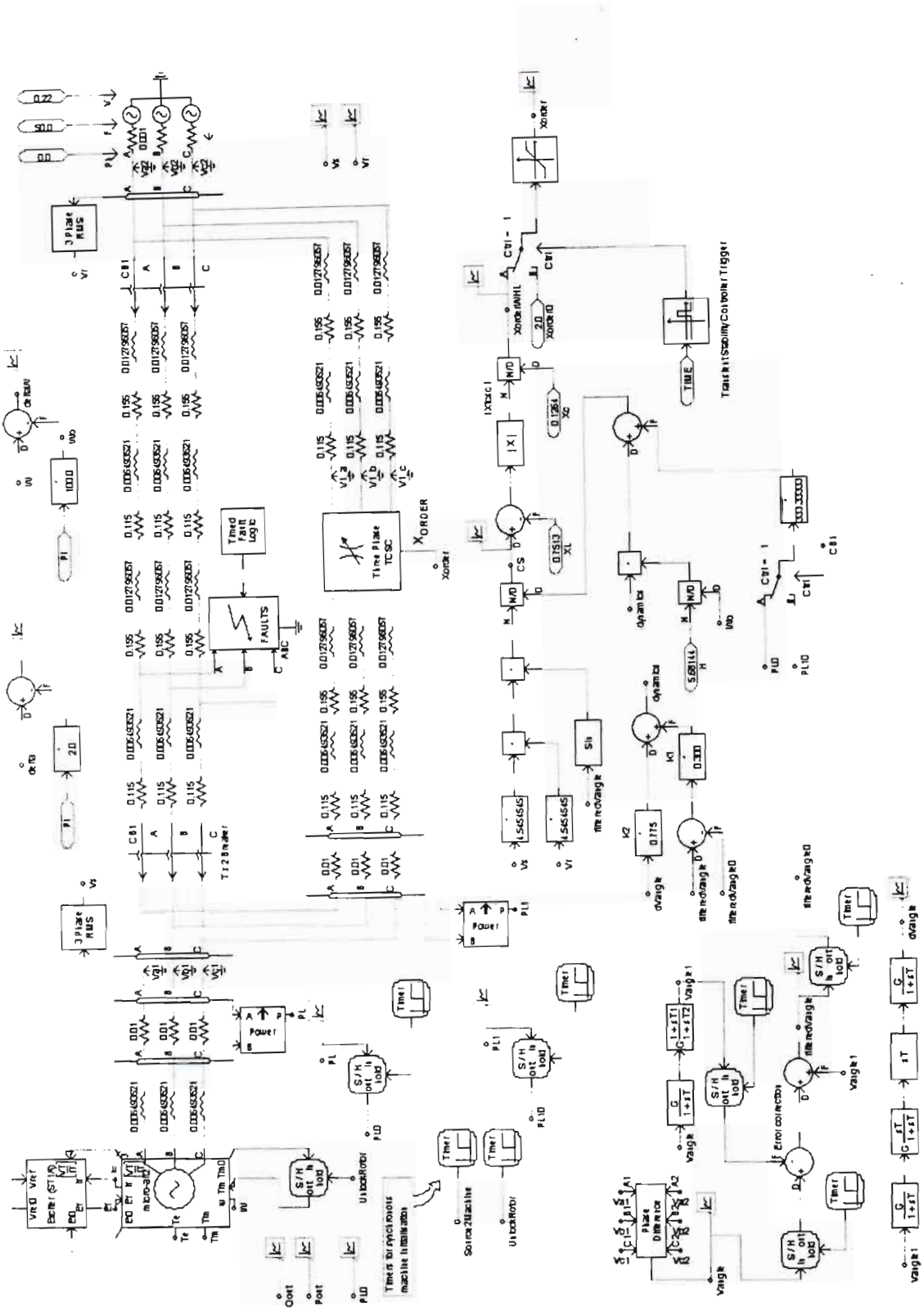

Fig. D.12: PSCAD simulation model for the results in Table 6.2.

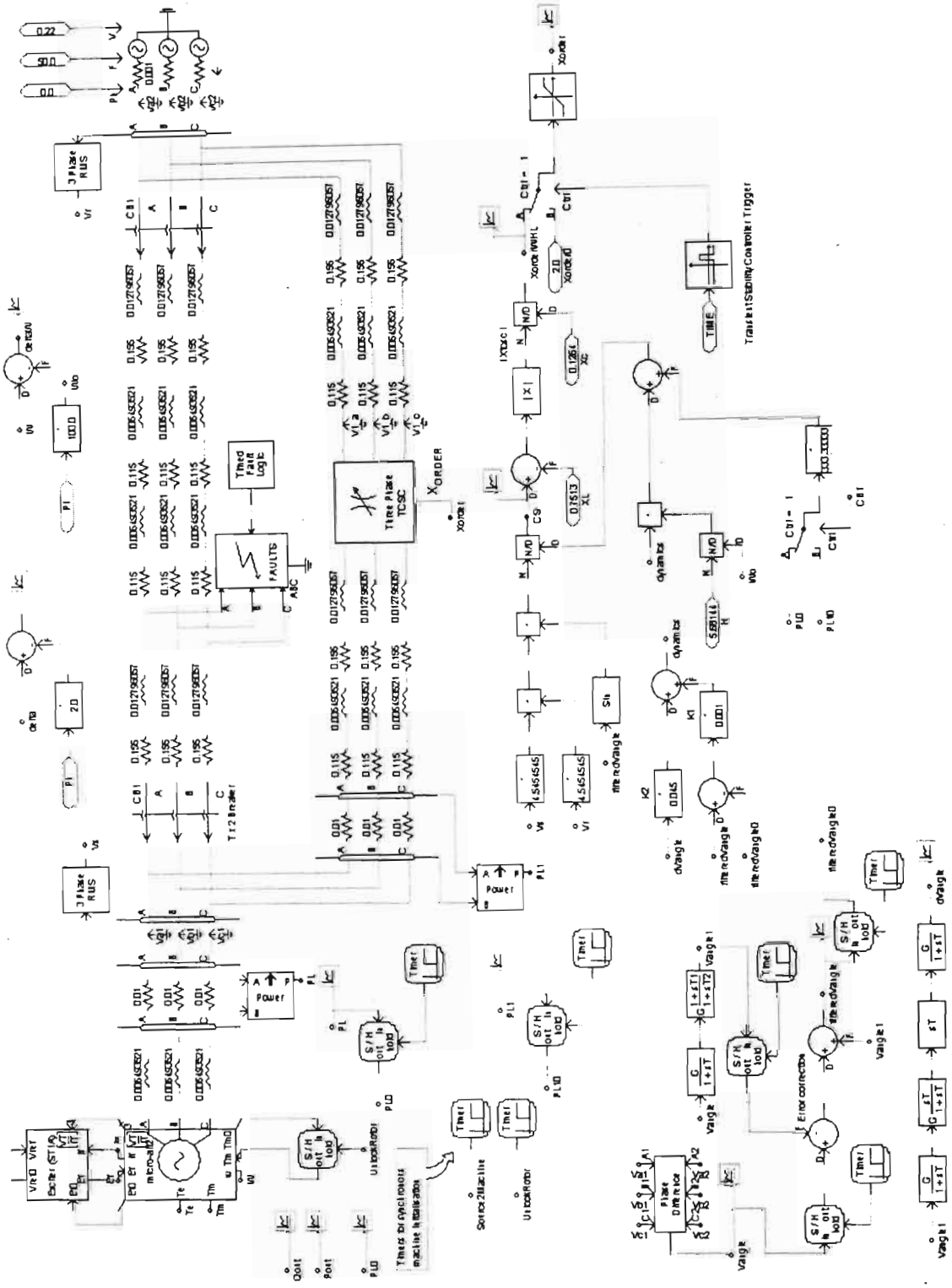

Fig. D.13: PSCAD simulation model for the results in Table 6.3.

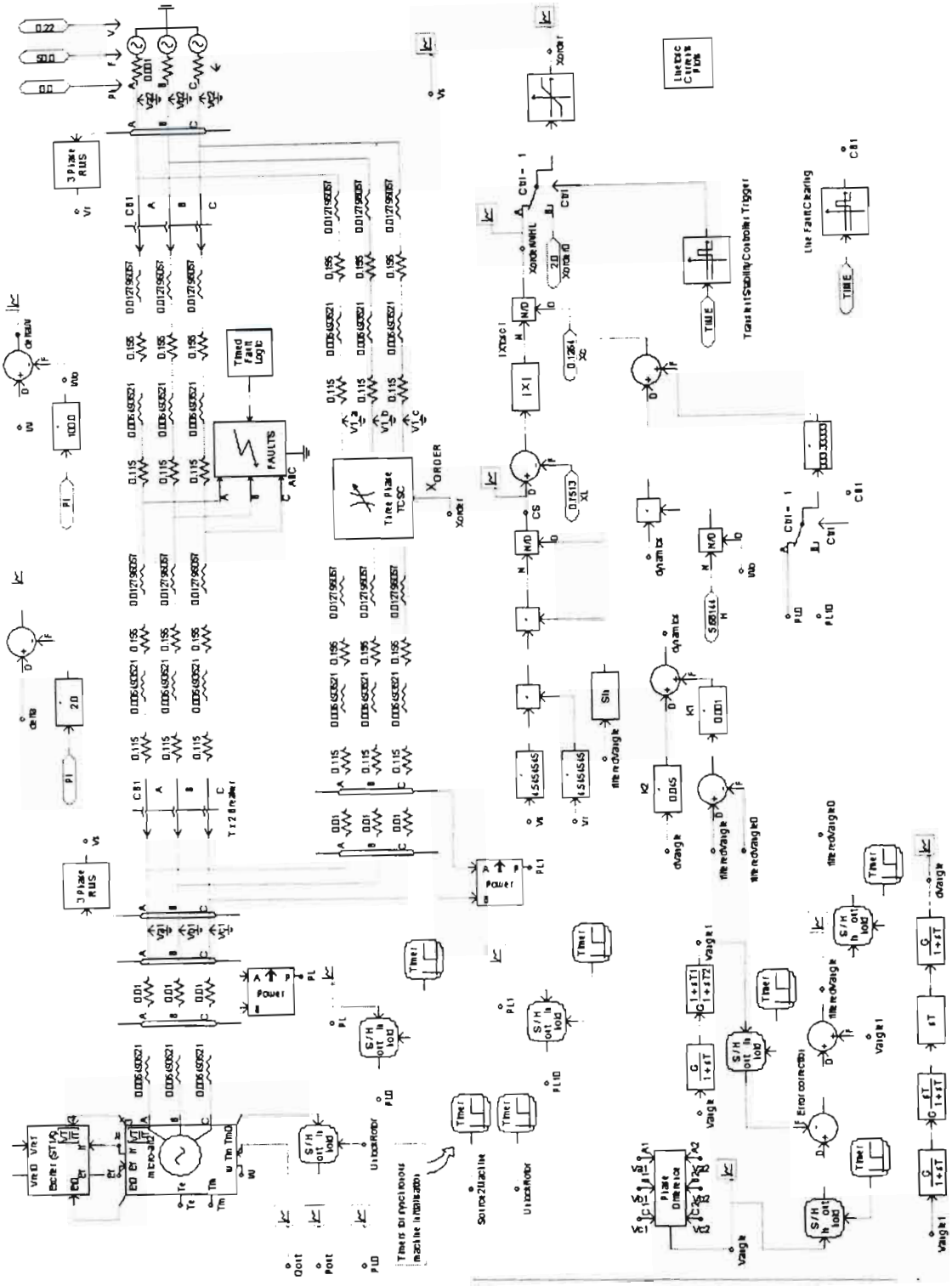

Fig. D.14: PSCAD simulation model for the results in Table 6.4.

APPENDIX E

DERIVATION OF THE NONLINEAR ADAPTIVE CONTROL SCHEME AND THE DESIGN OF CONTROL PARAMETERS

E.1 Introduction

Chapter Six of this thesis considered nonlinear adaptive variable impedance control approach that is based on locally measured signals synthesised for use as controller input. This appendix shows the derivation of the control law and the design of the control parameters.

E.2 Derivation of the control law

Suppose there is a nonlinear system which has a single control variable:

$$\dot{\mathbf{X}} = \mathbf{f}(\mathbf{X}) + \mathbf{g}(\mathbf{X})u(t) \tag{E.1}$$

where $\mathbf{X}$ is a n-dimensional state vector,

$\mathbf{f}(\mathbf{X})$ and $\mathbf{g}(\mathbf{X})$ are R_n valued mappings,

$u(t)$ is the only control variable.

With the theory of differential geometry, a nonlinear system can be linearised through coordinate transformation [28]. The nonlinear equations can be transformed to the following linear system:

$$\dot{\mathbf{Z}} = \mathbf{A}\mathbf{Z}(\mathbf{t}) + \mathbf{B}y(t) \tag{E.2}$$

According to the linear optimal technique LQR, $u(t)$ is selected to minimise the cost function J where

$$J = \int_{t_0}^{t} \left(\mathbf{Z}^{\mathrm{T}}(\mathbf{t})\mathbf{Q}\mathbf{Z}(\mathbf{t}) + ry^2(t) \right) dt \qquad \text{(E.2.1)}$$

and to minimise the cost function J :

$\frac{dJ}{dt} = 0$ which is the Riccati equation and r is a positive parameter for a single input system.

By choosing:

$y(t) = -\mathbf{K}\mathbf{Z}(\mathbf{t})$, the design boils down to the determination of the elements of the matrix $\mathbf{K}$.

Consider a simple power system shown in Fig. E.1, with the following dynamic equations:

$$\dot{\delta} = \omega - \omega_0 \qquad \text{(E.3)}$$

$$\dot{\omega} = \frac{\omega_0}{2H}\left(P_m - \frac{E'_q V_2}{X_\Sigma} \sin\delta \right) \qquad \text{(E.4)}$$

where $X_\Sigma = X'_d + X_T + X_L + X_C = X_{L\Sigma} + X_C$.

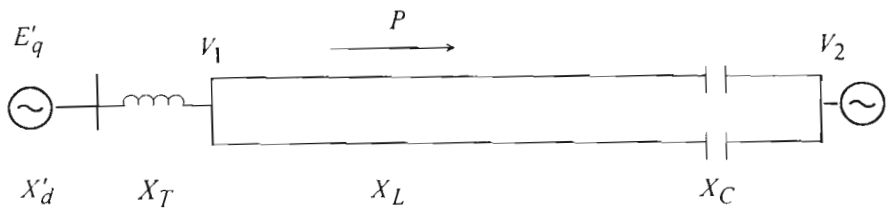

Fig. E.1: One-line diagram of a simple power system.

The equations (E.3) and (E.4) can be written in matrix form as follows:

$$\begin{bmatrix} \dot{\delta} \\ \dot{\omega} \end{bmatrix} = \begin{bmatrix} \omega - \omega_0 \\ \frac{\omega_0 P_m}{2H} \end{bmatrix} + \begin{bmatrix} 0 \\ -\frac{\omega_0 E'_q V_2 \sin\delta}{2H} \end{bmatrix} \frac{1}{X_\Sigma} \qquad \text{(E.5)}$$

By comparing equations (E.1) and (E.5), the following terms to can be defined:

$$\mathbf{X} = \begin{bmatrix} \delta \\ \omega \end{bmatrix} \tag{E.6}$$

$$\mathbf{f}(\mathbf{X}) = \begin{bmatrix} \omega - \omega_0 \\ \dfrac{P_m \omega_0}{2H} \end{bmatrix} \tag{E.7}$$

$$\mathbf{g}(\mathbf{X}) = \begin{bmatrix} 0 \\ -\dfrac{\omega_0 E'_q V_2 \sin\delta}{2H} \end{bmatrix} \tag{E.8}$$

$$u(t) = \frac{1}{X_\Sigma(t)} \tag{E.9}$$

By using the nonlinear control theory [28], the following coordinates transformation from $\mathbf{X}$ space to $\mathbf{Z}$ space as follows:

$$Z_1 = \delta - \delta_0 = \Delta\delta \tag{E.10}$$

$$Z_2 = \omega - \omega_0 = \Delta\omega \tag{E.11}$$

From equations (E.3) and (E.10),

$$\Delta\dot{\delta} = \dot{\delta} = \Delta\omega = \omega - \omega_0 \quad \Rightarrow \quad \dot{Z}_1 = Z_2 \tag{E.12}$$

and choosing $\Delta\dot{\omega} = \dot{\omega} = y(t) \quad \Rightarrow \quad \dot{Z}_2 = y(t)$ (E.13)

Thus, by writing equations (E.12) and (E.13) in matrix form:

$$\begin{pmatrix} \dot{Z}_1 \\ \dot{Z}_2 \end{pmatrix} = \begin{pmatrix} 0 & 1 \\ 0 & 0 \end{pmatrix} \begin{pmatrix} Z_1 \\ Z_2 \end{pmatrix} + \begin{pmatrix} 0 \\ 1 \end{pmatrix} y(t) \tag{E.14}$$

and hence by comparing equations (E.2) and (E.14), the following matrices and be obtained:

$$\mathbf{A} = \begin{pmatrix} 0 & 1 \\ 0 & 0 \end{pmatrix} \text{ and } \mathbf{B} = \begin{pmatrix} 0 \\ 1 \end{pmatrix}.$$

From equation (E.13),

$$y(t) = \dot{Z}_2 = \dot{\omega} = \frac{\omega_0}{2H}\left(P_m - \frac{E'_q V_2 \sin\delta}{X_\Sigma} \right) \tag{E.15}$$

Since for the linear quadratic regulator LQR,

$$y(t) = -\mathbf{KZ(t)} = -\begin{bmatrix} K_1 & K_2 \end{bmatrix}\begin{bmatrix} Z_1 \\ Z_2 \end{bmatrix} = -K_1 Z_1 - K_2 Z_2 \tag{E.16}$$

Replacing (E.16) and (E.9) in equation (E.15) and re-arranging:

$$u(t) = \frac{P_m - \frac{2H}{\omega_0}\left(K_1 \Delta\delta + K_2 \Delta\omega\right)}{E'_q V_2 \sin\delta} \tag{E.17}$$

Since $u(t) = \frac{1}{X_\Sigma} = \frac{1}{X_{L\Sigma} + X_C}$, by replacing in equation (E.17) and re-arranging:

$$X_C = \frac{E'_q V_2 \sin\delta}{P_m - \frac{2H}{\omega_0}\left(K_1 \Delta\delta + K_2 \Delta\omega\right)} - X_{L\Sigma} \tag{E.18}$$

By using the voltage angle difference ϕ between the sending and receiving buses and the initial active power transfer P_{L0} in the lines, equation (E.18) can be written in a local control scheme as follows:

$$X_{TCSC} = \frac{V_1 V_2 \sin\phi}{P_{L0} + \frac{2H}{\omega_0}\left(K_1 \Delta\phi + K_2 \frac{d\phi}{dt} \right)} - X_L \tag{E.19}$$

which is the nonlinear adaptive control scheme considered in Chapter Six for the different transient stability studies that were investigated.

E.3 Design of control parameters

As explained in the previous section, $y(t) = -\mathbf{KZ}(t)$ was chosen and the design boils down to the determination of the elements of the matrix $\mathbf{K}$. From the LQR technique:

$$y(t) = -\mathbf{KZ}(t) = -\frac{1}{r}\mathbf{B}^{\mathrm{T}}\mathbf{PZ}(t) \tag{E.20}$$

where $\mathbf{P}$ is the solution of the following Ricatti equation:

$$\mathbf{A}^{\mathrm{T}}\mathbf{P} + \mathbf{PA} + -\mathbf{PB}\frac{1}{r}\mathbf{B}^{\mathrm{T}}\mathbf{P} + \mathbf{Q} = 0 \tag{E.21}$$

The matrix $\mathbf{Q}$ was chosen as $\begin{bmatrix} 1 & 0 \\ 0 & 0 \end{bmatrix}$ which means that in the performance index J define by equation (E.2.1) where the first term is given by:

$$\mathbf{Z}^{\mathrm{T}}\mathbf{QZ} = \begin{bmatrix} Z_1 & Z_2 \end{bmatrix}\begin{bmatrix} 1 & 0 \\ 0 & 0 \end{bmatrix}\begin{bmatrix} Z_1 \\ Z_2 \end{bmatrix} = Z_1^2 = (\Delta\delta)^2 \tag{E.22}$$

and $$y(t) = \dot{\omega} \tag{E.23}$$

By replacing equations (E.22) and (E.23) in equation (E.2.1),

$$J = \int_{t_0}^{t}\left((\Delta\delta)^2 + r(\dot{\omega})^2\right)dt \tag{E.24}$$

which means the performance will depend both rotor angle deviation and the rate of change of the rotor speed where r is a positive gain of the control input signal $y(t)$.

To determine the diagonal matrix $\mathbf{P} = \begin{bmatrix} p_1 & p_2 \\ p_2 & p_3 \end{bmatrix}$,

$\mathbf{A}$, $\mathbf{B}$ and $\mathbf{Q}$ were replaced in the Ricatti equation (E.21) to obtain the following:

$$\begin{bmatrix} 1-\frac{p_2^2}{r} & p_1-\frac{p_2 p_3}{r} \\ p_1-\frac{p_2 p_3}{r} & p_2-\frac{p_3^2}{r} \end{bmatrix}=0$$ and thus the following elements of $\mathbf{P}$ can be determined:

$$p_1=\left(\sqrt{2}\right)r^{\frac{1}{4}} \tag{E.25}$$

$$p_2=\sqrt{r} \tag{E.26}$$

$$p_3=\left(\sqrt{2}\right)r^{\frac{3}{4}} \tag{E.27}$$

From equation (E.20),

$$\mathbf{K}=-\frac{1}{r}\mathbf{B}^{\mathrm{T}}\mathbf{P} \tag{E.28}$$

By replacing the matrices $\mathbf{B}$ and $\mathbf{P}$ in equation (E.29), the matrix $\mathbf{K}$ can be determined:

$$\mathbf{K}=\begin{bmatrix} K_1 & K_2 \end{bmatrix}=\begin{bmatrix} \sqrt{\frac{1}{r}} & \sqrt[4]{\frac{4}{r}} \end{bmatrix} \tag{E.29}$$

From equation (E.29), the following correlating function that relates K_1 and K_2 can be derived:

$$K_2=\sqrt{2K_1} \tag{E.30}$$

The eigenvalues λ of the linearised system defined by equation (E.2) can be determined by the following equation:

$$\left|\lambda \mathbf{I} - (\mathbf{A} - \mathbf{BK})\right| = 0 \tag{E.31}$$

Thus by replacing $\mathbf{A}$, $\mathbf{B}$, $\mathbf{K}$ and $\mathbf{I}$ in equation (E.31), the eigenvalues are determined:

$$\lambda = -\sqrt[4]{\frac{1}{4r}}(1 \pm j) \tag{E.32}$$

Thus from equations (E.29) and (E.32), when the control gain r is chosen to be small, K_1 and K_2 become large and the real part of the eigenvalues become more negative. Hence, large values of K_1 and K_2 would be preferable if only design criteria was based on the positions of the eigenvalues.

However, from equation (E.19), large values of K_1 and K_2 means large TCSC reactance. Since the TCSC's control range has an upper limit $X_{orderMAX}$ due to limitation in the firing angle α (as discussed in Chapter Three), proper values of K_1 and K_2 must be chosen to avoid saturation in the control action where the reactance order is clamped to $X_{orderMAX}$ while trying to settle at a higher post-fault value of compensation. As the control gains K_1 and K_2 are correlated, by specifying the value K_1 automatically specifies the value of K_2. Furthermore, from equation (E.19), another factor that influences the TCSC reactance is the initial active power transfer P_{L0} in the line. Thus, different values K_1 corresponding to different P_{L0} were chosen such that the response of the nonlinear adaptive controller's output stayed within the permissible range $[X_{orderMAX}, X_{orderMIN}]$. For the study system of Fig. 6.1, the following combinations:

$$P_{L0} = 0.8pu \Rightarrow K_1 = 0.3$$

$$P_{L0} = 1.0pu \Rightarrow K_1 = 0.001$$

were found to be the appropriate values that kept X_{TCSC} within the permissible range.

REFERENCES

[1] Paserba J. J., "How FACTS Controllers Benefit AC Transmission Systems", *Proceedings of the IEEE PES Transmission and Distribution Conference and Expo*, Dallas, TX, USA, 2003.

[2] Zhou X., Guo J., Zhang C., Yonghua Y., Hu X., Chen Q., Weisheng W., Baohua L., Chen Y., Li Z., Tao J., Zhang Z., Jing J., "Analysis and control of Yimin-Fengtun 500kV TCSC system", *Electric Power Systems Research*, Vol. 46, 1998, pp.157-168.

[3] Gyugyi L., "Solid-State control of AC Power Transmission", *Proceedings of the EPRI FACTS conference 1,* Cincinnati, 1990, pp.(1.7-1)-(1.7-44).

[4] Kimbark E. W., "Improvement of System Stability by Switched Series Capacitors", *IEEE Transactions on Power Apparatus and Systems*, Vol. PAS-85 No. 2, 1966, pp.180-188.

[5] Gyugyi L., Hingorani N. G., "Understanding FACTS: Concepts and Technology of Flexible AC Transmssion Systems", *IEEE Press,* Piscatway NJ, 2000.

[6] Larsen E., Bowler C., Damsky B., Nilsson S., "Benefits of Thyristor Controlled Series Compensation", *Cigre Annual Meeting*, Paris 1992.

[7] Kundur P., "Power System Stability and Control", *McGraw-Hill Inc*, 1994.

[8] Mathworks, "Using MATLAB Version 6, Computation, Visualization and Programming", *The Mathworks Inc*, 2002.

[9] Manitoba HVDC Research Centre, "PSCAD/EMTDC Version 3.0.8 User's Manual", *The Manitoba HVDC Research Centre Inc*, 2001.

[10] Pillay Carpanen R. and Rigby B. S., "The application of the thyristor controlled series capacitor for enhancing generator transient stability", *Proceedings of the 13th Southern African Universities Power Engineering Conference*, Stellenbosch, 2004.

[11] Pillay Carpanen R. and Rigby B. S., "Transient stability enhancement using a thyristor controlled series capacitor", *Proceedings of the 7th IEEE Africon Conference*, Gaborone. Botswana 2004.

[12] Pillay Carpanen R. and Rigby B. S., "Energy function control versus bang-bang control of the TCSC for enhancing the stability of power systems", *Proceedings of the 14th Southern African Universities Power Engineering Conference*, Johannesburg, 2005.

[13] Smith O. J. M., "Power System Transient Control by Capacitor Switching", *IEEE Transactions on Power Apparatus and Systems*, Vol. PAS-88 No. 1, 1969, pp.28-35.

[14] Webster R. H. and Smith O. J. M., "Series Capacitor Switching to Quench Electromechanical Transients in Power Systems", *IEEE Transactions on Power Apparatus and Systems*, Vol. PAS-90 No. 2, 1971, pp.427-433.

[15] Ramarao N. and Reitan D. K., "Improvement of Power System Transient Stability using Optimal Control: Bang-Bang Control of Reactance", *IEEE Transactions on Power Apparatus and Systems*, Vol. PAS-89 No. 5/6, pp.975-984, 1970.

[16] Machowski J., Bialek J. W., Bumby J. R., "Power System Dynamics and Stability", *John Wiley & Sons Ltd*, 1997.

[17] Wang Y., Mohler R.R., Mittelstadt W., "Variable-Structure FACTS controllers for Power System Transient Stability", *IEEE Transactions on Power Systems*, Vol. 7 No. 1, 1992, pp.307-313.

[18] Kosterev D. N., Kolodziej W. J., "Bang-Bang Series Capacitor Transient Stability Control", *IEEE Transactions on Power Systems*, Vol. 10 No. 2,1995, pp.915-924.

[19] Kosterev D. N. and Kolodziej W. J., "Robust Transient Stability Control Using Thyristor Controlled Series Compensation", *Proceedings of the 4th IEEE conference on Control Applications*, 1995, pp.215-220.

[20] Padiyar K. R. and Rao K. U., "Discrete Control of TCSC for Stability Improvement in Power Systems", *Proceedings of the 4th IEEE conference on Control Applications*, 1995, pp.246-251.

[21] Padiyar K. R. and Rao K. U., "Discrete Control of Series Compensation for Stability Improvement in Power Systems", *International Journal of Electrical Power & Energy Systems*, Vol. 19 No. 5, 1997, pp.311-319.

[22] Chang J., Tatanto G. N., Chow J. H., "Dynamic state estimation using a nonlinear observer for optimal series-capacitor switching control", *International Journal of Electrical Power & Energy Systems*, Vol. 19 No. 7, 1997, pp.441-447.

[23] Jiang D., Lei X., "A nonlinear TCSC control strategy for power system stability enhancement", *Proceedings of the 5th International Conference on Advances in Power System Control, Operation and Management, APSCOM 2000,* Hong Kong, Oct 2000, pp.576-581.

[24] Lerch E., Povh D., Xu L., "Advanced SVC control for damping power system ocillations", *IEEE Transactions on Power Systems*, Vol. 6 No. 2, 1991, pp.524-535.

[25] Wang Y., Tan Y. L., Guo G., "Robust nonlinear co-ordinated excitation and TCSC control for power systems", *IEE Proceedings on Generation, Transmission and Distribution*, Vol. 149 No. 3, 2002, pp.367-372.

[26] Yu C. S., Liu C. W., "Self-correction two-machine equivalent model for stability control of FACT system using real-time phasor measurements", *IEE Proceedings on Generation, Transmission and Distribution*, Vol. 149 No. 4, 2002, pp.389-396.

[27] Zhou X. and Liang J., "Overview of control schemes for TCSC to enhance the stability of power systems", *IEE Proceedings on Generation, Transmission and Distribution*, Vol. 146 No. 2, 1999, pp.125-130.

[28] Zhou X. and Liang J., "Nonlinear adaptive control of TCSC to improve the performance of power systems", *IEE Proceedings on Generation, Transmission and Distribution*, Vol. 146 No. 3, 1999, pp.301-305.

[29] Dai X., Liu J., Tang Y., Li N., Chen H., "Neural network αth-order inverse control of thyristor controlled series compensator", *Electric Power Systems Research*, Vol. 45, 1998, pp.19-27.

[30] Dai X., He D., Li N., Chen H., "Improved ANN αth-order inverse TCSC controller for enhancing power system transient stability", *IEE Proceedings on Generation, Transmission and Distribution*, Vol. 146 No. 6, 1999, pp.550-556.

[31] Mei S., Chen J., Lu Q., Song Y., Goto M., Yokoyama A., "Nonlinear multitarget H_∞ controller for thyristor controlled series compensation", *IEE Proceedings on Generation, Transmission and Distribution*, Vol. 148 No. 6, 2001, pp.557-561.

[32] Tan X., Tong L., Zhang N., Yin Z., Zhang D., Wang Z., , "A Fuzzy Control for Thyristor Controlled Series Compensation in Transients of Power Systems", *1998. Proceedings of IEEE International Conference on Power System Technology*, POWERCON '98, Beijing August 1998, Vol. 1, pp441 – 445.

[33] Rajkumar V., Zhu W., Mohler R. P., Spée R., Mittelsatdt W. A., Maratukulam D., "A bilinear self-tuning controller for Multimachine Transient Stability", *IEEE Transactions on Power Systems*, Vol. 9 No. 3, 1994, pp.1379-1384.

[34] Rajkumar V., Mohler R. P., "Bilinear Generalized Predictive Control using the Thyristor-Controlled Series Capacitor", *IEEE Transactions on Power Systems*, Vol. 9 No. 4, 1994, pp.1987-1993.

[35] Yu C. S, Liu C.W., "A Practical Design of TCSC Controllers for Inter-area Transient Stability Control Using Real-Time Measurements", *Proceedings of IEEE PES Winter Meeting*, Jan 1999, pp. 661-666.

[36] Venkatasubramaniam V., Taylor C. W., "Improving Pacific Intertie Stability Using Slatt Thyristor Controlled Series", *Proceedings of IEEE PES Winter Meeting*, Jan 2000, pp. 1468-1470.

[37] Rigby B. S., Harley R. G., "A Solid-State Controllable Series Capacitive reactance for Improved Utilization of High-Power Transmission Lines", *Proceedings of CIGRE Third Southern African Regional Conference*, Midrand, Johannesburg, SA 1998.

[38] Noroozian M. Andersson J., "Damping of Power System Oscillations by use of Controllable Components", *IEEE Transactions on Power Delivery*, Vol. 9 No. 4, 1994, pp.2046-2053.

[39] Song Y. H., Johns A. T., "Flexible AC Transmission Systems (FACTS)", *IEE Power and Energy Series*, London 1997.

[40] Kimbark E. W., "Improvement of Power System Stability by Changes in the Network", *IEEE Transactions on Power Apparatus and Systems*, Vol. PAS-88 No. 5, 1969. pp.773-778.

[41] Reitan D. K , RamaRao N., "A Method of Improving Transient Stability by Bang-Bang Control of Tie-line Reactance", *IEEE Transactions on Power Apparatus and Systems*, Vol. PAS-93, Jan/Feb. 1974, pp. 303-311.

[42] Miniesy S. M., Bohn E. V., "Optimum Network Switching in Power Systems", *IEEE Transactions on Power Apparatus and Systems*, Vol. PAS-90, Jan/Feb. 1971, pp. 2118-2123.

[43] Olwegard A., Walve K., Waglund G., Frank H., Torseng S., "Improvement of Transmission Capacity by Thyristor Controlled Reactive Power", *IEEE Transactions on Power Apparatus and Systems*, Vol. PAS-100, No. 8, August 1981, pp. 3930-3939.

[44] Nelson R. J., Bian J., Ramey D. G., Rietman T. R., Hill J. E., "Transient Stability Enhancement with FACTS Controllers", *IEE International Conference on AC and DC Power Transmission*, 29 April-3 May 1996, pp. 269-274.

[45] Ishimaru M., Yokoyama R., Shirai G., Niimura T., "Robust Thyristor Controlled Series Capacitor Controller design based on linear matrix inequality for a Multi-Machine Power System", *International Journal of Electrical Power & Energy Systems*, Vol. 24, No. 5, 2002, pp.621-629.

[46] Hingorani N. G., "Flexible AC Transmission", *IEEE Spectrum*, April 1993.

[47] Chonco N. S., "The Application of Controllable Inverter-Based Series Compensation to Power Oscillation Damping", MSc Thesis, University of Natal, Durban, South Africa, 2000.

[48] Mazibuko R. H., "Design and Implementation of Thyristor Controlled Series Capacitor for Research Laboratory Application", MSc Thesis, University of Natal, Durban, South Africa, 2003.

[49] Stankovic G. E., Mattavelli P., Ortega R., "On the Nonlinear control of TCSC", *Proceedings of the 35th Hawaii IEEE International Conference on System Sciences*, 2002.

[50] Rigby B. S., "An AC Transmission Line Power Flow Controller using a Thyristor Controlled Series Capacitor", *Proceedings of 6th IEEE Africon Conference*, George, South Africa, 2002. pp 773-778.

[51] Mazibuko R. H., Rigby B. S., Harley R. G., "Design of a Three-Phase Thyristor Controlled Series Capacitor", *Proceedings of 10th Southern African Universities Power Engineering Conference*, Cape Town, South Africa, 2001. pp 221-224.

[52] Li B. H., Wu Q. H. Wang P. Y., Zhou X. X., "Influence of the Transient Process of TCSC and MOV on Power System Stability", *IEEE Transactions on Power Systems*, Vol. 15, No. 2, 2000, pp. 798-803.

[53] Li B. H., Wu Q. H., Turner D. R., Wang P. Y., Zhou X. X., "Modelling TCSC Dynamics for Control and Analysis of Power System Stability", *International Journal of Electrical Power & Energy Systems*, Vol. 22, No. 1, 2000, pp.43-49.

[54] Martins N., Herminio J. C. P., Paserba J. J., "Using a TCSC for Line Power Scheduling and System Oscillation Damping – Small Signal and Transient Stability Studies", *Proceedings of IEEE PES Winter Meeting*, Jan 2000.

[55] Gama C., Tenório R., "Improvement for Power Systems Performance: Modelling, Analysis and Benefits of TCSCs", *Proceedings of IEEE PES Winter Meeting*, Jan 2000.

[56] Mihalič R., "Power Flow Control with Controllable Reactive Series Elements", *IEE Proceedings on Generation, Transmission and Distribution*, Vol. 145 No. 5, 1998, pp.493-498.

[57] Rigby B. S., Ndlovu C. K., Harley R. G., "A Thyristor Controlled Series Capacitor Design for Research Laboratory Application", *Proceedings of 5th IEEE Africon Conference*, Cape Town, South Africa, 1999. pp 903-908.

[58] Gama C., "Brazilian North-South Interconnection - Control Application and Operating Experience with TCSC", *Proceedings of IEEE PES Summer Meeting*, Jun, 1999.

[59] Edris A. A., Adapa R., Baker M. H., Bohmann K., Habashi K., Gyugyi L., Lemay J., Mehraban A. S., Myers A. K., Reeve J., Sener F., Torgerson D. R., Wood R. R., "Proposed Terms and Definitions for Flexible AC Transmission System (FACTS)", *IEEE Transactions on Power Delivery*, Vol. 12, No. 4, 1997, pp. 1848-1853.

[60] Jalali S. G., Hedin R. A., Pereira M., Sadek K., "A Stability Model for the Advanced Series Compensator (ASC)", *IEEE Transactions on Power Delivery*, Vol. 11, No. 2, 1996, pp. 1128-1137.

[61] Paserba J. J., Miller N. W., Larsen E. V., Piwko R. J., "A Thyristor Controlled Series Compensator Model for Power System Stability Analysis", *IEEE Transactions on Power Delivery*, Vol. 10, No. 3, 1995, pp. 1471-1478.

[62] Scott J.K., Mittelstadt W. A., Suhrbier R. W., "Test Results and Initial Operating Experience for the BPA 500kV Thyristor Controlled Series Capacitor Unit at Slatt Substation", *Proceedings of the EPRI FACTS conference 3,* Baltimore, Maryland, 1994, pp.(3-1)-(4-15).

[63] Jalali S. G., Lasseter R. H. Dobson I., "Dynamic Response of a Thyristor Controlled Switched Capacitor", *IEEE Transactions on Power Delivery*, Vol. 9, No. 3, 1994, pp. 1609-1615.

[64] Helbing S. G., Karady G. G., "Investigations of an Advanced Form of Series Compensation", *IEEE Transactions on Power Delivery*, Vol. 9, No. 2, 1994, pp. 939-945.

[65] Larsen E. V., Clark K., Miske S. A., Urbanek J., "Characteristics and Rating of Thyristor Controlled Series Compensation", *IEEE Transactions on Power Delivery*, Vol. 9, No. 2, 1994, pp. 992-1000.

[66] Nyati S., Wegner C. A., Delmerico R. W., Piwko R. J., Baker D. H., Edris A., "Effectiveness of Thyristor Controlled Series Capacitor in Enhancing Power System Dynamics: An Analog Simulation Study", *IEEE Transactions on Power Delivery*, Vol. 9, No. 2, 1994, pp. 1018-1027.

[67] Urbanek J., Piwko R. J., Larsen E. V., Damsky B. L., Furumasu B. C., Mittlestadt W., Eden J. D., "Thyristor Controlled Series Compensation Prototype Installation at the Slatt 500kV substation", *IEEE Transactions on Power Delivery*, Vol. 8, No. 3, 1993, pp. 1460-1469.

[68] Christi N., Hedin R., Johnson R., Kruase A., Montoya A., "Power System Studies and Modelling for Kayenta 230kV substation Advanced Series Compensation", *IEE International Conference on AC and DC Power Transmission*, Sep 1991, pp. 33-37.

[69] Zhongdong Y., Luyuan T., Yongtin C., Dongxia Z., Chunlin G., Zhonghong W., "A study on the characteristics of TCSC based on digital simulations and physical experiments", *Proceedings of IEEE International Conference on Power System Technology*, POWERCON '98, Beijing August 1998, Vol. 1 , pp328 – 332.

[70] IEEE Power System Relaying Committee WG K13, "Series Capacitor Bank Protection", *IEEE PES*, 1998.

[71] Ogata K., "Modern Control Engineering", *Prentice –Hall of India Pvt Ltd,* New Dehli, 1997.

[72] Athas M. and Falb P. L., "Optimal Control: An Introduction to the Theory and its Applications", *Mc Graw-Hill Inc.,* 1966.

[73] Larsen E. V., Juan J., Sanchez-Gasca, Chow J. H., "Concepts for the Design of FACTS Controllers to Damp Power Swings", *IEEE Transactions on Power Systems*, Vol. 10, No. 2, 1995, pp.948-955.